Grid Amplifiers

Thesis by

Moonil Kim

In Partial Fulfillment of the Requirements

for the Degree of

Doctor of Philosophy

California Institute of Technology

Pasadena, California

1993

(Submitted December 11, 1992)

Acknowledgements

First of all, I would like to thank my advisor, Professor David Rutledge who allowed me to be a member of his prestigious group at Caltech, and supported me financially over the past five years. Under his guidance, I have had a chance to work on many interesting projects such as MESFET grid oscillators, Gunn-diode grid oscillators, diffraction analysis, beam-steering grids, grid amplifiers, and monolithic grid oscillators. He encouraged me never to give up on these experiments even after numerous failures.

I would like to thank my colleagues who ride bicycles to preserve a better environment: Jon Hacker, Mike DeLisio, Victor Lubecke, and Alina Moussessian. I will remember the three-kicking sparrings, basketball fights, hallway soccer, and space-war games. Without them, my life at Caltech would have been much more difficult. The rest of the MMIC group members; Shi-jie Li, Jung Chi Chiao, Jeff Liu, and Renee Watson - I admire them for their patience and quietness. I will never forget the friendship of the former members of the group, Robert Weikle, Zoya Popović, Gabriel Rebeiz, Wyman Williams, Phil Stimson, and Scott Wedge. They spent their valuable time, teaching me the practical side of microwaves. I am grateful to Yong Guo, Karen Lee, Lars Foged, Olga Borić, Arthur Sheiman, David Haub, Dayalan Kasilingham, Maisy Ng, and Randy Salvatore for being my friends. I also appreciate the kindness that Kent Potter and Irene Laura have shown over the years.

I should mention that many of the ideas in this thesis were originated by Professor Jim Rosenberg at Harvey Mudd Collage and Dr. Pete Smith at JPL. Lance Sjogren at UCLA and Dr. Larry Epp at JPL also helped me understand how quasi-optical grids work in general. Dave Gagnon at NWC kindly performed many important measurements for me. The most important contribution in completing this thesis came from Dr. Emilio Sovero at Rockwell International. Dr. Sovero provided transistors, measurement equipment, and even photographs for publications along with helpful advice. Without his help, this thesis would have been about twenty pages long.

Grid Amplifiers

Abstract

Presented in this thesis are two grid amplifiers for operation in the microwave range. The first 5×5 MESFET amplifier grid verified the design approach by showing a gain of 11 dB at 3.3 GHz. The second 10×10 amplifier grid, which has a metal layout pattern suitable for future monolithic integration, has shown a gain of 10 dB at 10 GHz with a 3 dB bandwidth of 1 GHz. The active devices in the grid were custom-designed HBT differential-pairs with a self-biasing resistor network for the base. This amplifier grid has produced a saturated output power of 450 mW while exhibiting a noise figure of 6.5 dB. The amplifier grid was also converted into an oscillator with smooth frequency-tuning between 8 and 11 GHz by using external feedback. A grid-array system of an oscillator and the amplifier was built to show the conservation of propagation angle for an rf beam through the amplifier grid. Amplitude modulation of the grid amplifier gain was demonstrated by applying a modulating signal to the grid's dc bias lines.

Contents

Chapter 1

Introduction

During the last few years, different types of quasi-optical power-combining grids for the microwave and millimeter-wave bands have been investigated. A number of grids were successfully built with MESFET transistors and Schottky diodes. This chapter provides a brief review of these grids and an outline of the thesis.

1.1 MICROWAVE AND MILLIMETER-WAVE POWER-COMBINING

For high power applications in the millimeter-wave range, the power of the vacuum-tube devices surpass the solid-state devices as indicated in Figure 1.1. However, paralleling the rapid growth of the semiconductor industry at lower frequencies, it would be desirable to replace tubes with solid-state devices. This suggests that we should consider combining the outputs of many solid-state devices. The idea of free-space power-combining was first introduced by Wandinger and Nalbandian in 1983 [1]. They built an oscillator that combined the output powers of two Gunn diodes at 60 GHz using tapered dielectric rod antennas coupled to a Gaussian resonator. In 1986, Mink [2] suggested using monolithic source arrays in an optical resonator to obtain an efficient power combining of solid-state millimeter-wave sources. Later, Stephan *et al.* investigated combining output powers from two Gunn diodes in free-space [3]. There, the microstrip ground plane and a spherical reflector formed a Gaussian beam cavity. A good overview of the millimeter-wave radiation source and various types of power-combining method is provided in the introductory chapter of Weikle's Ph.D. Thesis [4].
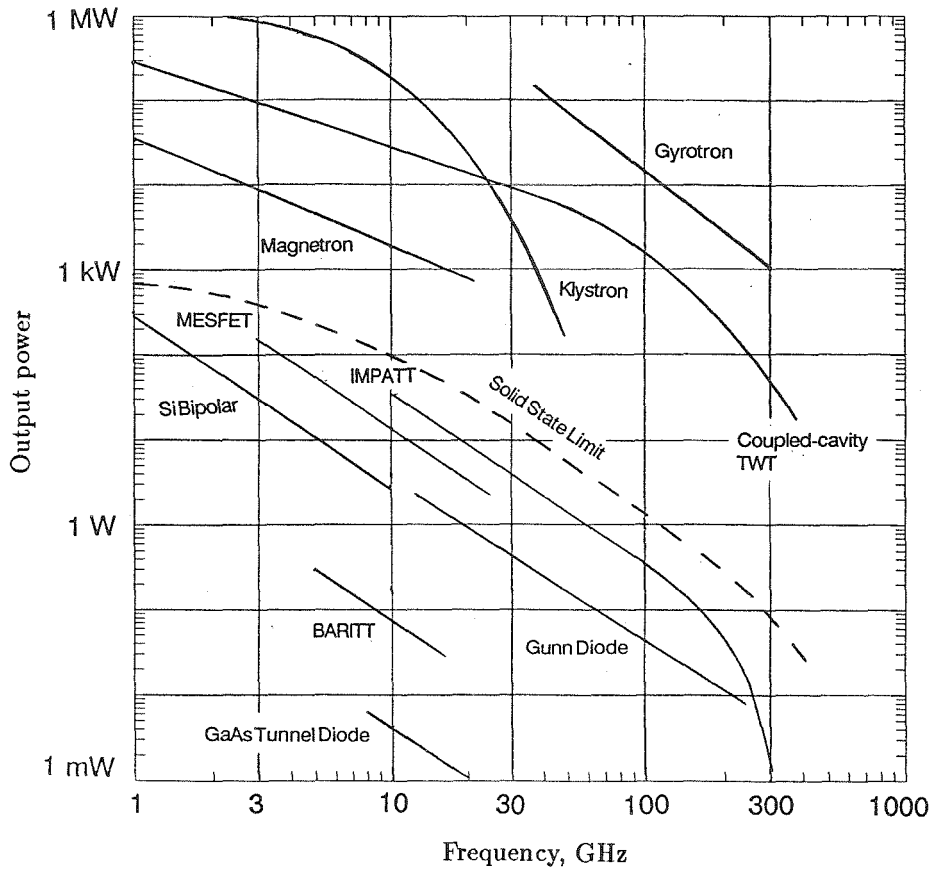
Figure 1.1 Output power vs. frequency for vacuum-tube and solid-state devices. This data was collected and updated by DeLisio at Caltech.

1.2 PAST GRID ARRAYS

Periodic arrays with embedded solid-state devices have been extensively studied over the past five years as a means to accomplish an effective power-combining of many solid-state devices. The majority of the grid arrays built in this period are oscillators for signal generation in the microwave range. However, construction of complete quasi-optical grid-array systems requires control components as well. To this end, several diode grids, both monolithic and hybrid, were built to demonstrate phase-shifting, beam-steering, and frequency-multiplying.

1.2.1 THE 25-ELEMENT MESFET GRID

Gunn diodes are good candidates for application in oscillator grids [5]. In order
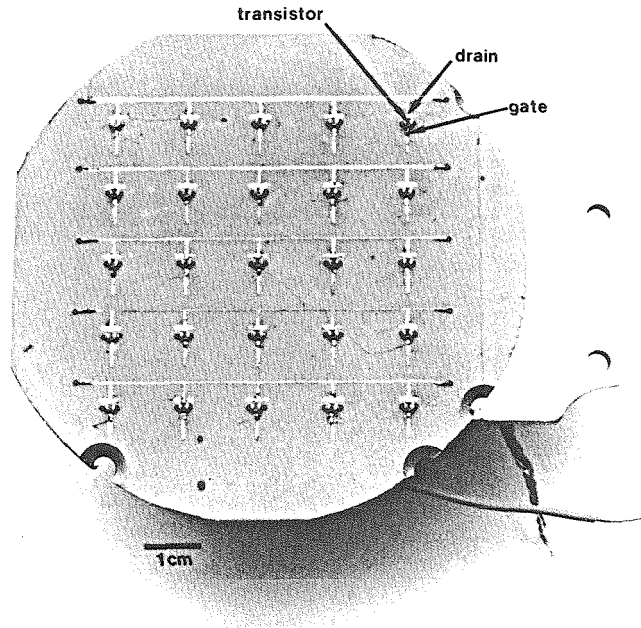
Figure 1.2 The first 25-element grid oscillator. The packaged devices (*Fujitsu* FSC10LF) were mounted on top of a *Rogers* Duriod substrate with $\epsilon_r = 10.5$.
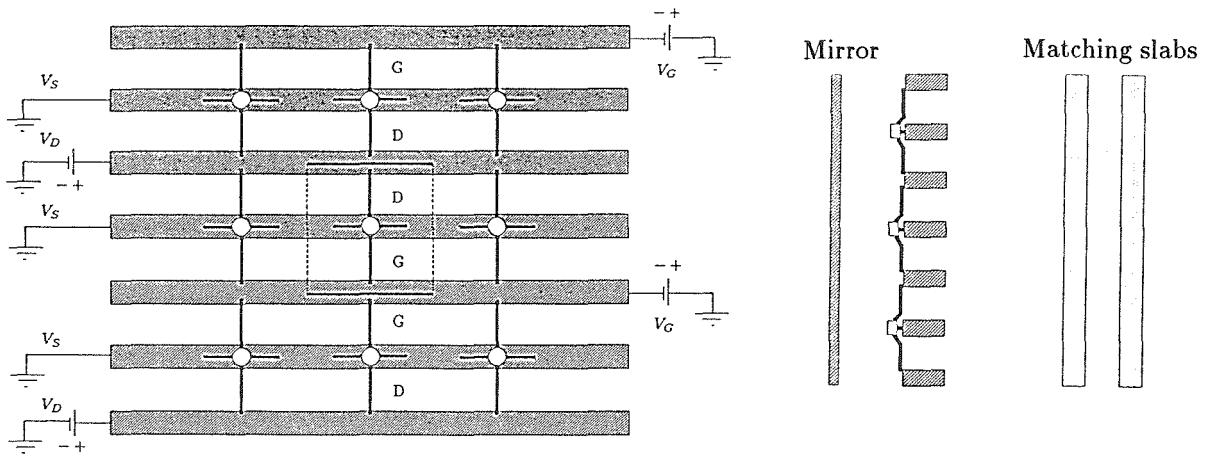
Figure 1.3 The bar grid oscillator [7]. The front and the side views are shown. Symmetry allows us to impose a certain set of boundary conditions on the edge of a unit cell. The solid lines indicate electric walls, while the dashed lines show magnetic walls.

to frequency-lock the whole grid, however, it is sometimes necessary to bias each diode separately. This separate biasing may not be convenient for grids with a large number of elements. As an alternative, MESFET transistors can be used in grid oscillators. Transistors usually provide high gain over a wide frequency range. Consequently, small differences among devices can be tolerated as the necessary feedback exists in the passive metallic grid structure outside the active device. The demonstration of the first 25-element oscillator grid [6] shown in Figure 1.2 showed us that transistors are in fact adequate active devices for larger-size grid oscillators.

1.2.2 THE BAR GRID

The first grid oscillator had a complicated structure and was rather difficult to analyze. On the other hand, the bar grid [7] has a relative simple geometry where the copper bars form TEM waveguides for individual rows in the array. The waveguide to the device connection was made by the transistor package leads that acted as inductive dipole antennas (Figure 1.3). For the first time, the oscillation frequency of the grid was predicted from an equivalent circuit model. FM modulation on the gate bias line was successfully demonstrated as well.

1.2.3 THE PLANAR 100-ELEMENT GRID

The planar grid [8] shown in Figure 1.4 possesses a relatively simple cross-shape metal pattern on a single plane. Such a grid structure can easily be integrated into a monolithic circuit. The total radiated rf output power of this grid was more than half a watt. The induced EMF method was used to calculate the imbedding impedance that the device sees when placed in the grid [4]. The shape of the grid structure and the equivalent circuit model developed for this grid have been adopted for more recent grid oscillators as well.
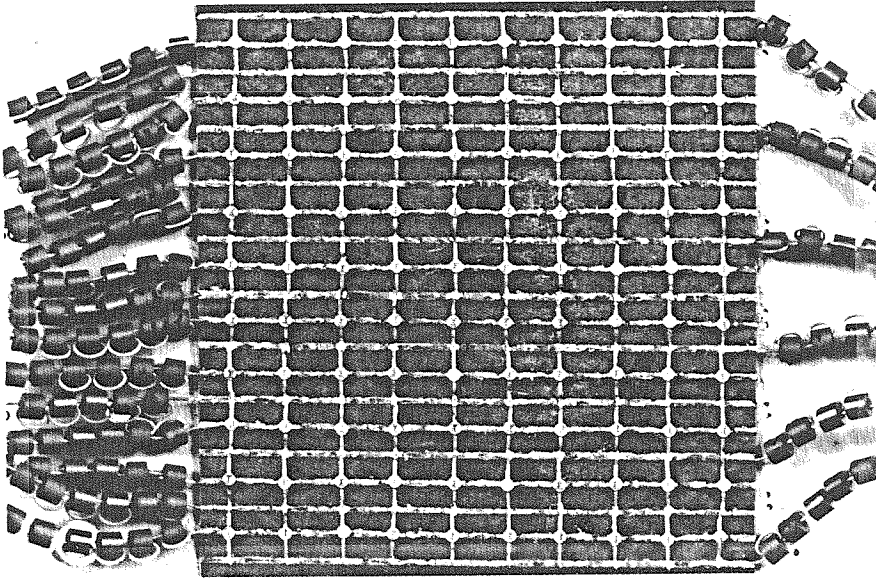
Figure 1.4 The 100-element MESFET planar grid oscillator [8].

	Name (number of devices)	Unit cell size (mm)	Oscillation frequency (GHz)	Output power (mW)
1	First Oscillator Grid, (25)	13	9.7	460
2	Bar Grid, (36)	10	3	220
3	Planar Grid, (100)	8	5	550
4*	X-band Grid, (16)	9	11.6	335
5*	Ku-band Grid, (36)	5	17	235

Table 1.1 Hybrid grid oscillators in chronological order. All the grids used *Fujitsu* FSC11 MESFET transistors. An (*) on the assigned number denotes the grid with transistors in chip form. Other grids used packaged transistors.

1.2.4 THE COMMON-GATE FEEDBACK GRID

In the earlier grids, the drain and the gate leads were usually aligned vertically, and two source leads horizontally. This arrangement was chosen simply because it

fits the existing transistor package style. However, even without rigorous theory, it is easy to see that this may not be the best arrangement for grid oscillators. First, the vertically polarized output power is drawn from the gate and the drain leads. In MESFET's, the gate rf current is much smaller than the source or the drain rf currents. Therefore, we are wasting the large source of rf current. Also, in MESFET's, the gain between the gate and the drain is greater at low frequencies, and drops as $1/f^2$ at higher frequencies. When the gate and the drain leads share the same polarization, it is more likely to produce oscillations at lower frequencies. Later grid oscillators [9] utilize the common-gate configuration, where the drain and the source leads are aligned in the same direction. The feedback path between the gate and the drain now depends heavily on the shape and the size of the passive grid structure. With this improved feedback control, the two grids have produced oscillations at 11.6 and 17 GHz respectively.
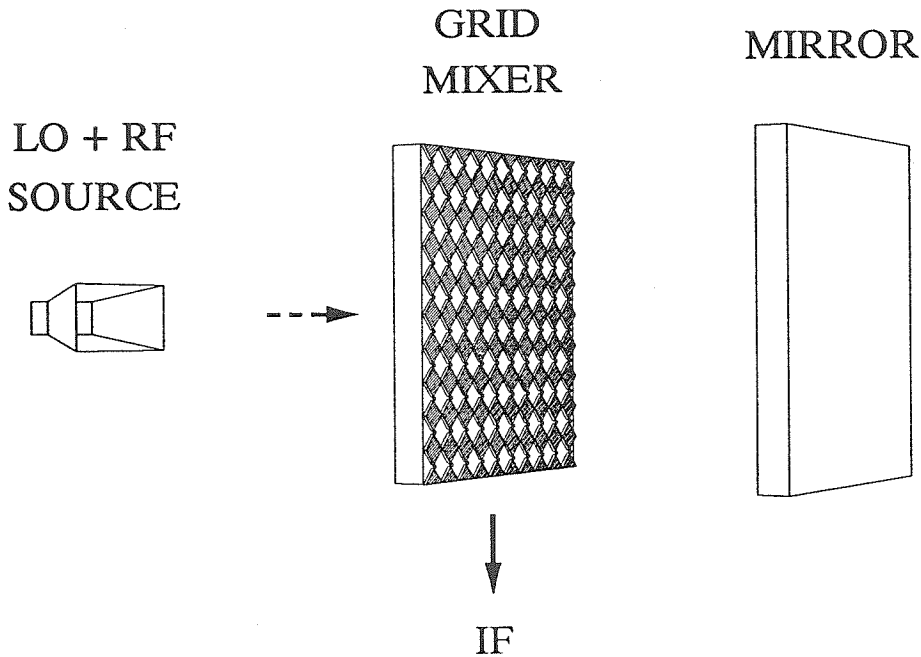
Figure 1.5 The mixer grid setup [12]. A mixer grid can also be used as an up converter where an incident LO signal will produce an RF signal that is modulated by an IF signal.

1.2.5 PHASE-SHIFTER SCHOTTKY DIODE ARRAY

To test phase-shifting of quasi-optical beams, diode grids were fabricated on 2 cm × 3 cm GaAs wafers with 2000 aluminum Schottky diodes [10]. A 70° phase shift with a 6.5 dB loss was measured at 93 GHz when the incident beam is reflected off the diode grid and a mirror. The same grid could be used for frequency-doubling [11] from 33 to 66 GHz with a conversion efficiency of 9.5%.

1.2.6 100-ELEMENT SCHOTTKY DIODE MIXER GRID

A 10 GHz, 100-element bow-tie grid mixer [12] has shown an improvement in dynamic range of 16.3 to 19.8 dB over an equivalent single diode mixer. The conversion loss and noise figure of the grid are equal to that of a conventional mixer. Recently, monolithic diode grids have been fabricated to build a frequency-tripler [13], and an electronic beam attenuator [14].

1.3 ORGANIZATION OF THE THESIS

The major fraction of this thesis is devoted to two grid amplifiers that were built in 1991 and 1992. These amplifiers are expected to complement other grid arrays as a critical component in millimeter-wave systems. The way we approach the amplifier design is described in Chapter 2, where differences between oscillators and amplifiers are also pointed out. In order to test our design approach, we built the first amplifier grid [15] with packaged MESFET transistors. The results of the first grid are presented in the same chapter.

In chapter 3, an improved grid amplifier for X-band [16] is discussed. The new unit cell design along with the custom-made differential-pair HBT chip transistor configuration are shown. The grid amplifier is then thoroughly characterized in gain, power, and noise performance. Results of additional experiments to test the results of failures in the grid are included. In chapter 4, we discuss

several applications of this particular X-band grid amplifier [17]. The applications include an external positive feedback oscillator, a grid array system made of an oscillator and an amplifier, and a variable-gain AM modulator.

Chapters 5 and 6 describe two grids that are closely related to the previous grid work. First, the theory developed in the past hybrid oscillator is borrowed to fabricate the first monolithic oscillator at 35 GHz [18]. The output power and the measured patterns are shown. Then the feasibility of a beam-steering grid is tested with a passive structure. The structure had gaps in the inductive leads in the place of the varactor diodes. By varying the gap sizes, the structure presents reactances necessary for a fixed beam shift of 30° at 93 GHz [19]. In the final chapter, two future projects related to the grid amplifier are discussed.

REFERENCES

[1] L. Wandinger and V. Nalbandian, " Millimeter-Wave Power Combining Using Quasi-Optical Techniques," *IEEE Trans. Microwave Theory Tech., MTT-31,* pp. 189–193, February 1983.

[2] James W. Mink, "Quasi-Optical Power Combining of Solid-State Millimeter-Wave Sources," *IEEE Trans. Microwave Theory Tech., MTT-34,* pp. 273–279, February 1986.

[3] S. Young and K. D. Stephan, "Stabilization and Power Combining of Planar Microwave Oscillators with an Open Resonator," *IEEE MTT-S International Syposium Digest,* vol. 1, pp. 185–188, Las Vegas, NV, 1987.

[4] R.M. Weikle, "Quasi-Optical Planar Grids for Microwave and Millimeter-Wave Power Combining," Ph.D. Thesis, California Institute of Technology, Pasadena, CA, 1992.

[5] R.A. York, and R.C. Compton, "Quasi-Optical Power Combining Using Mutually Synchronized Oscillator Arrays," *IEEE Trans. Microwave Theory Tech., MTT-39,* pp. 1000–1009, June 1991.

[6] Z.B. Popović, M. Kim, and D.B. Rutledge, "Grid Oscillators," *Int. J. Infrared and Millimeter-Waves,* vol. 9, pp. 647–654, 1988.

[7] Z.B. Popović *et al.,* " Bar Grid Oscillators," *IEEE Trans. Microwave Theory Tech., MTT-38,* pp. 225–230, March 1991.

[8] Z.B. Popović, R.M. Weikle, M. Kim, and D.B. Rutledge, "A 100-MESFET Planar Grid Oscillator," *IEEE Trans. Microwave Theory Tech., MTT-39,* pp. 193–200, February 1992.

[9] R.M. Weikle, M. Kim, J.B. Hacker, and D.B. Rutledge, "Planar MESFET Grid Oscillators using Gate Feedback," to be published in *IEEE Trans. Microwave Theory Tech.*

[10] W.W. Lam *et al.*, "Millimeter-Wave Diode-Grid Phase Shifters," *IEEE Trans Microwave Theory Tech.*, *MTT-36*, pp. 902–907, May 1988.

[11] C.F. Jou *et al.*, "Millimeter-Wave Diode Grid Frequency Doubler," *IEEE Trans Microwave Theory Tech.*, *MTT-36*, pp. 1507–1514, November 1988.

[12] J.B. Hacker, R.M. Weikle, M. Kim, M.P. De Lisio, and D.B. Rutledge, "A 100-Element Planar Shottky Diode Grid Mixer," *IEEE Trans. Microwave Theory Tech.*, *MTT-40*, pp. 557–562, March 1992.

[13] H-X King *et al.*, "Monolithic Millimeter-Wave Quasi-Optical Frequency Multiplier Arrays,"*Int. Semiconductor Device Research Symposium*, pp. 68–72, December 1991.

[14] L.B. Sjogren *et al.*, "Monolithic Millimeter-Wave Diode Array Beam Controllers: Theory and Experiment," *Int. Symposium on Space Terahertz Technology*, Ann Arbor, MI, March 1992.

[15] M. Kim, J.J. Rosenberg, R.P. Smith, J.B. Hacker, M.P. DeLisio, D.B. Rutledge, " A Grid Amplifier," *IEEE Microwave Guided Wave Lett.*, *MGWL-1*, pp. 322–324, November 1991.

[16] M. Kim, E.A. Sovero, J.B. Hacker, M.P. DeLisio, J.C. Chiao, J.J. Rosenberg, D. Gagnon, and D.B. Rutledge, "An X-Band HBT Grid Amplifier," submitted to *IEEE Trans Microwave Theory Tech.*

[17] M. Kim, E.A. Sovero, J.B. Hacker, M.P.DeLisio, S. Li, J.J. Rosenberg, and D.B. Rutledge, "Applications of an X-Band Grid Amplifier," submitted to *IEEE Trans Microwave Theory Tech.*

[18] M. Kim, E.A. Sovero, R.M. Weikle, J.B. Hacker, M.P. DeLisio, S. Li, and D.B. Rutledge, "A 35 GHz HBT Monolithic Grid Oscillator," submitted to *IEEE Trans Microwave Theory Tech.*

[19] M. Kim *et al.*, "A Beam Diffration by a Planar Structure at 93 GHz," *IEEE AP-S Syposium*, London, Ontario, 1988

Chapter 2

The C-Band MESFET Grid Amplifier

The basic design approach for grid amplifiers is presented. In this approach, the beam is amplified while transmitting through the amplifier grid. The chosen grid configuration utilizes cross-polarization for the input and the output field. The first 50-MESFET amplifier grid [1] based on the design approach was built and showed a gain of 11 dB at 3.3 GHz. The 3 dB gain bandwidth was 90 MHz.

2.1 DESIGN APPROACH

Work on oscillator grids has been conducted for many years. Though limited to a specific metal shape, grid oscillators can now be designed analytically. The accuracy of the analytic model has been demonstrated by successfully predicting the oscillation frequencies for oscillators at 11 GHz and 17 GHz [2]. Many ideas and concepts about grid amplifiers are borrowed from oscillator grid research. Designing amplifier grids is complicated compared to designing oscillators. The biggest task in building an amplifier grid is to prevent unwanted oscillations. Stabilizing an array of very high-gain solid-state devices at all frequencies is not an easy problem. Transistors packed together may behave in many different modes. A single transistor in array can obtain feedback from the surrounding metallic structures as in the case of grid oscillators. It is also possible that two neighboring transistors with a certain phase-offset might produce a different feedback path for a different kind of an oscillation. In some cases, a specific unit cell design which operated successfully in a 4 × 4 grid exhibited an oscillation in a 10 × 10 grid.
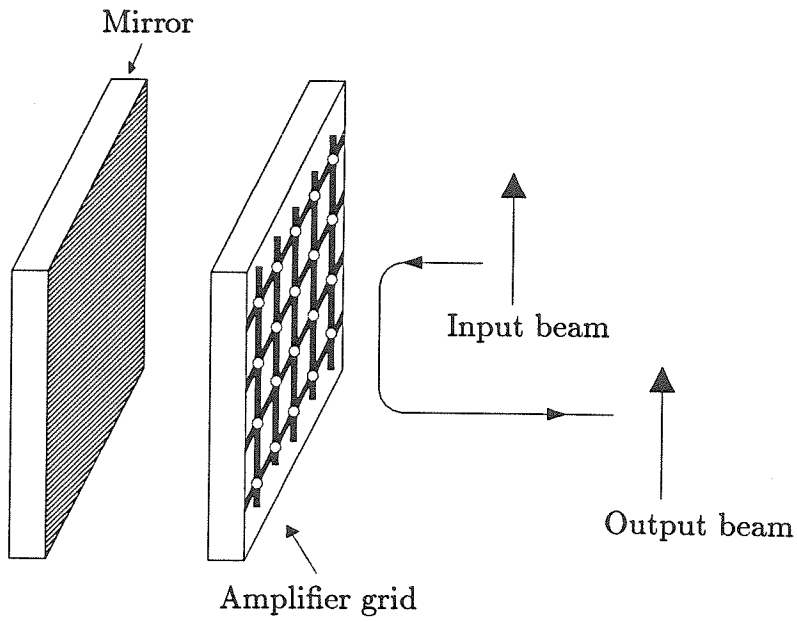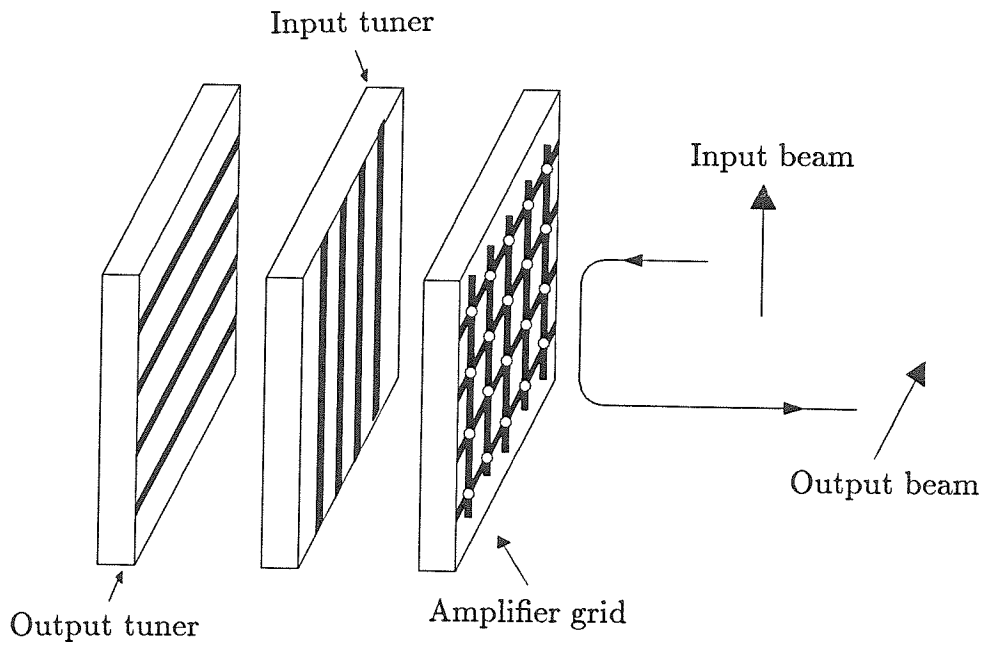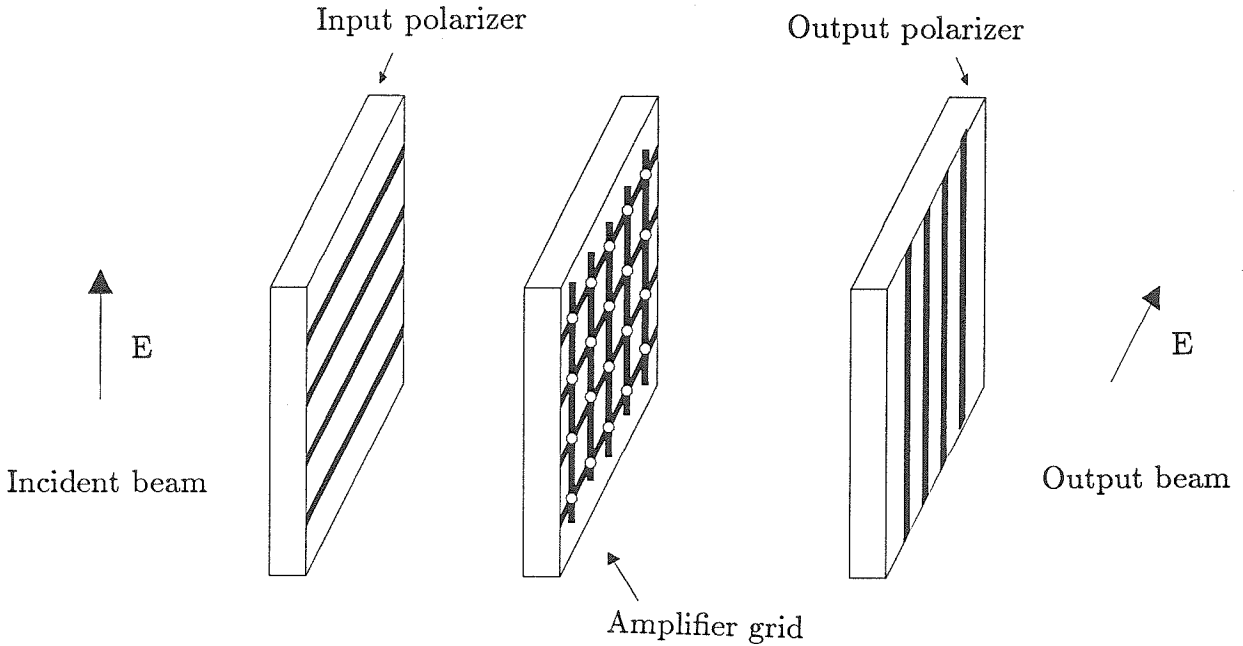
Figure 2.1 Two different schemes for amplifier grids with a reflected amplified beam. (a) Both the input and the output beam share the same polarization. (b) The input and the output beams are cross-polarized.

Input polarizer   Output polarizer

E

Incident beam   E

                                       Output beam

Amplifier grid

Figure 2.2 Transmission cross-polarized grid amplifier scheme.

Initially, several different amplifier configurations were examined. The first was very closely related to an oscillator grid. In many cases, oscillator grids can be separated into an active sheet and a partially reflecting mirror. The active sheet can be modeled as a load with negative resistance whose reflection coefficient is grater than unity [3]. If the oscillator grid is stable when the reflector is removed, then the oscillator can be used as an amplifier (Figure 2.1a). However, in a quasi-optical grid system, unless the object in front of such a grid amplifier is perfectly matched, reflection onto the grid could easily induce an oscillation.

A stable circuit that can tolerate a certain degree of output beam reflection is the design goal. This could be done by separating the input beam from the output by utilizing two cross-polarized fields (Figure 2.1b). This way, if the output beam is reflected back to the grid, it would not couple strongly to the input. This is advantageous compared to the earlier approach in that the two input and the output circuits can be tuned independently using different polarizers. Convenient

polarizers for microwave beams are simple dielectric slabs with etched copper strips. This scheme has one drawback. It is difficult to use this amplifier in conjunction with other grid arrays. In the case where a signal is generated by an oscillator grid with a back short, both the oscillator and the amplifier would be enclosed by two mirrors. The amplifier could be tilted so that the incident beam and the output beam could be separated, however, this adds complication to an already complex circuit.

Figure 2.2 shows the most desirable amplifier configuration. Vertically polarized power is incident from the left, and passes through a polarizer. The grid amplifies the beam and radiates it as horizontally polarized power, which passes through an output polarizer to the right. The polarizers provide isolation between the input and the output.
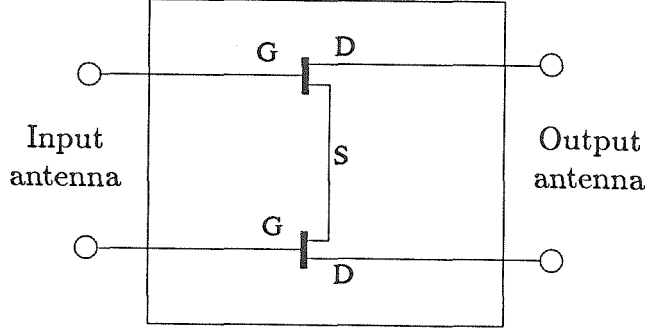
For a cross-polarized amplifier grid, the active device configuration should be adjusted appropriately. The active device has to pick up the voltage difference developed in the gap between the two input antenna leads, and produce a larger voltage difference at the two output terminals. A single three-terminal transistor could be used as shown in Figure 2.3a. This requires one port of the transistor to be shared by both input and output antennas which may result in poor isolation between the input and the output. Better isolation can be achieved with two transistors connected as shown in Figure 2.3b. One of the three terminals of the two transistors is tied together to produce a four port device, two for the input and the other two for the output. When the transistor pair is working in the differential-mode, the voltage difference at the input terminals will be amplified and appear across the output terminals.

2.2 SIMPLIFIED EQUIVALENT CIRCUIT

Previous oscillator grids exhibit a current distribution which permits electric and magnetic walls on the boundaries of a unit cell. This allows the reduction of
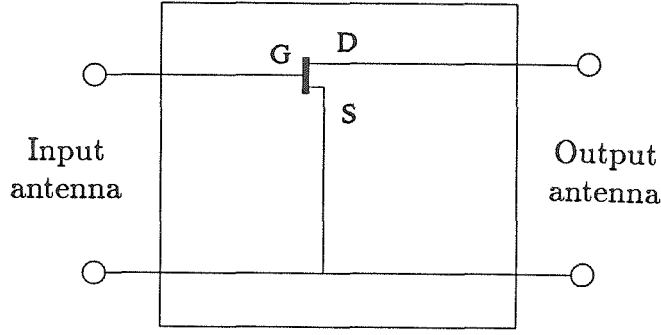
(a)

(b)

Figure 2.3 Two different device configurations for an amplifier grid. (a) A single transistor in a unit cell. (b) Two transistors forming a differential-pair. For a cross-polarized amplifier grid application, the differential-pair is ideal.

the problem of the entire grid to that of a single unit cell [4]. The theory that predicts the oscillator performance is independent of the grid size, provided that the grid is reasonably large. However, the current distribution in an amplifier grid does not allow any boundary conditions to be imposed on the edge of a unit cell (Figure 2.4).

The problem can be simplified by assuming that an incident beam would only couple to the antenna that is polarized in the same direction. A simple example is shown in Figure 2.5. Here, we find the coupling network between the vertical

(a)   (b)
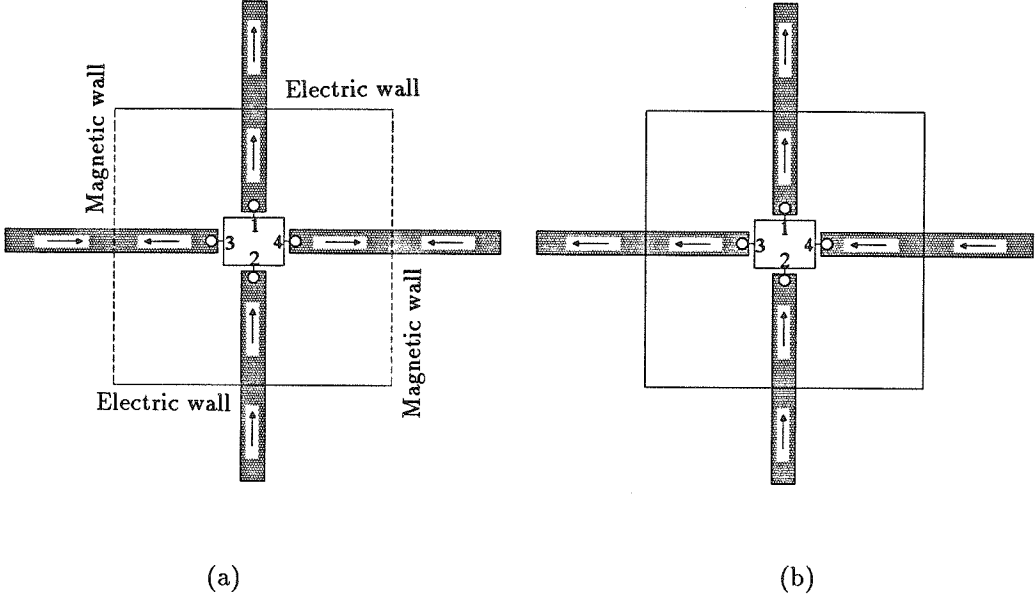
Figure 2.4 Current distribution on the unit cell for (a) an oscillator grid, and (b) an amplifier grid. Note that an oscillator grid has convenient boundary conditions for the unit cell, and a single unit cell can be used to predict the performance of the whole grid. The coupling antennas are all assumed to be inductive leads.

beam and two vertical leads by ignoring the coupling between the vertical beam and horizontal leads. When the frequency is low, the coupling between the antenna and the cross-polarized beam is small and mainly capacitive. The same process is applied with the horizontal beam and the two horizontal leads. Once the two coupling networks are found, a complete equivalent circuit can be found by connecting them to the active devices.

## 2.3 FABRICATION OF THE C-BAND AMPLIFIER GRID

A grid amplifier designed to test the feasibility of the cross-polarized fields approach was constructed. Figure 2.6 is a diagram of a unit cell. The vertical leads pick up the incident radiation. These leads are attached to the gates of two MESFET's. The amplified signal radiates from the horizontal drain leads. There are 25 transistor pairs in the 5×5 grid. The transistors were FSC10LG packaged
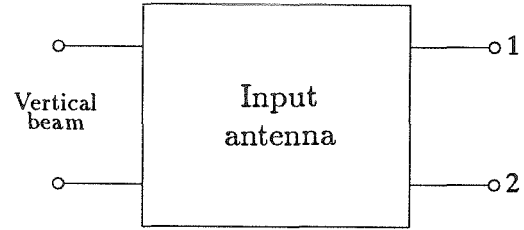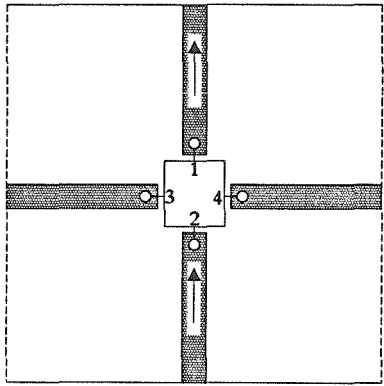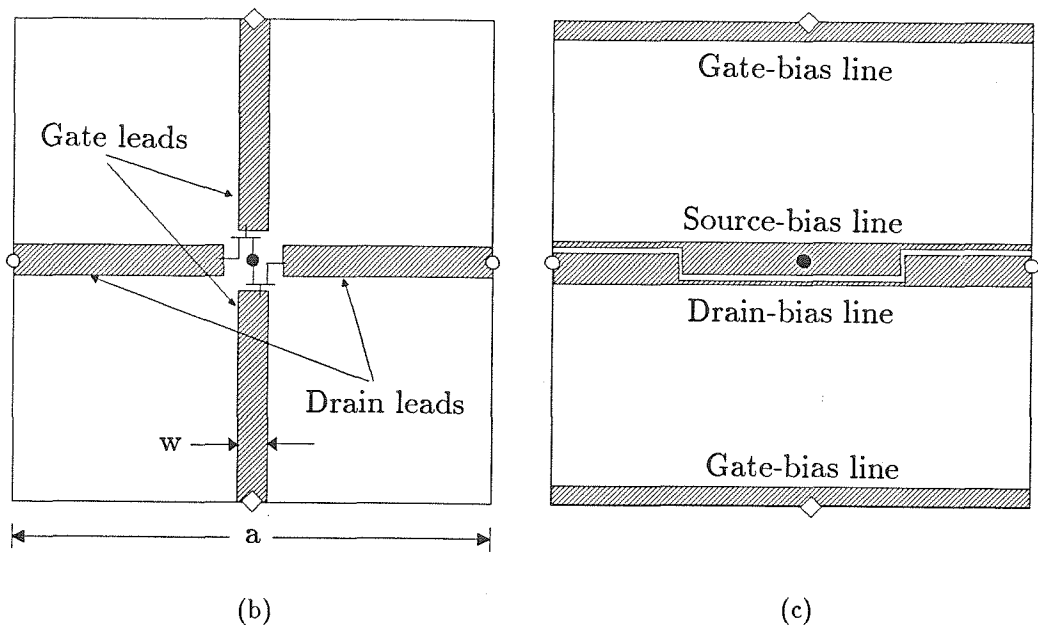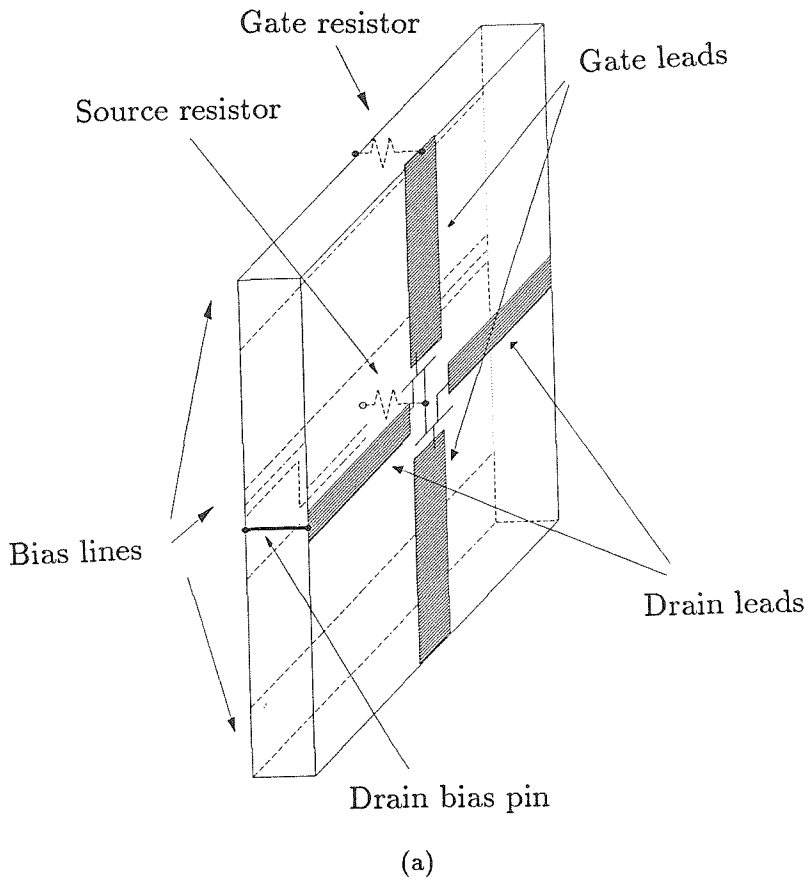
(a)
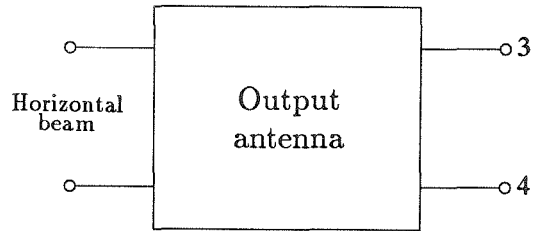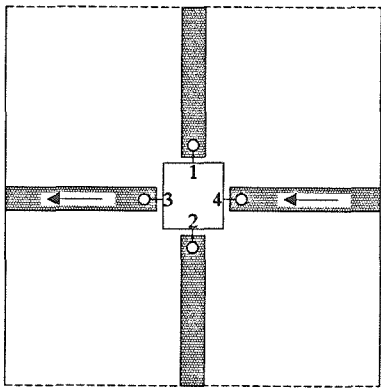
(b)
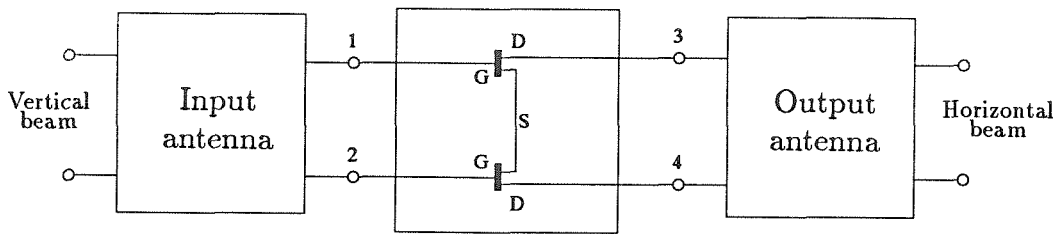
(c)

Figure 2.5 Example of the cross-polarized amplifier cell equivalent circuit. (a) Input coupling network. (b) Output coupling network. (c) Complete equivalent circuit. Electric walls are shown as solid lines, and magnetic walls as dashed lines on the boundaries on the unit cell.

MESFET's manufactured by *Fujitsu*. The substrate was a 2.54-mm thick *Duroid* board ($\epsilon_r = 10.5$) manufactured by Rogers Corporation. An identical second *Duroid* board with the copper removed was placed behind the amplifier to help tune the circuit. In addition, there were two polarizers for input and output circuit tuning. The input polarizer was made of thin copper strips on top of a 3.5 mm-thick teflon board, and it presented 1.6 nH inductance to the beam polarized in the horizontal output direction. The output polarizer was made from a 1.3 mm-thick *Duroid* board ($\epsilon_r = 10.5$) and it tuned the input beam with a shunt inductance of 0.5 nH. During gain measurements, the output polarizer was placed 45 mm away from the active grid array surface, and the input polarizer was placed 30 mm behind the extra *Duroid* substrate which provided additional tuning. The copper strips for both polarizers were facing toward the active grid array.

One of the most challenging areas of grid amplifier design is designing dc bias schemes for the transistors. For this first grid, the bias lines were placed on a separate plane in order not to disturb the coupling between the antennas and the rf beams. The bias strips, etched on the other side of the *Duroid* substrate that holds the transistors, were 2.8 mm-wide with 8 mm-spacing. A shunt inductance of roughly 0.5 nH is presented to the output matching circuit. Holes punched in the substrate allow connections to be made between the two surfaces of the substrate. The drain-bias connections were metal pins at the cell boundaries, and the gate-bias connections were 1-kΩ carbon resistors. The source-bias was connected with 120-Ω resistors to suppress common-mode oscillations. These resistors do not affect the differential gain, which determines the overall grid gain.

A simple equivalent circuit for the amplifier grid is shown in Figure 2.7. Free-space is represented as a transmission line with a characteristic impedance of 377 Ω. The *Duroid* substrate appears as a section of line with an impedance of

Gate resistor

Source resistor

Gate leads

Bias lines

Drain leads

Drain bias pin

(a)

Gate leads

Drain leads

w

a

(b)

Gate-bias line

Source-bias line

Drain-bias line

Gate-bias line

(c)

Figure 2.6 The unit cell of a grid amplifier. (a) Perspective view, (b) front view and (c) back view. The symbols indicate different connections between the front and the back of the grid amplifier. •: 120-Ω source-bias resistor, ◇: 1-kΩ gate-bias resistor, o: drain-bias pin.
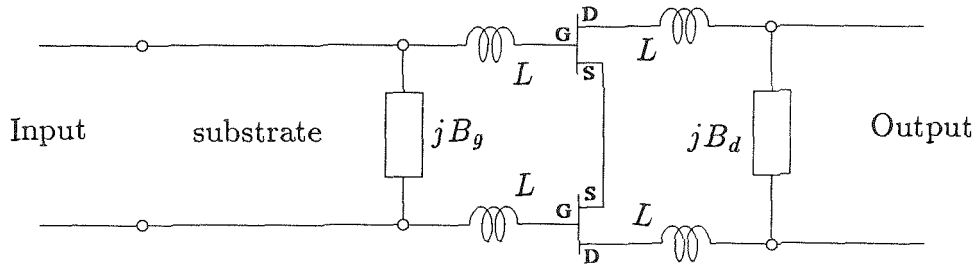
20

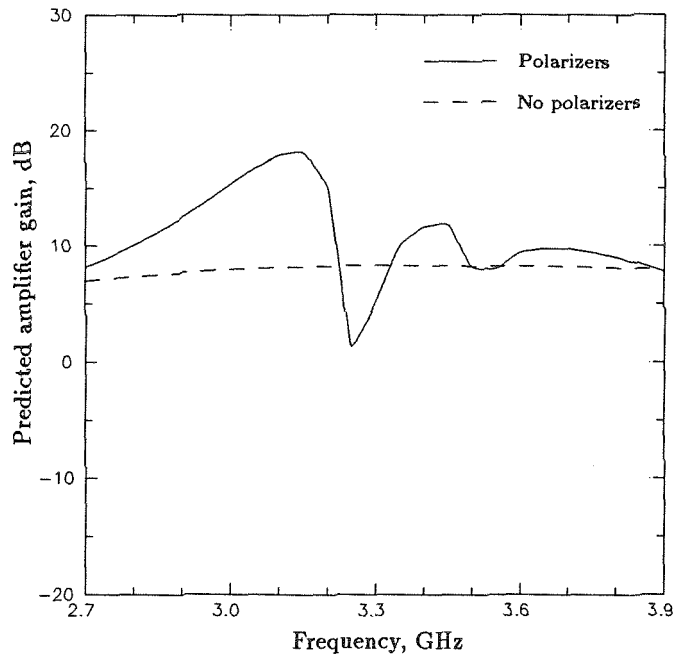**Figure 2.7** Transmission-line model for the unit cell.

Figure 2.8 A linear simulation using *Puff* predicts that the grid has a gain of 19 dB and 8 dB with and without the polarizers respectively.

$116\,\Omega$. The gate and drain leads are represented by an inductance that can be calculated from a quasi-static formula [5]

$$L = \left(\frac{\mu_0 a}{4\pi}\right) \ln\left[\left(\frac{\pi w}{2a}\right)\right] \qquad (2.1)$$

where a is the period, and w is the lead width. For our grid, $a = 16\,\mathrm{mm}$ and $w = 2\,\mathrm{mm}$, so that $L = 2.6\,\mathrm{nH}$. The susceptance B_g represents the output polarizer, and B_d accounts for the bias lines and the input polarizer. A linear circuit simulation using *Puff* [6] of this model using the manufacturer's scattering parameters for the transistors, predicted a gain of 18 dB at 3.15 GHz with the 3 dB bandwidth of 200 MHz. The single *Duroid* substrate containing the active array and the bias strips alone and neglecting polarizers, had a predicted gain of 8.4 dB at 3.3 GHz, with a 3-dB bandwidth of 2.4 GHz.

2.4 MEASUREMENTS

Figure 2.9 shows how the gain was measured. A signal generator transmits a vertically polarized beam from a small horn. The beam is incident on the grid, amplified, and transmitted with horizontal polarization. Another horn receives the amplified beam. We define the grid amplifier gain G by the equation

$$P_r = G P_t \left(\frac{G_t A}{4\pi r^2}\right)\left(\frac{G_r A}{4\pi r^2}\right) \qquad (2.2)$$

where P_r is the received power and P_t is the signal generator power. G_t and G_r are the gains of the transmitting and receiving horns, A is the geometrical area of the grid, and r is the distance between the grid and each horn. The terms in parentheses are the input and output space-loss factors. The grid gain G is the ratio of the power radiated by the grid to the incident power, reduced by the losses from amplitude and phase errors across the grid. This equation has quite a few parameters, but we can eliminate some of them by making a calibration

measurement with the grid removed (Figure 2.9b) and the receiving horn rotated 90° to match the polarization of the transmitting horn. The received power P_c is then given by

$$P_c = \frac{P_t G_t G_r \lambda^2}{(4\pi)^2 (2r)^2} \tag{2.3}$$

From these two equations, we can write an expression for the amplifier gain as


(a)

(b)
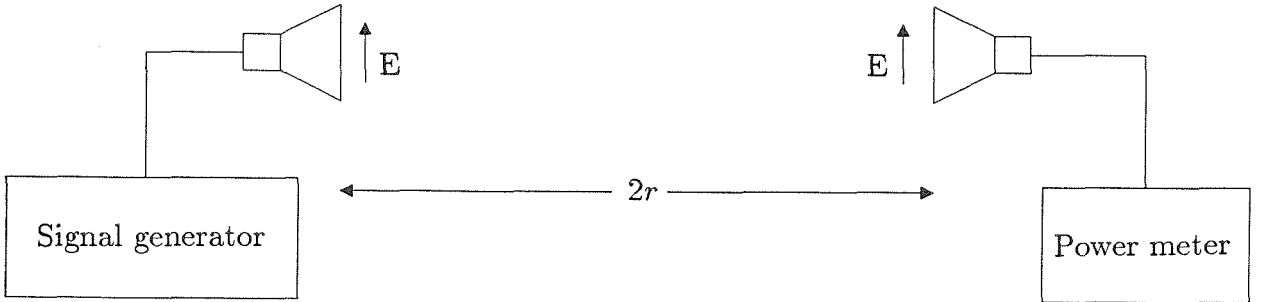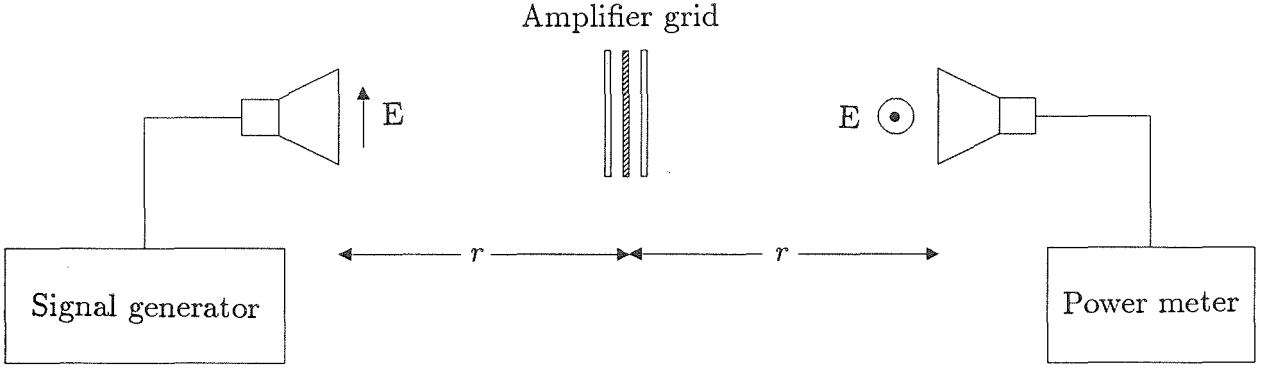
Figure 2.9 (a) Measuring the amplifier gain. The gain of each horn is about 10 dB in this frequency range. (b) Calibration measurement with the grid removed and the receiving horn rotated 90° to match the transmitter polarization.

$$G = \frac{P_r}{P_c} \left(\frac{\lambda r}{2A} \right)^2 \tag{2.4}$$

This simple formula allows us to calculate the gain from a relative power measurement and three well-known parameters. In our measurements, r was 50 cm and A was 64 cm^2.

Figure 2.10 is a plot of the measured amplifier gain. The largest value is 11 dB at 3.3 GHz, with a 3-dB bandwidth of 90 MHz. The bias line strips just behind the radiating structure are probably responsible for the narrow gain bandwidth. The tuning provided by polarizers is important, and no gain was seen without them. Compared to the predicted gain curve, the peak gain is down by 8 dB with or without the polarizers. Throughout the measurements, the gate bias-line voltage was −0.25 V relative to the source bias-line, and the drain bias-line voltage was 4 V. The drain current was 6.6 mA per MESFET. For comparison, the gain was also measured with the bias turned off, and found to be below −5 dB everywhere (Figure 2.11). The received signal was monitored with a spectrum analyzer to insure that there were no spurious oscillations. As an additional check, the measurements were repeated at different power levels to ensure that the output power varied linearly with input power.

The initial configuration of this device (which had no bias resistors) suffered from an oscillation. The oscillation was suppressed by replacing the metal pins with the small carbon bias resistors for the front-back side connections. This indicates that the oscillation may be due to the common-mode current flowing on the source bias line. A possible feedback path is described in Figure 2.12. The total distance the common-mode current travels before it comes back to the same position is 4.8 cm which corresponds to a multiple of the wavelength at 8 GHz assuming the effective dielectric constant is the average of the air and the dielectric substrate. The unwanted oscillation was observed at 8 GHz, supporting this assertion.
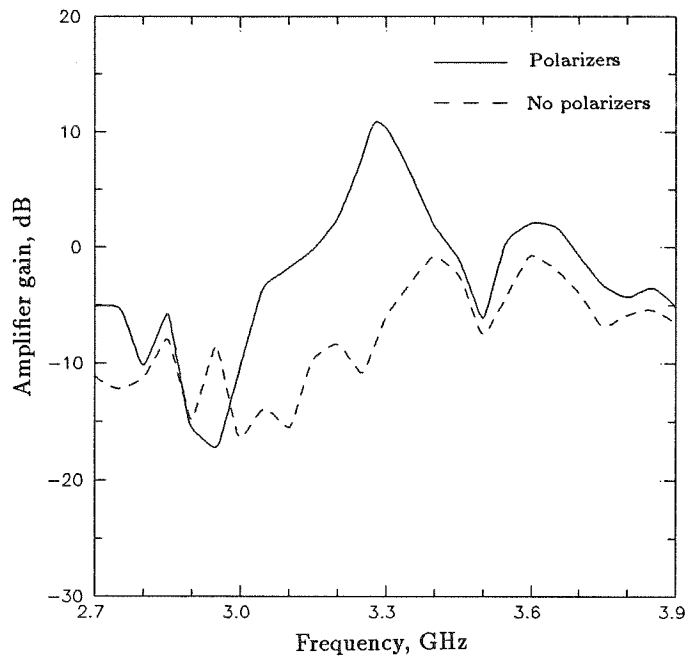
Figure 2.10 Measured grid amplifier gain with (solid line) and without (dashed line) the polarizer
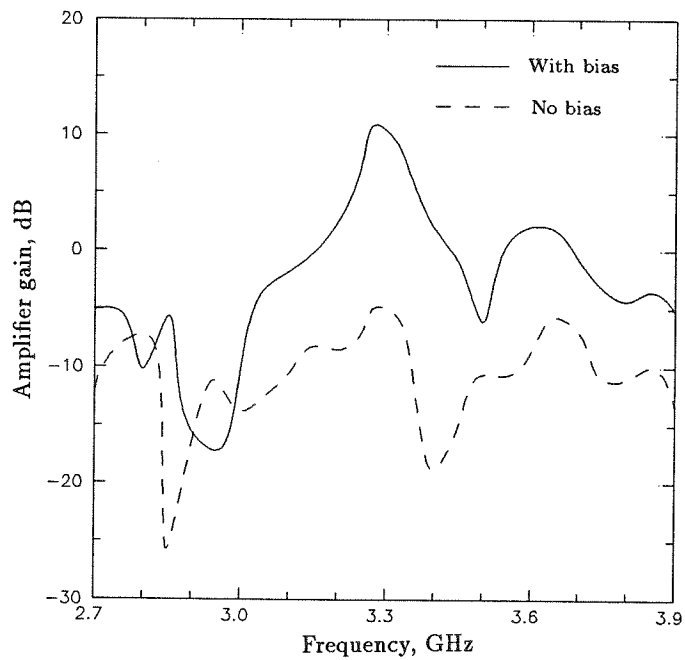
Figure 2.11 Measured grid amplifier gain with (solid line) and without (dashed line) bias. The total incident power was about $300\,\mu$W.

Gate bias line

Gate antenna lead

rf current

Source bias line
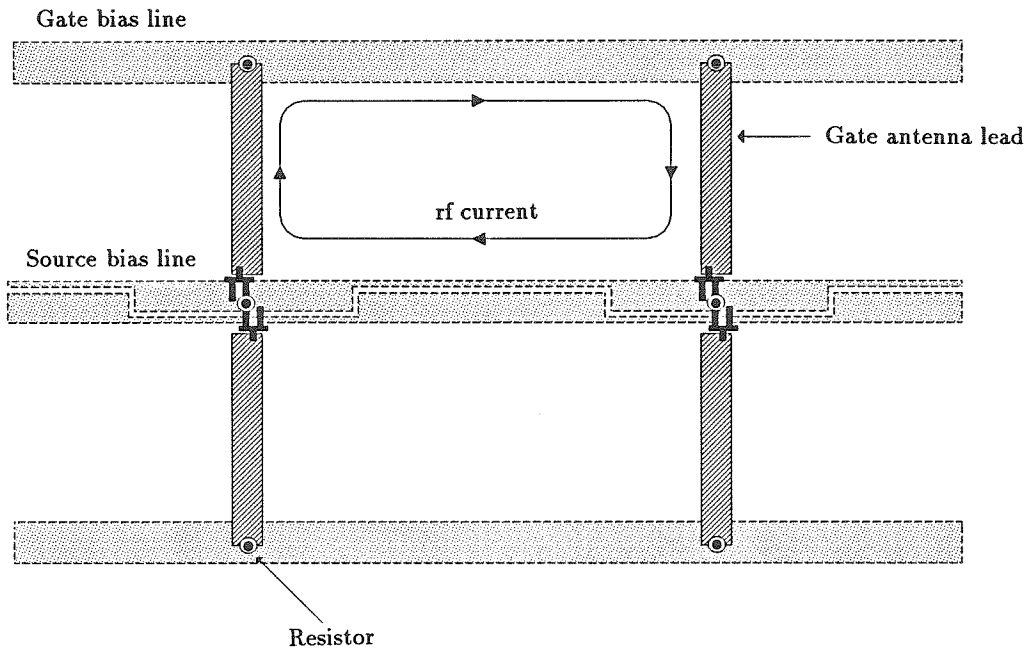
Resistor

Figure 2.12 A possible feedback path for a common-mode oscillation in the amplifier. Resistors at the drain and source ends help stop the rf current flowing along this path, and suppress the unwanted oscillation.

REFERENCES

[1] M.Kim *et al.*, "A Grid Amplifier," *IEEE Microwave Guided Wave Letters, MGWL-1*, pp. 322–324, May 1991.

[2] R.M. Weikle *et al.*, "Planar MESFET Grid Oscillators using Gate Feedback," to be published in the *IEEE Trans. Microwave Theory Tech.*

[3] G. Gonzales, "Microwave Transistor Amplifiers," pp. 194–199, Prentice-Hall, 1984.

[4] R.M. Weikle, "Quasi-Optical Planar Grids for Microwave and Millimeter-wave Power Combining," Ph.D Thesis, California Institute of Technology, 1992.

[5] G.G. MacFarlane, "Quasi-Stationary Field Theory and its Application to Diaphragms and Junctions," *Proc. of the IEE, 93, part 3a*, pp. 1523–1527, 1946.

[6] S.W. Wedge, R. Compton, D. Rutledge, "Puff – Computer Aided Design for Microwave Integrated Circuits," California Institute of Technology, 1991.

Chapter 3

The X-Band HBT Grid Amplifier

A 100-element X-band grid amplifier with improved performance is presented. The active devices in the grid are custom designed heterojunction bipolar transistor (HBT) differential-pair discrete chips that include a resistive network to provide self-bias to the base. The passive metallic grid structure was empirically designed to provide an effective coupling between the HBT's and free space. Two independent measurements, one with beam-focusing lenses, the other without, were used to characterize the grid. In each case, the peak gain of the grid was 10 dB at 10 GHz with a 3 dB bandwidth of 1 GHz. The input and output return losses were better than 15 dB at 10 GHz. It is also shown that the output matching primarily determines the power performance of the amplifier grid. The dc to rf efficiency for the grid at 10 GHz was 10.5% with an rf output saturation power of 450 mW. Noise measurements indicate the grid has a 6.5 dB noise figure at 10 GHz.

3.1 DESIGN GOALS

The first 25-element MESFET grid amplifier [1] demonstrated a stable gain of 11 dB at 3.3 GHz. This grid had features that were different from previous oscillators and mixers. The grid utilized cross-polarization to isolate the input from the output. This helped prevent the amplifier from oscillating. It also allowed polarizers to tune the input and the output circuits of the amplifier independently. The cross-polarization approach also required a new active device configuration. Differential-pair transistors provided two gate terminals to collect an input beam
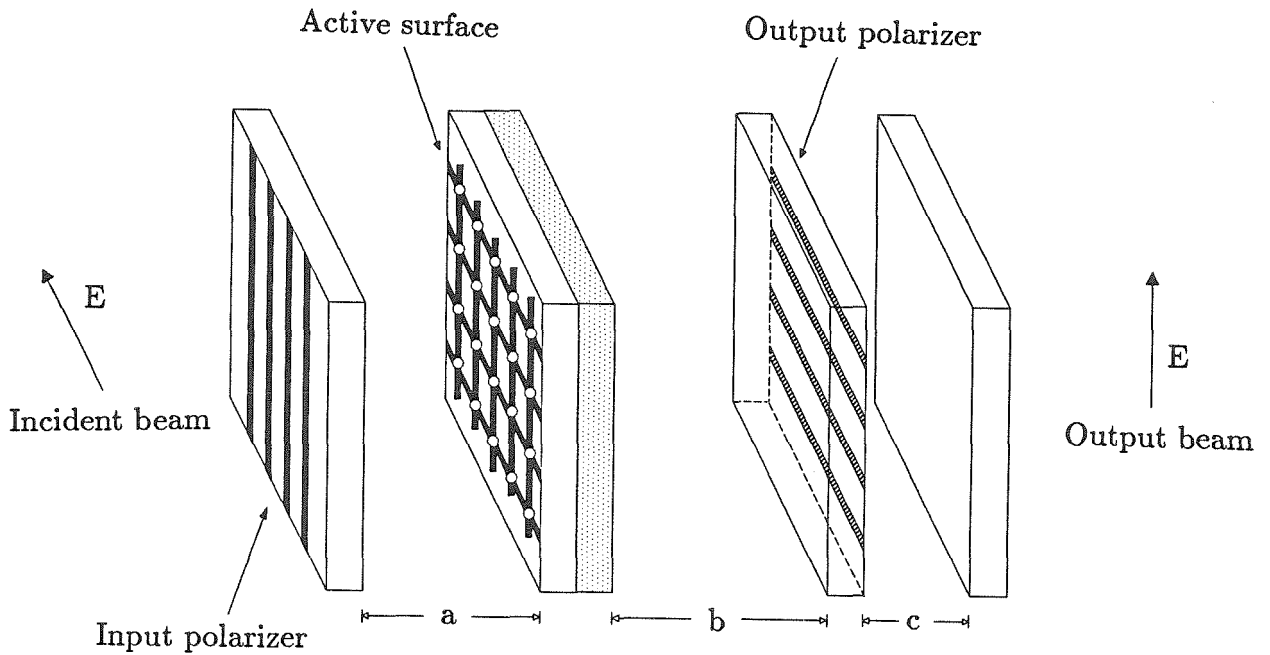
Figure 3.1 A perspective view of a grid amplifier. The input beam is horizontally polarized while the output beam is vertically polarized.

	dielectric constant(ϵ_r)	Physical length (mm)	Electrical length at 10 GHz (°)
a	1	14	168
b	1	15	180
c	1	10	120
▨	10.5	3.81	148
☐	2.2	3.18	57

Table 3.1 Optimum polarizer spacing for maximum gain at 10 GHz. These dimensions were determined empirically. By readjusting the polarizer positions the peak gain could be shifted to other frequencies.

in one polarization, and two drain terminals to radiate the amplified beam in cross-polarization.

The first amplifier grid also had metal strips on the back side of the substrate that held the transistors. These strips were necessary to provide dc bias to the transistors, but they also caused the grid to have a 3 dB bandwidth of only 2.7%. The connection between the strips and the transistors were made with metal pins and carbon resistors through via holes. Such a grid structure is not suitable for future monolithic integration. Furthermore, the transistors used were packaged devices that needed a large unit cell period, forcing the grid to work only at low frequencies. Therefore, our goal became to build a new grid for X-band operation with improved gain and bandwidth. The grid structure should also be suitable for a monolithic circuit design without major modifications.

A perspective sketch of a grid amplifier (Figure 3.1) shows how the amplifier grid operates. A horizontally polarized input beam passes through the input polarizer and reaches the amplifier grid. The metal strips on the grid couple the beam to the active devices, and radiate an amplified beam in the vertical direction through the output polarizer. The position of the polarizers determines the input and output matching frequency.

3.2 A FAILED ATTEMPT

Before the X-band HBT grid amplifier, an attempt was made to build an amplifier grid using high electron mobility transistors (HEMT's). Even though this 10×10 grid failed to work, the experience helped us build the next HBT amplifier grid. The sketch of the HEMT grid is shown in Figure 3.2. We incorporated the radiating structures and the bias lines on the same plane. The output radiating antenna was unchanged from the earlier C-band grid, but the input receiving antenna utilized a bow-tie structure. The bow-tie structure was previously used in the mixer grid [2] to provide broad-band matching. The arrows on the input
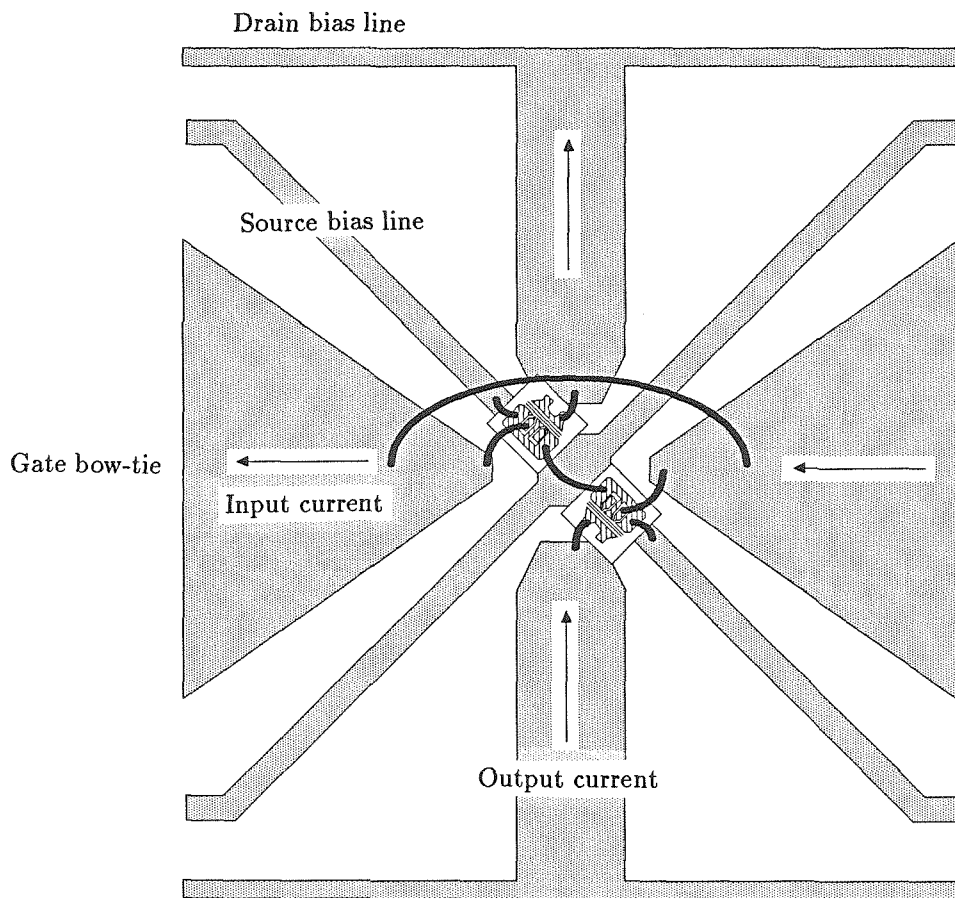
Figure 3.2 Unit cell sketch of the HEMT grid. Bow-tie structure was used as an input antenna to broaden the 3-dB gain bandwidth. The thin metal strips provide dc bias to the transistors.

and the output antenna structures indicate the flow of rf currents under the desired differential-mode operation. Thin metal strips were used for the source bias lines to present a large inductance to any common-mode rf current out of the transistors. The HEMT chip transistors, FHX35X, manufactured by *Fujitsu*, had their sources tied together with a single bond wire. More bond wires were used to connect the source terminals and the source dc bias lines. The drain bias was provided through the output radiating antenna. All the gate bow-ties were connected by long bond wires which formed an inductive bridge over the top of the devices. This allowed control of the gate dc bias voltages from the grid edges.

Figure 3.3 shows the completed HEMT grid. When the grid was biased with a drain voltage of 0.4 V, the cross-polarized output power was raised by 10 dB. This output power, however, was still 7 dB less than the input power. When a larger dc bias was applied, the amplifier began to oscillate at 7 GHz. It was suspected that the oscillation was due to the large common-mode gain. The distance between the source bias lines and other radiating structures were small, thus, the inductance of the bias lines was probably too low to suppress the common-mode gain. The bow-tie structure, which occupied a large area, also might have been responsible for feeding the output signal back to the input because of its relative high cross-polarization ratio of its radiation pattern. Finally, the photograph of the differential-pair chips taken under the microscope (Figure 3.4) shows how difficult it was to provide a good connection between the two source terminals. The transistors had extremely high gain, and were likely to oscillate without a good source to ground connection. The failure of this grid led us to design and fabricate new differential-pair transistor chips for the next X-band HBT grid amplifier.

3.3 DEVICE AND UNIT CELL

The layer structure of the AlGaAs/GaAs heterojunction bipolar transistor used in the grid amplifier is shown in Table 3.2. The HBT's were fabricated by Rockwell
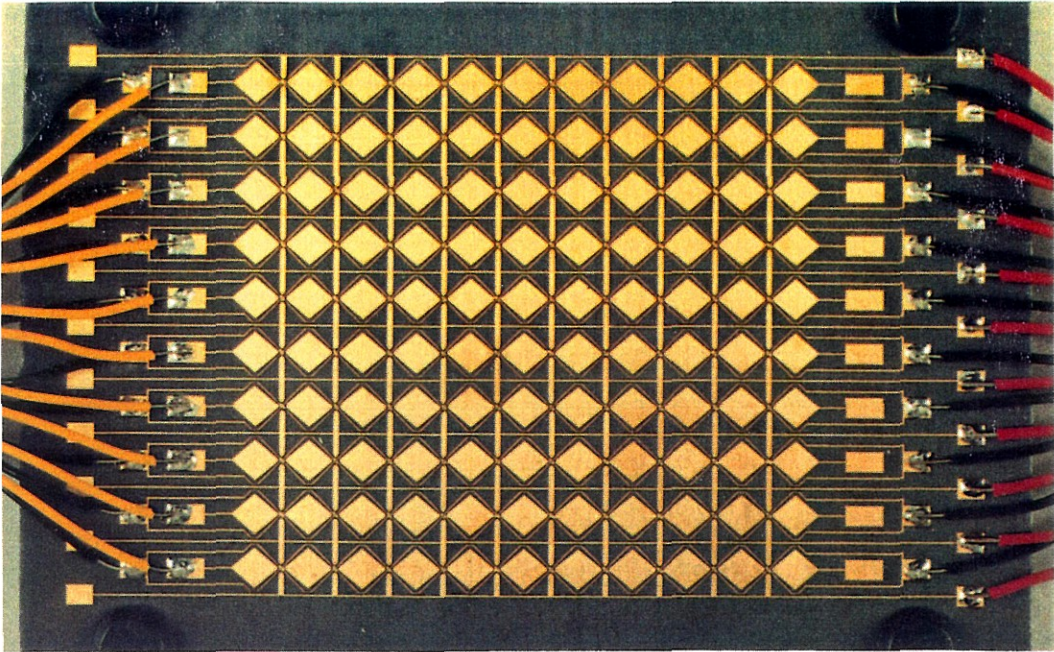
Figure 3.3 Photograph of the 200-element HEMT grid amplifier. The grid failed to produce a gain greater than 0 dB, and oscillated at 7 GHz.
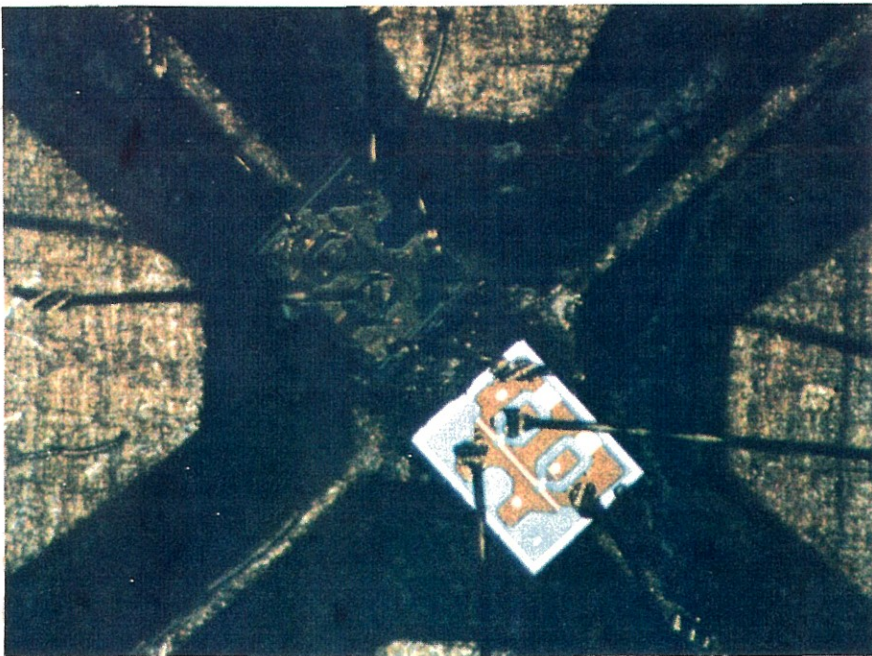
Figure 3.4 The photograph on the differential-pair chips taken under a microscope. The chips were *Fujitsu* FHX35X HEMT transistors. It was difficult to provide a good source-to-source contact.

International with a self-aligned dual lift-off process [3] after the epitaxial growth. Carbon and silicon are used as p-type and n-type dopants. With an emitter area of $40\,\mu m^2$, the HBT base resistance and the base-collector capacitance are estimated to be $10\,\Omega$ and $35\,fF$ respectively.

The performance of a single HBT, as shown in Figure 3.5 (a), was measured in order to predict the performance of the amplifier grid. The measured HBT was biased at $I_c = 20\,mA$ and $V_{ce} = 2.5\,V$, and exhibited a dc common-emitter current gain β_{dc} of 10. The measured common-emitter S_{21} was $11\,dB$ implying a unilateral gain close to $18\,dB$ at $10\,GHz$. The cutoff frequency, f_T, and the maximum frequency of oscillation, f_{max}, were estimated to be $65\,GHz$ and $90\,GHz$, respectively.

The differential-pair HBT chips used in the amplifier grid are slightly different from the measured single-element chips. The grid device, shown in Figure 3.6 contains two HBT's along with a simple bias network to provide self-bias to the base. The values of the resistors, $1.7\,k\Omega$ and $500\,\Omega$, were picked under the assumption that $\beta_{dc} = 10$, $V_{ce} = 3\,V$, and $I_c = 10\,mA$ give an optimal bias condition. This bias network eliminates the need for an extra bias line on the grid which would complicate the metal pattern. In addition, these resistors provide two additional advantages: The $1.7\,k\Omega$ collector to base resistor provides a negative shunt feedback that reduces the chances of unwanted spurious oscillations, and the $500\,\Omega$ emitter resistor suppresses the common-mode gain of the HBT pair forcing it to operate under the desired differential-mode. Unfortunately, the rf performance of the differential-pair HBT chip can only be estimated since its configuration contains different parasitic elements from the single chip HBT's used for the S-parameter measurements.

The passive metal structure in the grid array can be divided into two parts: one couples the input and output rf beams to the active devices, the other provides dc bias to the HBT chips. The design goal was to integrate both structures
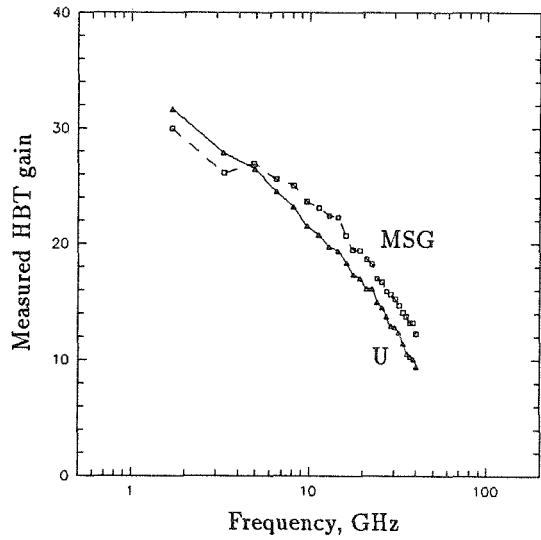
Layer	Thickness (μm)	Material	Doping(cm^{-3})	Content, x
Cap	0.15-0.25	n$^+$	4- 5x10^{18}	0
Emitter	0.07-0.12	n	3- 7x10^{17}	0.25
Base	0.05-0.10	p$^+$	3- 6x10^{19}	0
Collector	0.50-0.90	n	3- 8x10^{16}	0
Subcollector	0.60-0.90	n$^+$	4- 5x10^{18}	0

Table 3.2 Structural properties of Al$_x$Ga$_{1-x}$As/GaAs HBT grown by MOCVD.
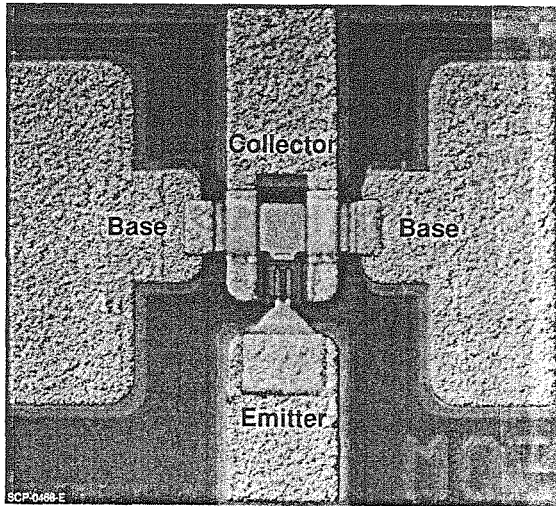
(a)   (b)

Figure 3.5 (a) The layout of an HBT used in device performance measurements. The device has two emitter fingers of $10\,\mu$m x $2\,\mu$m. The emitter and collector extend out to the top and bottom while the base is connected to the two horizontal pads. (b) Maximum stable gain (MSG) and unilateral gain (U) versus frequency for a single HBT.
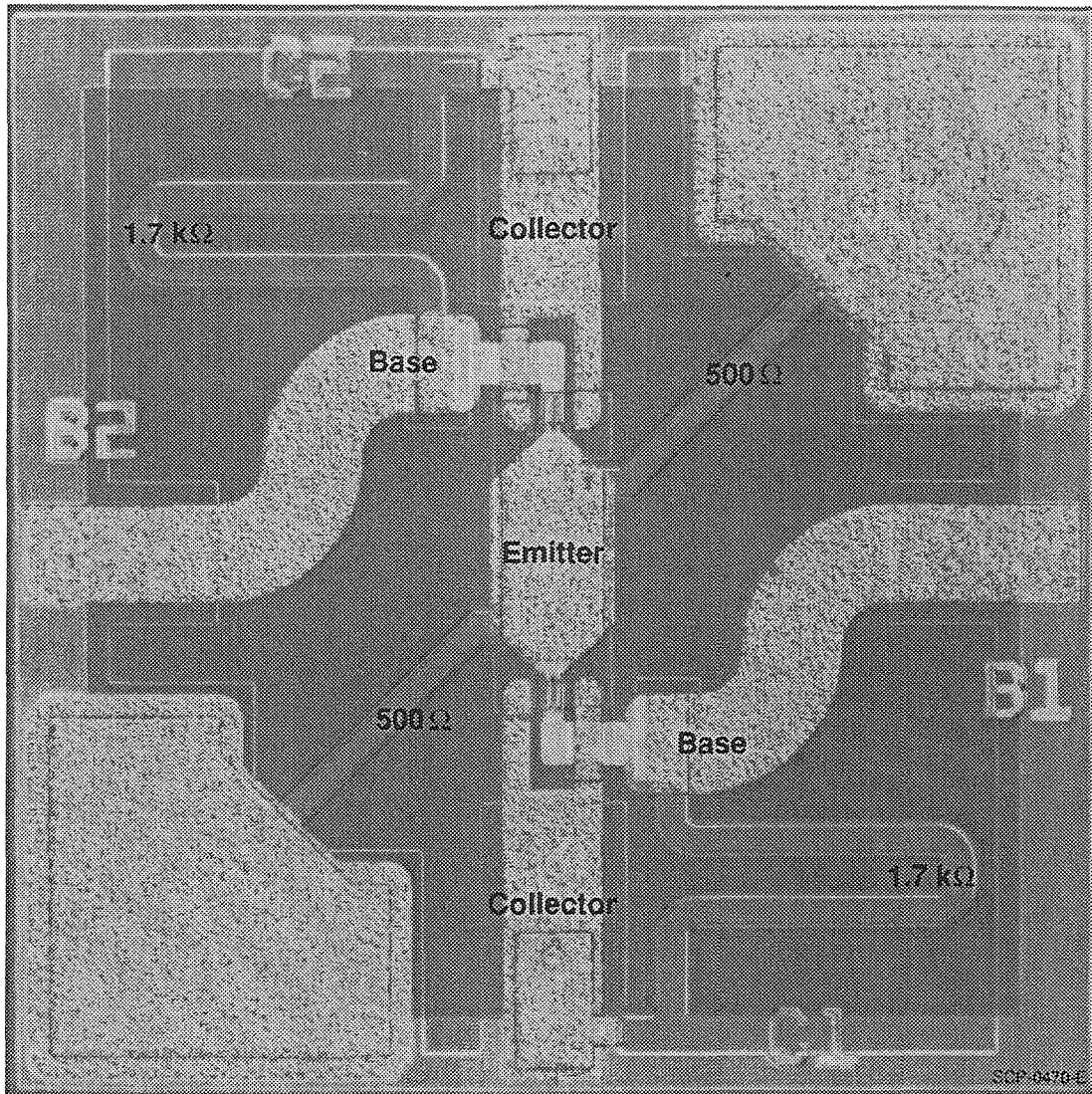
Figure 3.6 The differential-pair HBT chip layout. $1.7\,k\Omega$ and $500\,\Omega$ resistors provide self-bias to the base. The chip requires dc bias connections only to the collector and the emitter.
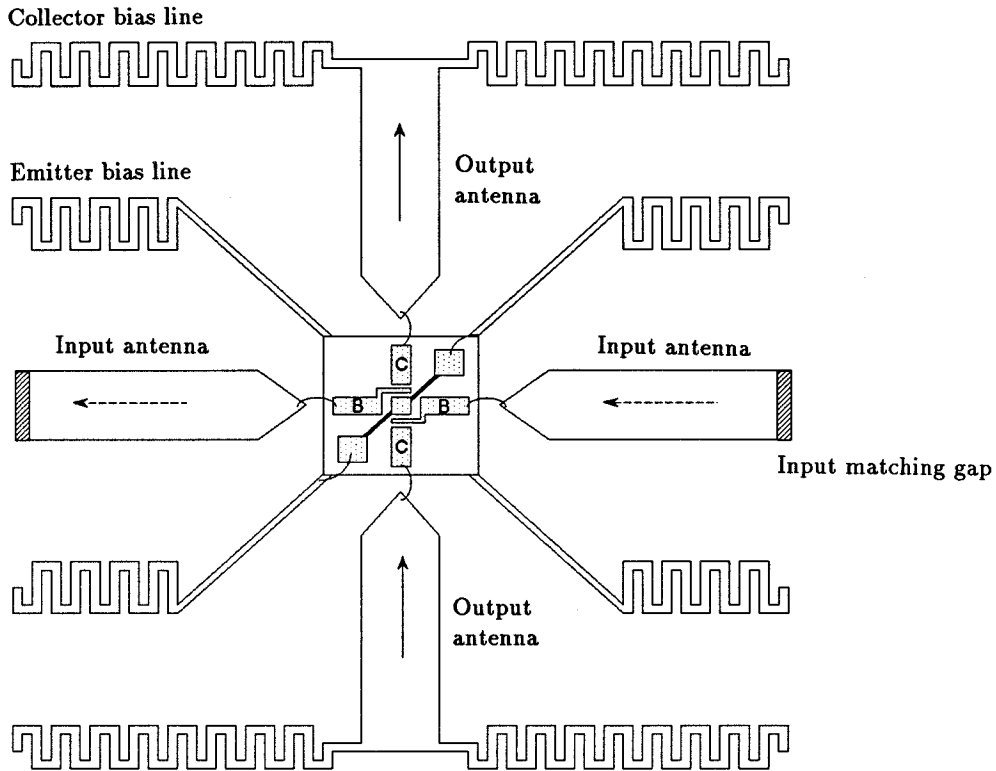
Figure 3.7 Sketch of a unit cell. The unit cell size is 8 mm. The radiating leads are 0.8 mm wide while the bias lines are 0.1 mm wide. The extremes of the meandering bias lines span 0.6 mm from top to bottom with a 0.1 mm gap size. The gap in the input antenna lead is 0.1 mm wide.

on the same plane. Various metal patterns were tested on smaller 4 × 4 grid arrays [4,5]. The best results were obtained from the grid that had the same unit cell dimensions as shown in Figure 3.7. This design was then adopted for a larger 10 × 10 grid array which would allow more accurate quasi-optical measurements. In this unit cell design, 100 μm wide meandering lines were used to provide dc bias to the HBT's. Ideally, the bias lines should not disturb fields incident upon and radiated from the grid. In other words, the bias lines should present a large reactance and become 'invisible' to the input and output beams. To examine the behavior of the meandering lines, two different structures, each containing a thin metal strip in a 2 mm TEM waveguide were examined on Hewlett-Packard's High Frequency Structure Simulator [6]. The results shown in Figure 3.9 indicate that the meandering lines used in the grid have roughly twice more inductance of a straight line for a beam that is polarized in the direction parallel to the metal lines.

Inductive strips are attractive as input and output antennas because their radiation patterns have good cross-polarization ratios. Thus, these strips provide good isolation between the input and the output, preventing unwanted oscillations. One drawback of the inductive strip is that it creates a severe input mismatch as the frequency increases. The estimated inductive reactance of a 0.8 mm-wide strip in a 8 mm unit cell is larger than 200 Ω near 10 GHz. Fortunately, the mismatch problem can be eliminated by opening a 100 μm-wide gap in the input antenna strip to add a series capacitance to cancel the inductance of the radiating lead.

3.4 GAIN AND MISMATCH

A lens-focused microwave Gaussian beam was used to measure the gain of the amplifier grid. The measurement setup included an HP 8510B network analyzer, two X-band standard gain horns, and two spherical bi-convex teflon lenses. Each
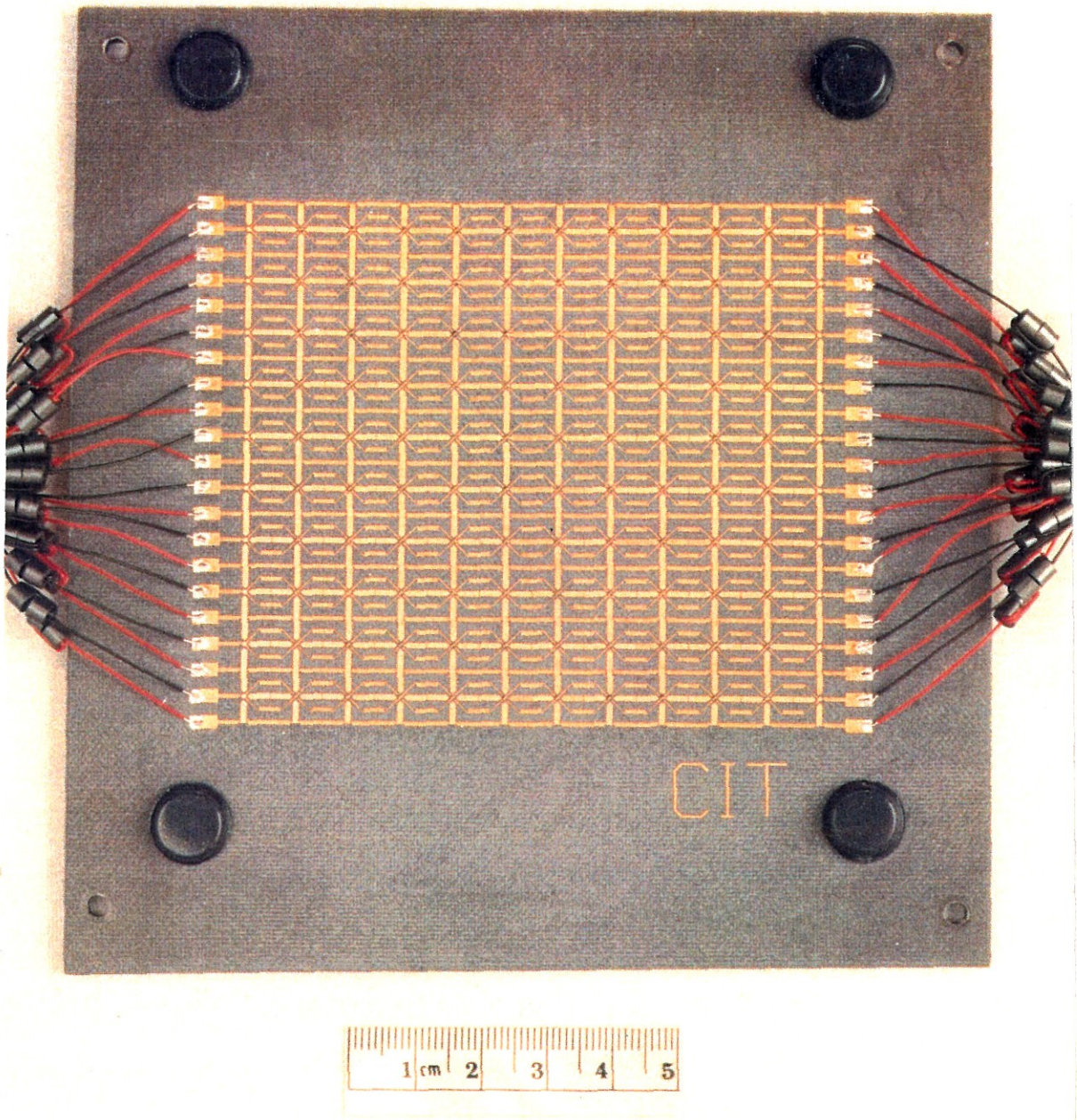
Figure 3.8 Photograph of the 100-element amplifier grid.

of the two identical bi-convex lenses were assembled from two plano-convex lenses placed back-to back. One plano-convex lens produces a plane-wave front from the spherical wave of the transmitting horn, the other lens refocuses the plane wave on the device under test to the opposite side. The lens that focused the beam on the grid had a diameter of 30 cm and a focal length of 46 cm, and provided a beam waist diameter of about 10 cm at 10 GHz. Previously, the same lenses were used in a reflectometer system for dielectric constant measurements in X-band, and produced very accurate results [7]. In order to measure the amplifier gain, the setup was first calibrated with an absorber screen that had an open aperture size equal to the amplifier grid, 64 cm². This absorber screen blocks about half of the power transmitted. After the calibration, the receiving horn was rotated 90° to collect the output beam from the inserted amplifier grid. The absorber was not required around the amplifier grid because the transmitting horn and the receiving horn were cross-polarized.

During the gain measurement, a dc bias of 5 V and 0.86 A was applied to the entire grid. Assuming that all the devices in the grid were identical, the collector-emitter voltage of each individual HBT was 2.85 V, and the emitter current was 4.3 mA. This dc bias current was only half of the predicted value for the given voltage bias, indicating the dc common-emitter current gain β_{dc} was less than what was previously measured for a single HBT chip. This implies that the gain of the differential-pair chips may be smaller than that of the single HBT chips. The amplifier grid, along with input and output polarizers, were arranged as shown in Figure 3.1. The positions of the polarizers were carefully adjusted to produce the largest amplifier gain. The optimum polarizer spacings are shown in Table 3.1. The results show that the peak amplifier gain was 10 dB at 10 GHz with a 3 dB bandwidth of 1 GHz (Figure 3.11). When the bias was removed, the gain dropped down below −10 dB everywhere. The shape of the gain curve was very sensitive to the positions of the input and the output polarizers. The peak
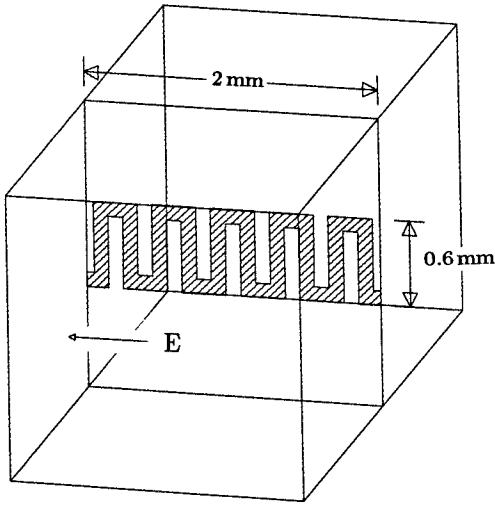
(a)
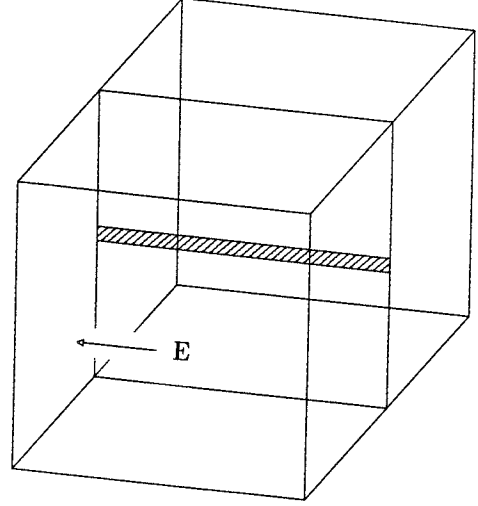
(b)
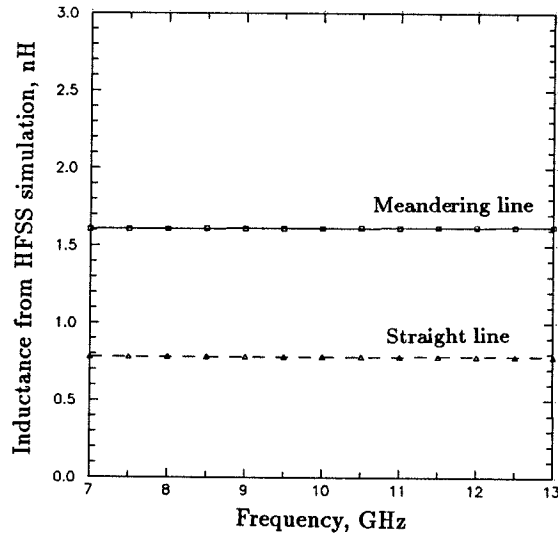
(c)

Figure 3.9 HFSS simulations on two different thin bias lines. (a) A meandering line, and (b) a straight line in a 2 mm unit cell waveguide were tested. The waveguide has boundary conditions to support the TEM mode of propagation. The waveguide beyond the metal strips was filled with a dielectric with $\epsilon_r = 2.2$ to simulate the substrate. (c) The inductance of the meandering lines was found to be 1.62 nH whereas the straight lines were only 0.78 nH between 7 and 13 GHz. Simulations for other unit cell sizes showed a similar ratio between the two types of lines.

(a)

(b)
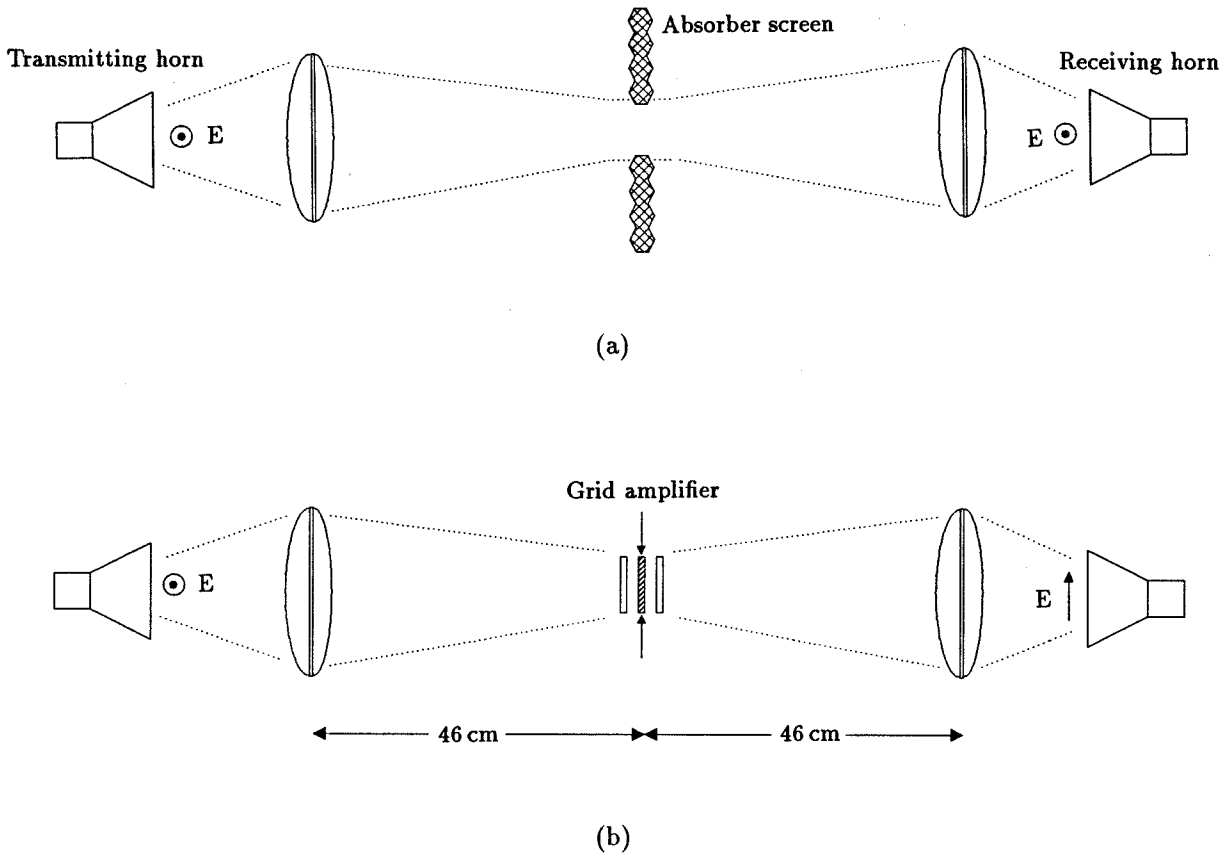
Figure 3.10 The lens-focused amplifier grid gain measurement system. The focusing lens has a circular aperture with a diameter of 30 cm and a focal length of 46 cm, producing a beam waist diameter of 10 cm at 10 GHz. (a) Calibration. (b) Amplifier gain measurements.

gain could be easily shifted from 8 GHz to 11 GHz by adjusting the polarizers.

The same measurement system can also be used as a reflectometer to allow the input and output mismatch to be measured. With the receiving horn removed, the reflectometer was first calibrated with a matched load, a short, and a delayed-short at a distance of 1 cm away from the reference plane. The short was a square metal plate about four times larger in area than the amplifier grid. During the test, absorber was placed behind the grid to prevent any reflections. The results in Figure 3.12 indicate that the grid is very well-matched at both the input and the output. The input match was more broad-band than the output match. However, both the input and the output were well-matched at 10 GHz. Since the
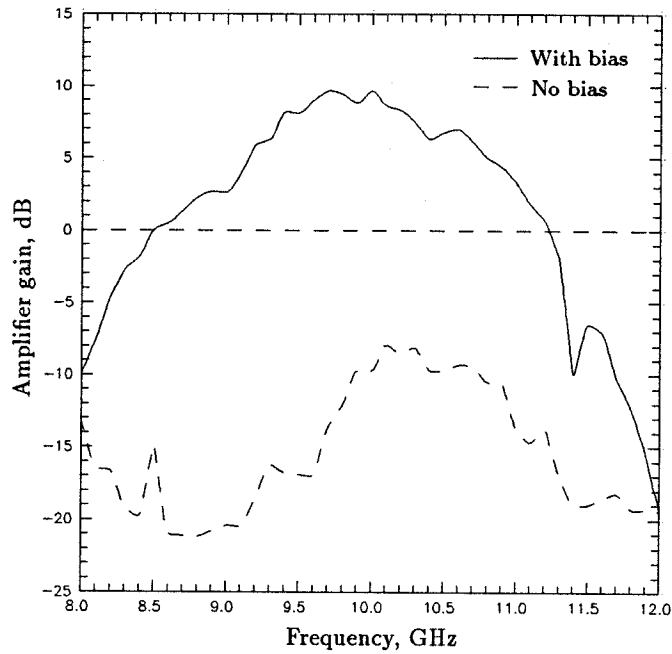
Figure 3.11 The amplifier grid gain versus frequency. When biased, the grid exhibits 10 dB of gain at 10 GHz. The 3 dB gain bandwidth was 1 GHz.

(a)   (b)
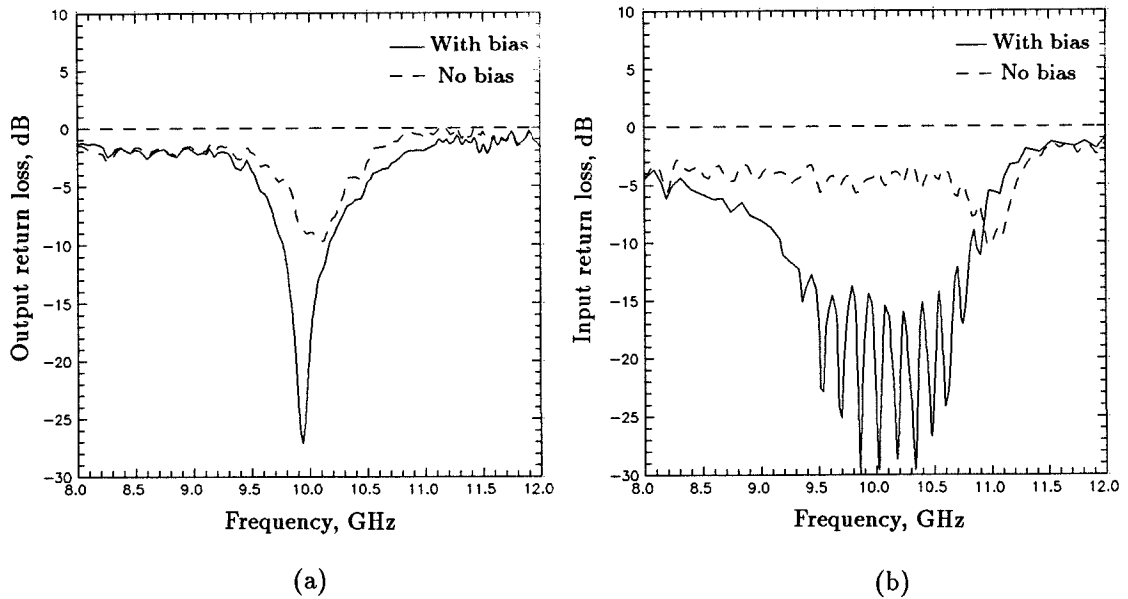
Figure 3.12 (a) Input return loss, and (b) output return loss vs. frequency. The small magnitude of the reflected signal into the network analyzer may be the cause of the ripples in the trace below -20 dB.
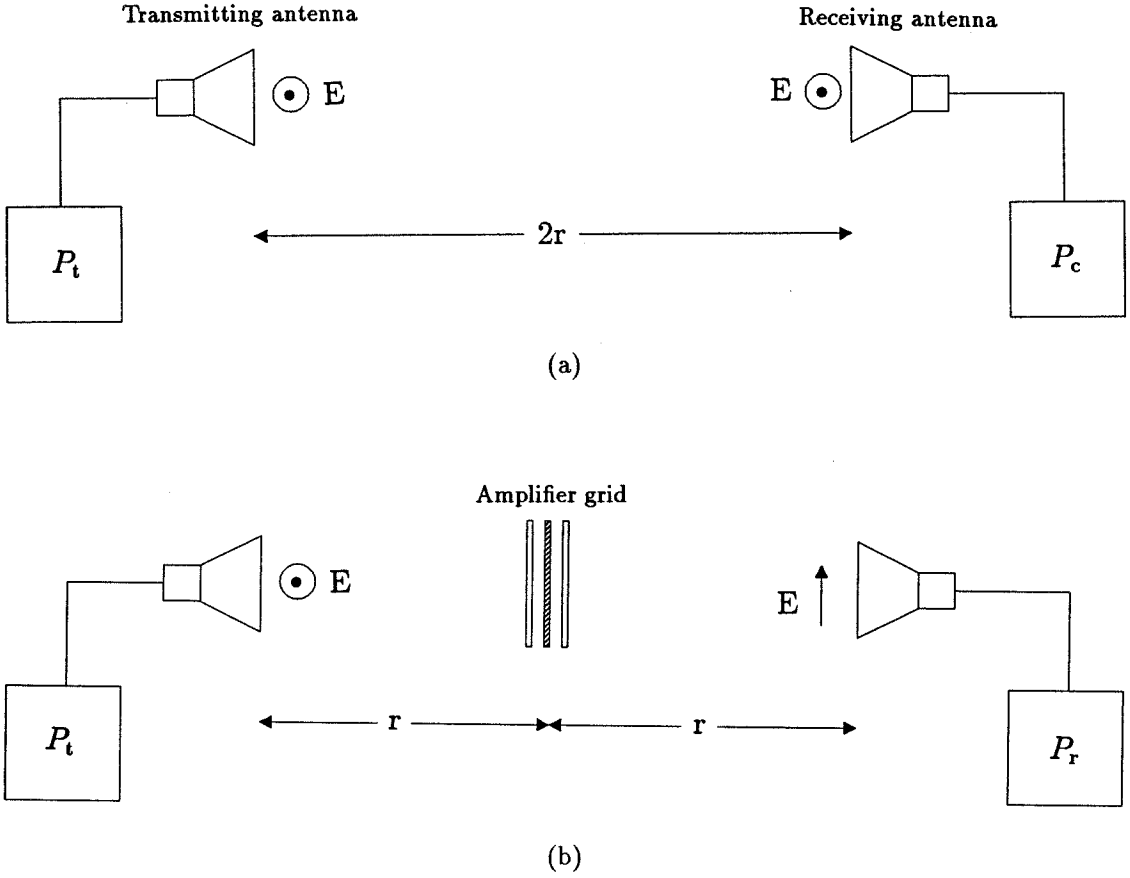
Figure 3.13 Amplifier grid gain measurements without lenses. (a) Calibration. (b) Measurements.

return loss dropped by 15 dB as the dc bias was applied, it was concluded that the match should be better than 15 dB even if there is a calibration error. It also indicated that the incident beam from one side of the grid was well-coupled to the devices, and did not pass through to the opposite side of the grid.

One can also measure the amplifier gain without using lenses. The measurements shown in Figure 3.13 give rise to a simple formula where the amplifier gain, G, can be expressed in terms of two measured powers, P_r and P_c, and three well-known parameters, as shown in [1],

$$G = \frac{P_r}{P_c} \left(\frac{\lambda r}{2A} \right)^2 \tag{3.1}$$

Here, r is the distance between the horn and the grid, and A is the area of the grid. By choosing A to be the geometric area, the grid gain G becomes the ratio of the power radiated by the grid to the incident power, reduced by the losses from the amplitude and phase errors across the grid. In our measurements, $r = 90\,\mathrm{cm}$ and $A = 64\,\mathrm{cm}^2$. Because the amplifier grid uses two different polarizations for the input and output, the two signals can be easily distinguished at the receiving horn. The grid and polarizers were aligned in the same fashion as in the lens measurement. The results were almost identical to the previous measurements using lenses, showing a peak gain of 10 dB at 10 GHz with a 3 dB gain bandwidth of 1 GHz. The similarity of the results obtained from the two different measurement methods gives us added confidence in our measurements.

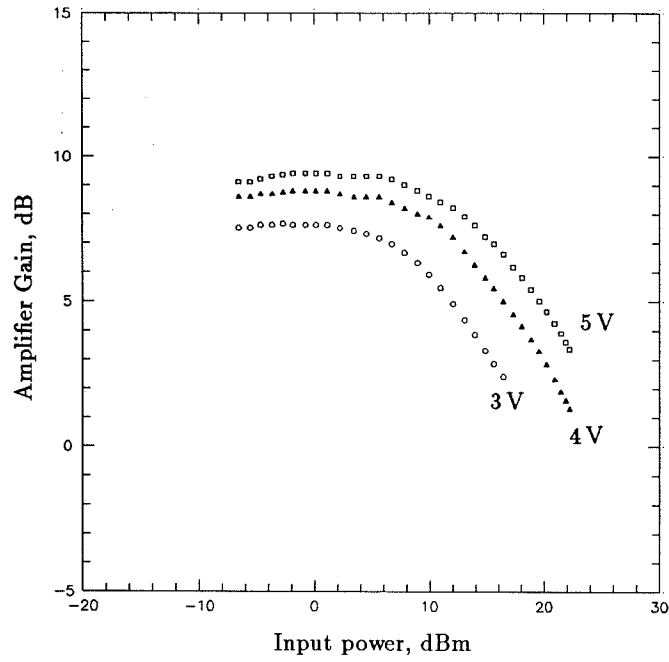## 3.5 POWER SATURATION MEASUREMENTS

The diffraction limited measurement system without focusing-lenses produces an input beam with a uniform phase and amplitude incident on the amplifier grid. This allows reasonably accurate power saturation measurements. The gain of the two identical horns , G_{horn}, used in the measurements, was first calculated from the known values of transmitted and received power, P_t and P_c [8].

$$G_{\mathrm{horn}} = \sqrt{\frac{P_c}{P_t}} \left(\frac{4\pi 2r}{\lambda} \right) \tag{3.2}$$

Then the beam incident on the grid from the transmitting horn, P_{in}, becomes

$$P_{\mathrm{in}} = P_t \left(\frac{G_{\mathrm{horn}}A}{4\pi r^2} \right) \tag{3.3}$$

where r is the distance between the horn and the grid, and A is the geometric area of the grid. With the same polarizer arrangement as before, the power saturation measurements were performed at three different frequencies, 9.6, 10.0, and 10.4 GHz. Figure 3.14 shows the grid power performance at 10 GHz. The 1 dB

(a)
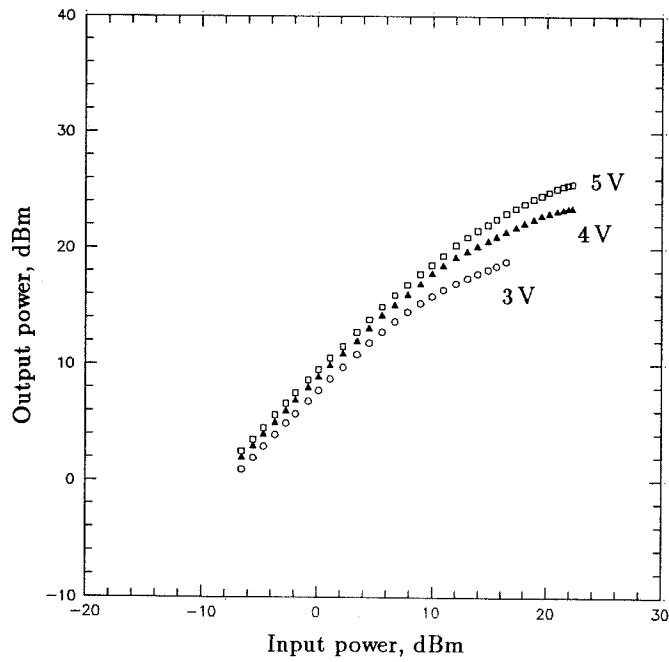
(b)

Figure 3.14 Power saturation measurements of the amplifier grid at 10 GHz with three different levels of dc bias. (a) Amplifier gain vs. input power. (b) Output power vs. input power.

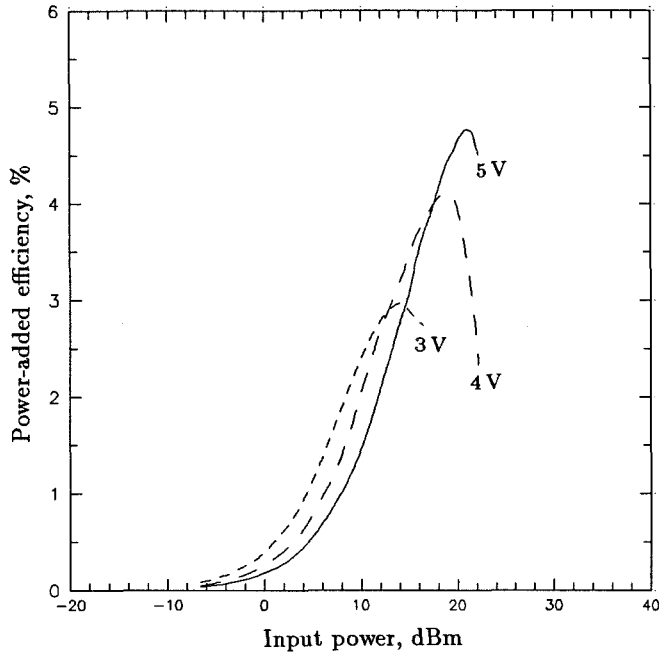**Figure 3.15** Power-added efficiency at 10 GHz for three different levels of dc bias. The maximum efficiency was 4.8%.

gain compression output power, $P_{1\,\mathrm{dB}}$, was 105 mW, and the saturated output power, P_{sat}, was 450 mW. The overall dc power supplied to the grid was 4.3 W, and the fraction of the power that was delivered to the HBT's was about 2.17 W. The dc to rf efficiency then becomes 10.5% overall and 20.7% if the loss in the bias resistors is ignored. Results at other frequencies, however, showed a sharp decrease in power-handling capability (Table 3.3). To explain this, the measured saturation powers are plotted on top of the output matching curve (Figure 3.16). It is clear that the power performance of the amplifier grid is largely governed by how well the output circuit is matched. In fact, by adjusting the polarizer positions slightly, thereby tuning the output matching circuit, the saturation power could be increased at the other frequencies.

Frequency (GHz)	P$_{1dB}$ (mW)	P$_{sat}$ (mW)	DC to rf efficiency (%)	HBT efficiency (%)
9.6	35	148	3.4	6.8
10.0	105	450	10.5	20.7
10.4	41	112	2.6	5.2

Table 3.3 The power performance of the grid at three different frequencies. The total DC power supplied to the grid is 4.3 W. Approximately 50% the total dc power was delivered to the transistors. The output power produced at 10 GHz is more than three times larger than those at the two other frequencies.
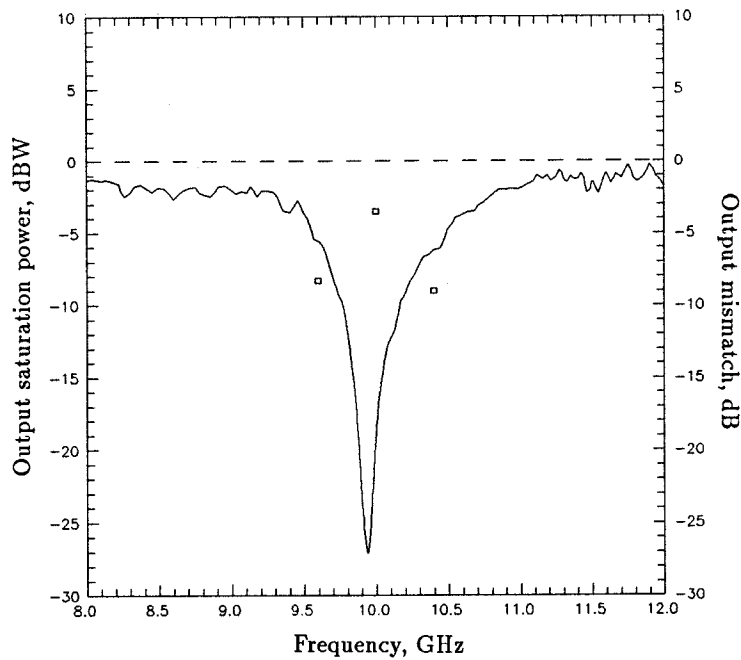
Figure 3.16 The output mismatch curve and the saturated output power vs. frequency. Both output mismatch and P_{sat} are plotted logarithmically. The mismatch is -5.6, -18.6, and -6.1 dB at 9.6, 10.0, and 10.4 GHz. It is evident that the output match affects the power performance of the grid amplifier.

3.6 Noise Figure Measurements

The amplifier grid noise performance was also measured. This measurement can be done using the diffraction-limited setup without lenses discussed earlier. As before, the grid is placed exactly in the middle of two identical horns (Figure 3.17). Using a Hewlett Packard HP8970 Noise Figure Meter and a Watkins Johnson M17C X-band mixer, the noise figure of the entire measurement setup including the two horns and the grid in free-space was measured. This noise figure was called the measured noise figure, F_m. The noise figure of the grid, F_{grid}, could then be extracted from the measured noise figure.

The total antenna temperature at the receiving horn, T_r, can be expressed in terms of the source temperature of the transmitting horn, T_t, and the added effective noise temperature of the amplifier grid, T_{grid} along with the room temperature, T_{room}.

$$T_r = GLT_{grid} + (1 - L)(GL + 1)T_{room} + GL^2 T_t \tag{3.4}$$

where G is the amplifier gain, and L is the input and output space-loss factor. Assuming the horns are lossless, the measured noise figure, F_m, can be written as,

$$F_m = 1 + \frac{1}{L}\frac{T_{grid}}{T_{ref}} + \frac{(1 - L)(GL + 1)}{GL^2}\frac{T_{room}}{T_{ref}} \tag{3.5}$$

and the amplifier grid noise figure, F_{grid} becomes

$$F_{grid} = 1 + L\left(F_m - 1 - \frac{(1 - L)(GL + 1)}{GL^2}\frac{T_{room}}{T_{ref}}\right) \tag{3.6}$$

where T_{ref} is the reference noise temperature. For this experiment, F_m varied from 28 to 33 dB, G from 0 to 10 dB, and L was about -17 dB. The measured noise
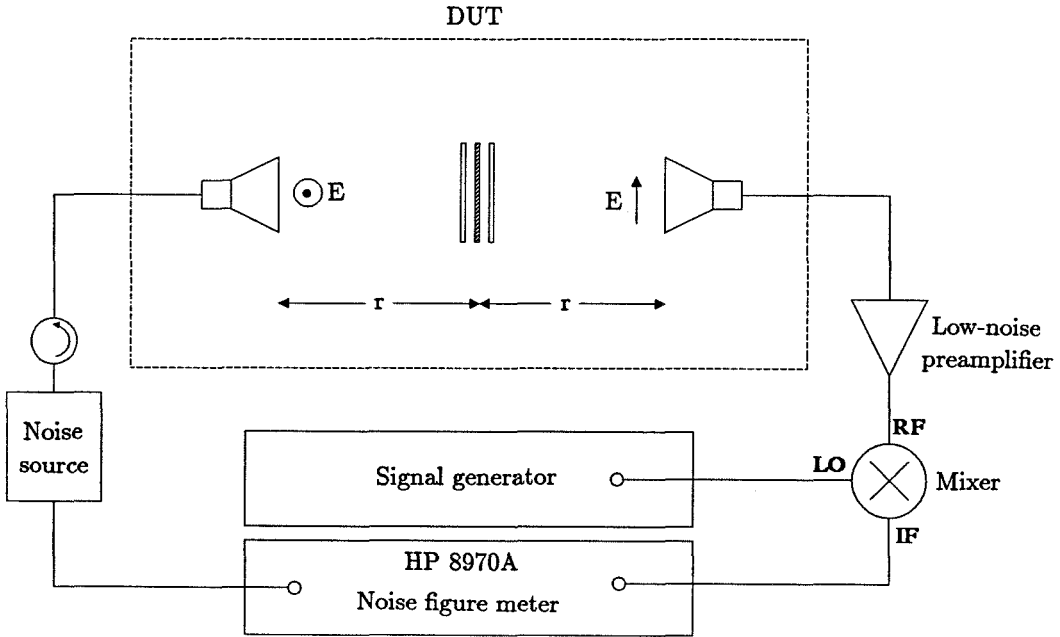
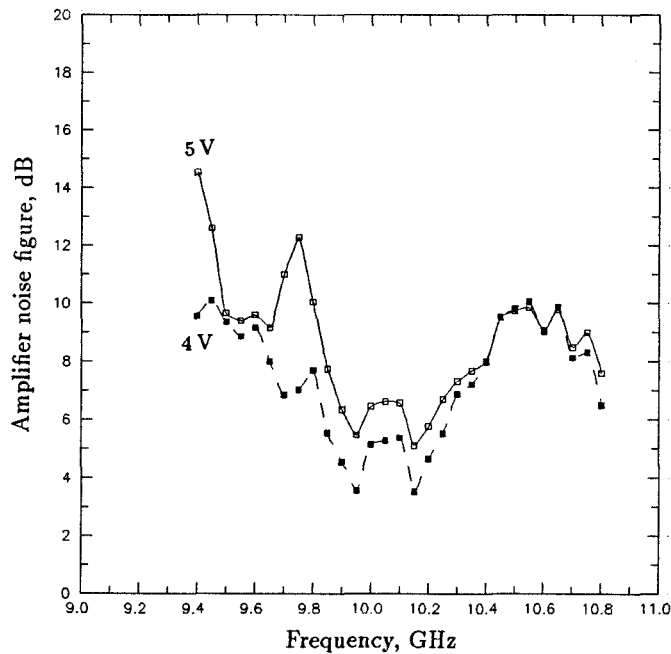**Figure 3.17** The amplifier grid noise figure measurement setup. In order to lower the measurement system noise, a low noise preamplifier may be required. In our experiments, an *Avantek* amplifier, AMT12034, which has about 30 dB gain and 4 dB NF between 7 and 12 GHz was used. This amplifier also provides necessary isolation at the receiving horn.

Figure 3.18 Noise performance of the amplifier grid at two different dc bias points. The numbers are comparable to the noise figure of a single chip circuits. This indicates that the noise power of the grid does not scale with the number of devices.
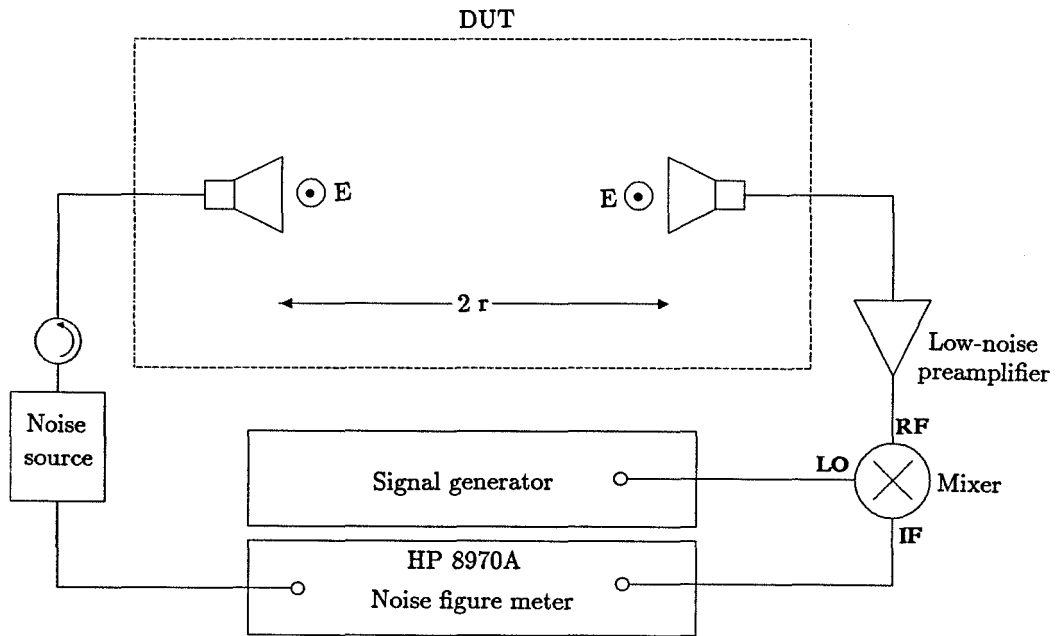
figures at two different dc bias points are shown in Figure 3.18. Here, T_{room} and T_{ref} were assumed to be 296.5 K. The noise figure was about 6.5 dB at 10 GHz with 5 V dc bias. As the dc bias was lowered from 5 to 4 V, the noise figure decreased by about 1.2 dB. The amplifier gain also dropped by 1 to 2 dB as well. For single HBT transistor circuits, 4 dB is a reasonable value for optimal noise figure [9]. Therefore, the noise figure of 6.5 dB for the entire grid indicates the noise power is not proportional to the number of devices in the grid, unlike the power handling capability of the amplifier grid which does scale with the number of the devices in the grid.

Noise figure is an extremely sensitive measurement, and many more factors affect the accuracy of the measurements. For example, signals can get coupled into the noise figure meter from many different external sources. Therefore, there is some uncertainty in the measured noise figure for the amplifier grid. One way to improve the measurement accuracy is to move the entire setup outdoors, and point the receiving horn into the sky. This would lower the room temperature, T_{room}, and the noise figure meter reading will be more sensitive to the grid effective temperature, T_{grid}.

In order to verify that there was no external interference, the room noise temperature surrounding the measurement setup was measured. This can be accomplished by measuring the noise figure of an 'empty' system, where the two horns are polarized in the same direction with the grid amplifier (Figure 3.19) removed. The total antenna temperature at the receiving horn, T_r, is then,

$$T_r = (1 - L^{'})T_{room} + L^{'}T_t \qquad (3.7)$$

where $L^{'}$ is the input and output space-loss factor between two horns, and $T^{'}_{room}$ is the measured room temperature. The measured noise figure for the 'empty' system, F_m, is given as.

Figure 3.19 The free-space noise figure measurement setup.
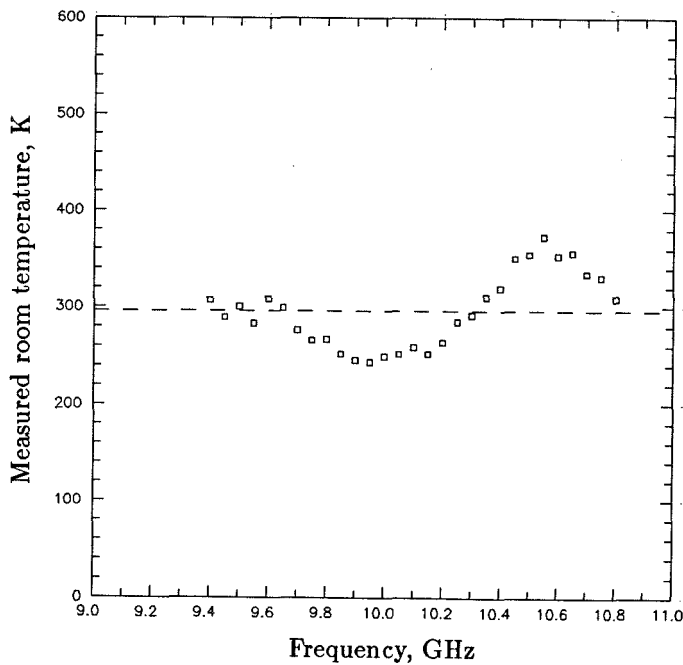
Figure 3.20 The measured room noise temperature surrounding our experimental setup.

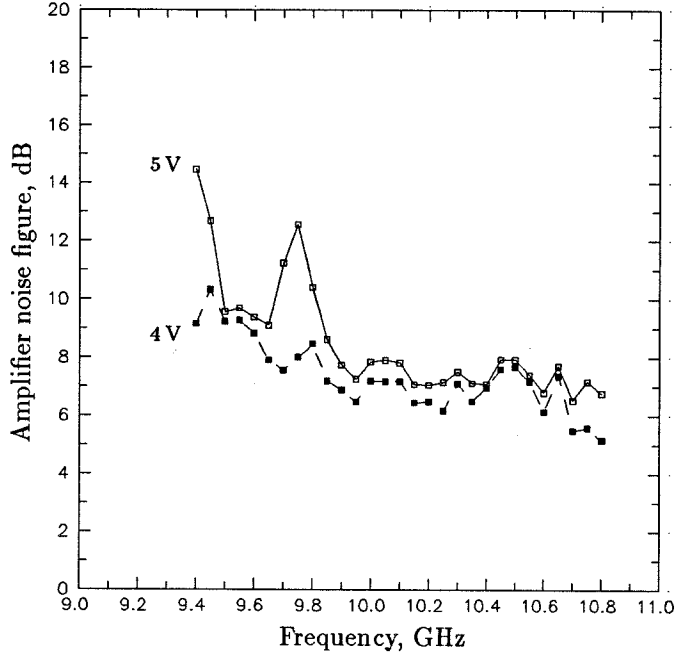**Figure 3.21** Calibrated noise figure of the amplifier grid at two different dc bias points. In Equation 3.6, the room temperature was changed from 296.5 K to the measured values that varies with the frequency as shown in Figure 3.20.

$$F_{\mathrm{m}} = 1 + \frac{1 - L'}{L'} \frac{T_{\mathrm{room}}}{T_{\mathrm{ref}}} \tag{3.8}$$

and the measured surrounding temperature, T_{room} becomes

$$T_{\mathrm{room}} = 296.5\mathrm{K} \left(L' + \frac{F_{\mathrm{m}} - 1}{1 - L'} \right) \approx 296.5\mathrm{K} L' F_{\mathrm{m}} \tag{3.9}$$

Figure 3.20 compares the measured room temperature to 296.5 K. The maximum deviation of the measured room temperature from 296.5 K was about 75 K. This implies that there is about 1 dB error in the free-space noise figure measurement system.

The measured room temperature can be applied to the noise figure calculation of the grid amplifier. Rather than 296.5 K, which was used ealier, the mesaured

room temperature was applied to Equation 3.6 instead. Figure 3.21 shows the calibrated noise figure of the amplifier grid. Between 10.0 and 10.8 GHz, the noise figure stays almost constant at 7 to 8 dB. The changes between Figure 3.18 and Figure 3.21 indicate how sensitive the noise measurement setup was to the noise sources other than the amplifier grid.

3.7 RELIABILITY OF THE AMPLIFIER GRID

In a quasi-optical grid array, the effect of a partial failure is a very important issue. Previously with FET transistors, the most common failure caused by an excessive dc bias voltage was usually a shorted gate-channel. In a grid where all the transistors are in a parallel configuration, one shorted device fails the entire grid. Throughout the measurements described in the earlier sections, however, the HBT grid has never failed to work. Furthermore, failures in the HBT grid can be checked rather easily with an IR camera connected to a microscope. When the
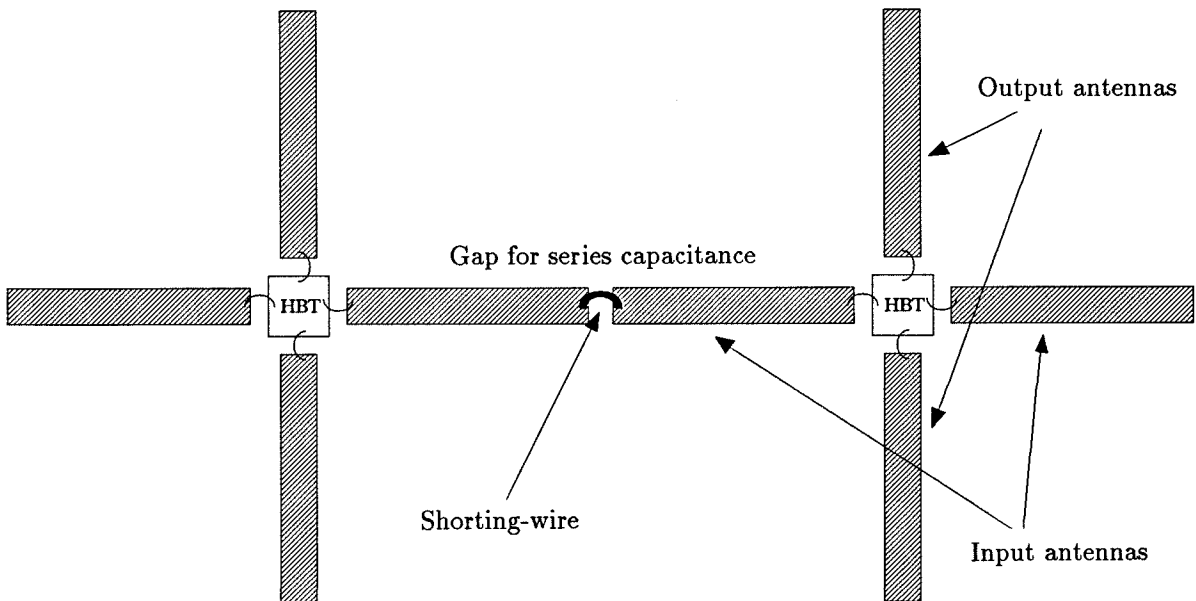
Figure 3.22 Sketch of the modified unit cells. The bond-wire across the input antenna gap had the effect of detuning the input match of the grid.

HBT chip is biased, there will be a recombination process of the minority carriers in the base junction. This process produces infrared light emission. Therefore, by checking for two bright spots with an IR camera, the failures in the differential-pair HBT chips could be detected. This method does not guarantee that all the chips in the grid are identical, but it does allow us to replace chips that are not dc-biased. The total number of chips replaced due to failure was about ten in the 10×10 array in a six month period of time.

Previously, a failure test was performed on a grid oscillator by physically removing transistors from the grid [10]. With an amplifier, we could simulate the effect of a failure by modifying the matching circuit for some unit cells in the grid. Earlier, the importance of the series capacitance gap in the input antenna lead was discussed. When this gap is closed with a single bond-wire as shown in Figure 3.22, the related unit cell should behave differently. This is obvious from the plot shown in Figure 3.23. When all the base-lead input antenna gaps were closed, the amplifier produced a gain that was 12 dB less than the previous gain. Different polarizer positions did not improve the gain. Therefore, the failure of a unit cell could be simulated to some degree with a closed antenna gap. Figure 3.24 shows the change in the measured amplifier gain when a fraction of the grid unit cells have their input matching gaps closed. The gain suffered the most when half of the gaps were closed. However, with 10% of unit cells having detuned matching circuits, the gain dropped by only 1 dB compared to the gain of the complete grid.
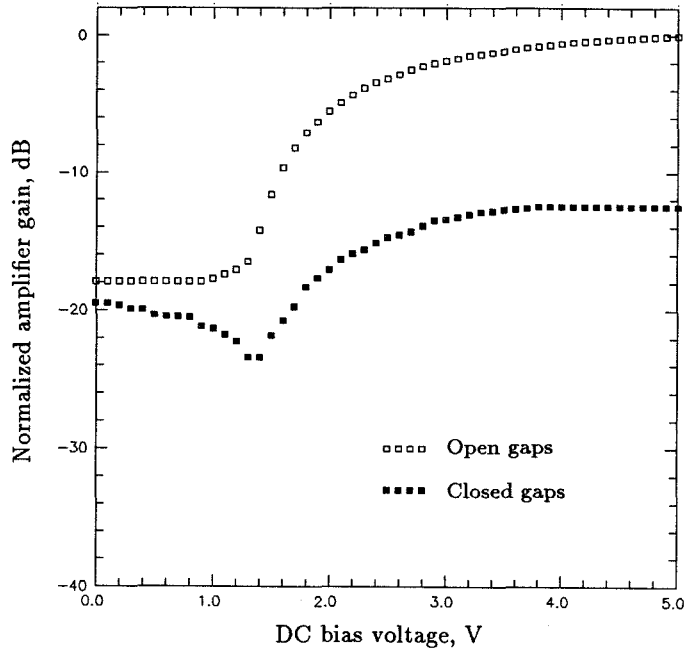
Figure 3.23 Amplifier gain response to the applied dc bias. (a) With all gaps opened, the gain was optimum. (b) When all the gaps were closed with bond-wire, the gain drops by more than 10 dB. The two curves were normalized to the maximum gain. Closing the gaps with bond-wires did not result in any spurious oscillations.
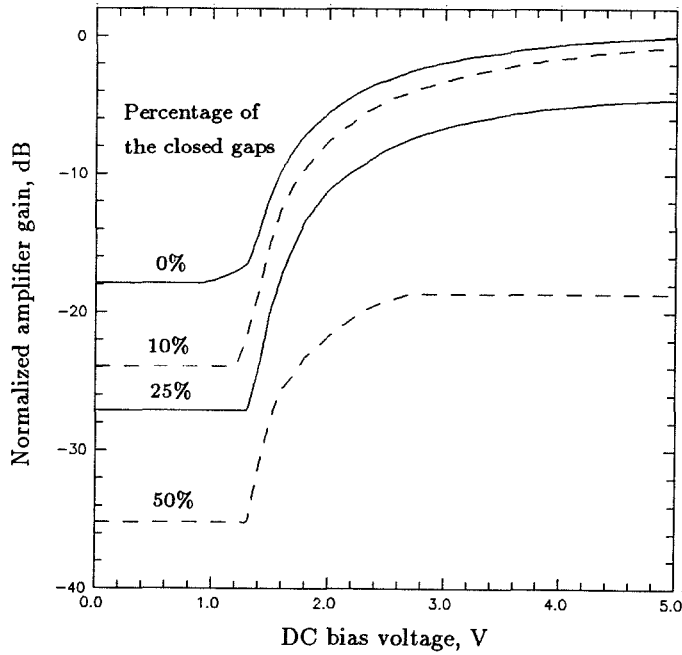
Figure 3.24 The changes in gain response when the gaps were closed for some unit cells in the grid. The locations of the closed-gap unit cells were chosen so that the unit cells were distributed equally in the grid. 10% modification of the grid showed less than 1 dB drop in the amplifier gain.

REFERENCES

[1] M. Kim *et al.*, "A Grid Amplifier," *IEEE Microwave and Guided Wave Letters*, *MGWL-1*, pp. 322–324, May 1991.

[2] J. B. Hacker *et al.*, "A 100-Element Schottky Diode Grid Mixer," *IEEE Trans. Microwave Theory Tech. MTT-38*, pp. 557-562, March 1992.

[3] M. Chang *et al.*, "AlGaAs/GaAs Heterojuction Bipolar Transistors Fabricated Using A Self-Aligned Dual-Lift-Off Process," *IEEE Electron Device Lett. EDL-8*, pp. 303-305, July 1987.

[4] M. Kim *et al.*, "A 10 GHz Quasi-Optical Grid Amplifier Using Integrated HBT Differential Pairs," *Device Research Conference*, Boston, MA, June 1992.

[5] D.B. Rutledge, J.B. Hacker, M. Kim, R.M. Weikle, R.P. Smith, E.A.Sovero, "Oscillator and Amplifier Grids," *Invited talk at IEEE MTT International Symposium*, Albuquerque, NM, June 1992.

[6] "HP 85180A High Frequency Structure Simulator," Hewlett-Packard, Networks Measurements Division, 1400 Fountaingrove Parkway, Santa Rosa, CA, 1992.

[7] D. Gagnon, "Highly Sensitive Measurements With a Lens-Focused Reflectometer," *IEEE Trans. Microwave Theory Tech. MTT-39*, pp. 2237–2240, December 1991.

[8] J.D. Kraus, " Antennas," Second Edition, pp. 828, McGraw-Hill, 1988.

[9] P.M. Asbeck, Mau-Chung F. Chang, J.A. Higgins, N.H. Sheng, G.J. Sullivan, and Keh-Chung Wang, " GaAs/AlGaAs Heterojuction Bipolar Transistors: Issues and Prospects for Application," *IEEE Trans. Electron Devices, ED-36*, pp. 2032–2035, October 1989.

[10] Z.B. Popović *et al.*, " Bar-Grid Oscillators," *IEEE Trans. Microwave Theory Tech., MTT-38*, pp. 225-230, March 1990.

Chapter 4

# Applications of the X-Band Grid Amplifier

Three different applications of the cross-polarized X-band HBT grid amplifier are discussed in this chapter. In the first experiment, the grid amplifier was converted into an oscillator with an external positive feedback. A quasi-optical feedback circuit made of a tilted polarizer and a mirror is described. During the operation, this circuit completed the oscillation feedback path by producing a horizontally polarized beam from a vertically polarized output beam without much loss. Oscillations at any frequency between 6.5 and 11.5 GHz could be generated. By varying the air gap spacing between the active grid-array surface and the half-wave plate feedback circuit, the oscillation frequency could be tuned continuously from 8.2 to 11.0 GHz. The measured peak ERP of 6.3 W was observed at 9.9 GHz. Next, a simple grid array system was built by coupling the grid amplifier to a 2 × 4 grid oscillator. The grid amplifier increased the peak power density of the grid oscillator by about 15 dB. Different spacings between the amplifier and the oscillator produced different radiation beam pattern for the amplifier grid. When the oscillator grid and the amplifier grid were far apart, the measured amplifier radiation pattern closely matched the pattern expected from a uniform source field with an aperture size of the amplifier grid. Pattern measurements are presented for the different incident beam angles to show that the propagation angle of the incident beam was preserved as it passed through the amplifier grid. The last experiment demonstrated the amplifier grid as an AM modulator. The modulation signal was fed into the dc-bias lines. AM modulation was performed at 10 GHz, where a modulation index of up to 0.65 was measured with a reasonable linearity.

4.1 AN EXTERNAL FEEDBACK OSCILLATOR

An amplifier is one of the most critical components in conventional millimeter-wave MMIC circuits. Likewise, an amplifier grid is a component that can greatly enhance the performance of other active grids in a cascaded grid-array system. A 100-element cross-polarized heterojuction bipolar transistor grid amplifier has already been discussed in Chapter 3 [1]. The grid exhibited a gain of 10 dB at 10 GHz with 3 dB gain bandwidth of 1 GHz. The maximum saturated power was 450 mW, which indicated a 10.5% dc-to-rf conversion efficiency. The noise figure of the amplifier grid was measured to be 6.5 dB at 10 GHz. This amplifier grid showed a vast improvement in overall performance over the first amplifier grid [2]. It also allowed additional experiments for testing the feasibility of an amplifier grid in a quasi-optical systems to be performed.

Many different types of quasi-optical grid-array components have been studied. Among them, the grid oscillator has been the primary subject of interest. Previous grid oscillators, whether hybrid [3,4] or monolithic [5], relied on a feedback path that was mainly determined by the shape and the size of the passive structure which contained the transistors. Therefore, the phase delay in the feedback path was difficult to change, and frequency tuning was rather limited. A grid amplifier, on the other hand, is stable since the cross-polarized input and output for the active array are well-isolated. In order to induce an oscillation, an additional feedback circuit is required. This feedback circuit provides the necessary conversion between the cross- polarized input and output. In this arrangement, the feedback path can be more clearly identified. By adjusting the phase delay in the feedback path, a wider oscillation frequency range can be obtained than is possible with past oscillator grids. Output power control is accomplished with the separate impedance tuning circuits outside the feedback loop.

The first step toward building a complete quasi-optical feedback circuit for X-band is to examine a tiled metal strip polarizer, which is positioned to make
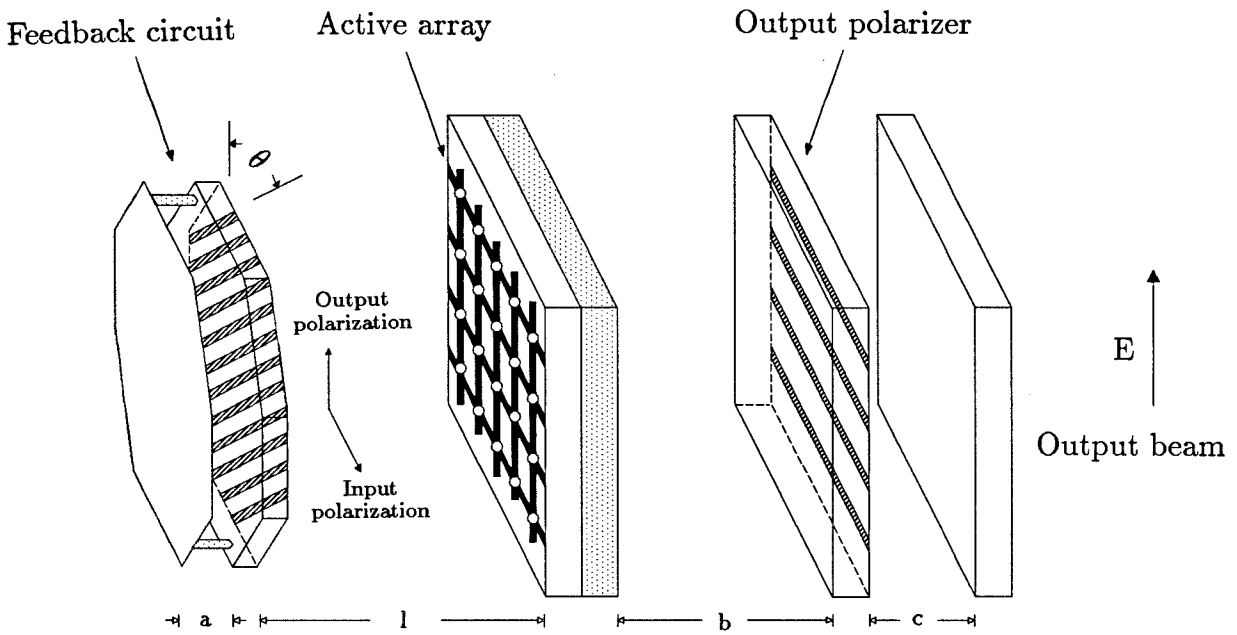
Figure 4.1 Sketch of the external feedback oscillator. The half-wave plate feedback circuit replaced the input polarizer of the standard grid amplifier.

	dielectric constant (ϵ_r)	Physical length (mm)	Electrical length at 10 GHz (°)
a	1	3	36
b	1	15	180
c	1	10	120
▨	10.5	3.81	148
☐	2.2	3.18	57

Table 4.1 Polarizer spacing for the oscillator. The spacings on the output side of the grid array is the same as the previous amplifier. The spacing between the active array surface and the feedback circuit, l in Figure 1, was varied to tune the oscillation frequency.

an angle, θ, with the vertical direction as shown if Figure 4.1. The polarizer is then assumed to be infinitely large. It is also assumed that the polarizer provides a total reflection for the beam polarized in the same direction, and a total transmission for the other polarization. Defining the four ports to be vertical polarization front side, vertical backside, horizontal front side, and horizontal backside, the tilted polarizer can be described in terms of an S-parameter matrix,

$$S = \begin{pmatrix} -\cos^2\theta & \sin^2\theta & -\sin\theta\cos\theta & -\sin\theta\cos\theta \\ \sin^2\theta & -\cos^2\theta & -\sin\theta\cos\theta & -\sin\theta\cos\theta \\ -\sin\theta\cos\theta & -\sin\theta\cos\theta & -\sin^2\theta & \cos^2\theta \\ -\sin\theta\cos\theta & -\sin\theta\cos\theta & \cos^2\theta & -\sin^2\theta \end{pmatrix} \tag{4.1}$$

The feedback circuit with a 45° tilted polarizer is shown the Figure as a part of the complete oscillator circuit. A 3.18 mm-thick *Duroid* substrate ($\epsilon_r = 2.2$), and an air-gap of 3 mm separated the tilted polarizer and a mirror. A simulation on the transmission-line model of this feedback circuit (Figure 4.2) indicated that the conversion between the incident vertical beam and the reflected horizontal beam was almost perfect over the frequency range of 8 to 11 GHz. This feedback circuit behaves under the same principle as a half-wave plate in optics [6]. The incident beam is first divided into two components, one parallel to the tilted polarizer and the other normal to the polarizer. Then, an extra 180° phase delay is added to the beam normal to the polarizer. The net result is a reflected beam with opposite polarization to the incident beam.

The input matching polarizer of the standard grid amplifier arrangement was replaced by the half-wave plate circuit. The output matching circuit remained unchanged. The oscillation frequency could be tuned smoothly between 8 and 11 GHz as the air-gap spacing between the active array surface and the feedback circuit was varied as shown in Figure 4.3a. Also shown is the repeatability of the oscillation frequency for every half-wavelength of the air-gap feedback delay. This suggests that a TEM transmission line-model could be used to characterize the delay. When the gap spacing was large, the multiple of 2π phase delay required
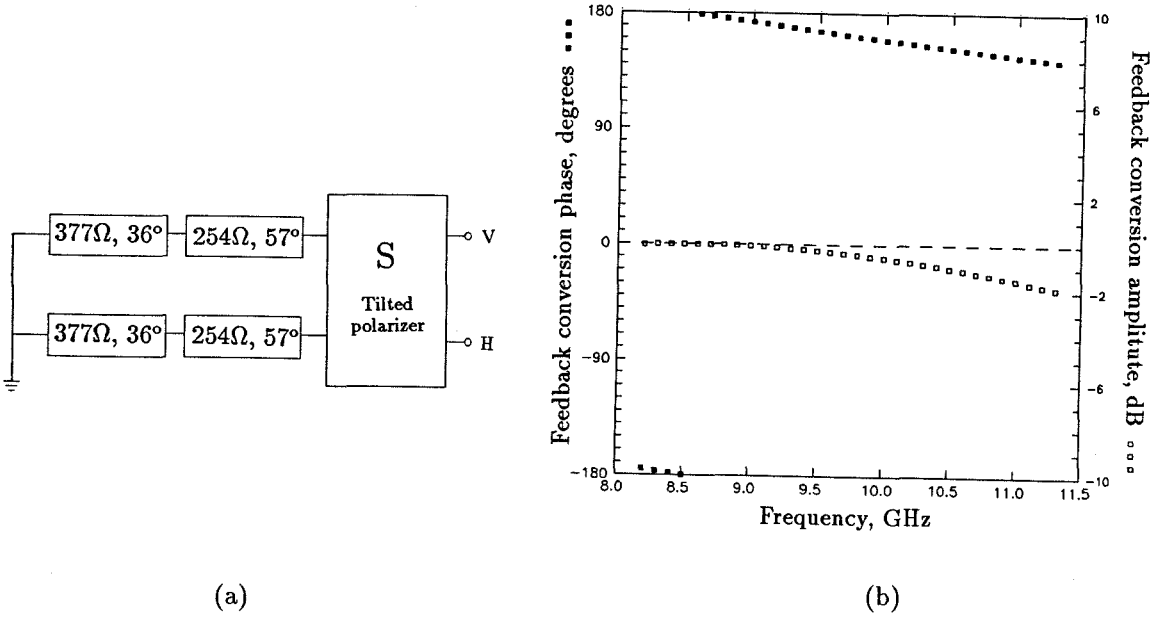
Figure 4.2 (a) The transmission line model for the half-wave plate feedback circuit. The S-parameters for the tilted polarizer are shown in equation (1). The 254 Ω transmission-line represents the *Duroid* substrate behind the tilted polarizer, and the 377 Ω transmission-line is the air gap between the substrate and the back-short. (b) The simulation shows that the feedback circuit converts the incident beam into a cross-polarized beam with almost no loss.

for an oscillation could be satisfied at more than one frequency. In this case, the frequency with a higher round trip gain dominates and produces the oscillation. In this circuit, the lower frequency round trip gain was larger. This explains why the high oscillation frequency range was shortened after each half-wavelength.

The measured output power (ERP) varied from -5 dBW to 8 dBW when the grid was biased at 3.5 V and 530 mA (Figure 4.3b). The oscillation frequency and the measured power were almost the same at every half-wavelength air-gap spacing. The maximum ERP of 6.3 W was obtained when the oscillation frequency was around 9.9 GHz. Under the assumption that the radiation pattern is determined by the physical size of the active grid array, the total transmitted power was estimated to be 72 mW, showing a dc-to-rf efficiency of 3.9 %. Ignoring the dc power loss in the resistor bias network, the efficiency for HBT's was 6.7%. The output power at other frequencies could be optimized with different output
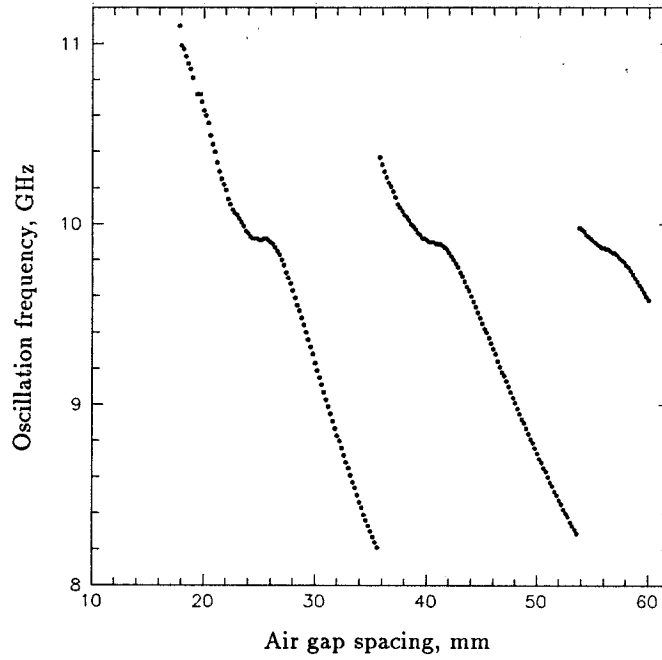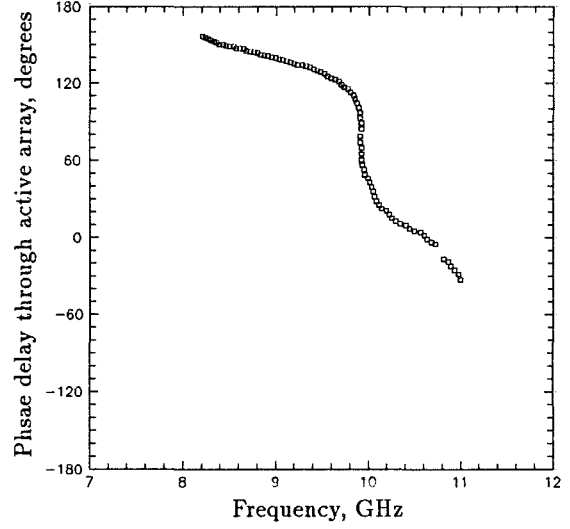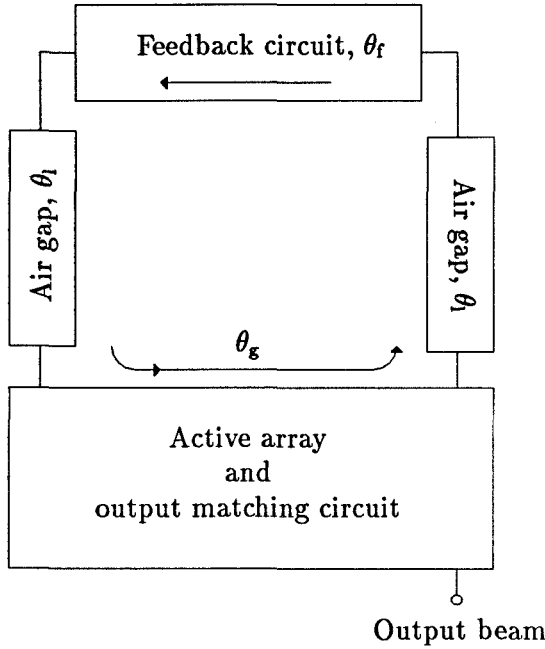
(a)
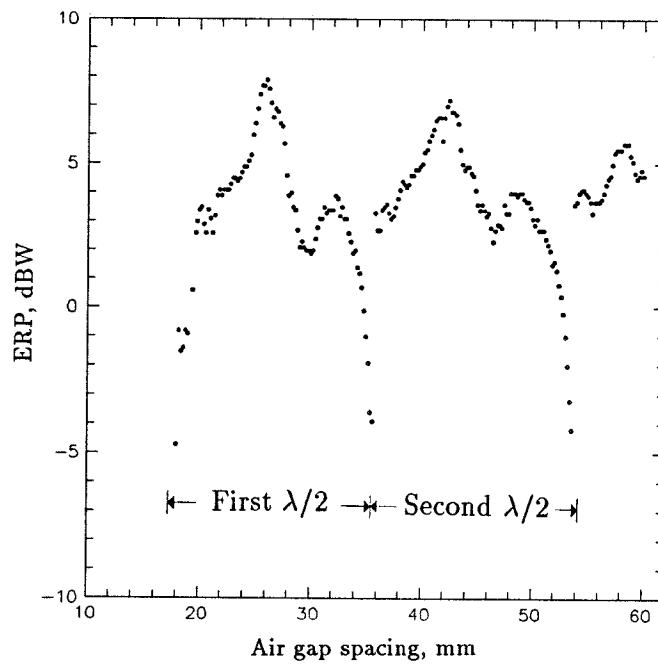
(b)

Figure 4.3 (a) Oscillation frequency vs. the air-gap spacing between the half-wave plate feedback circuit and the active array. (b) Measured ERP vs. air-gap spacing.

Figure 4.4 (a) Circuit diagram for the oscillator circuit. (b) Calculated phase delay in the active grid array as the incoming input signal was reflected back to the feedback circuit.

polarizer positions. The peak ERP diminished due to the increasing diffraction loss in the feedback system as the air-gap spacing increased.

For this oscillator, the frequency of oscillation is determined by the phase delays in the active array, the half-wave plate feedback circuit, and the air-gap in between. In the experiment just described, the air-gap spacing was changed to tune the frequency, however, electronic frequency tuning may be more desirable. Schottky/varactor diode grids have shown varying phase delays for a quasi-optical rf-beam [7, 8]. These diode grids can be placed in the feedback path along with a tilted polarizer and a mirror to tune the oscillation frequency. It is therefore interesting to calculate the amount of the phase delay, θ_g, added to the signal as it gets reflected back from the active grid array. The theory for the half-wave plate feedback circuit provides the phase delay in this case, θ_f. The experimental results give the delay in the air-gap spacing, θ_l. Figure 4.4b shows the phase delay

through the active grid for frequencies between 8 and 11 GHz. This was calculated for the first half-wavelength air-gap spacing. The results from the second half-wavelength were almost identical to the first. According to this curve, about 80° phase delay change at 10 GHz in the feedback circuit can tune the frequency from 8.2 to 9.8 GHz. Around 10 GHz, the oscillation frequency was less sensitive to changes in the external phase delay, and the frequency tuning would be more difficult.

There are many ways to obtain a phase-shifter from diode grids to accomplish electronic frequency-tuning. As an example, an electronically-tunned Fabry-Perot resonator is shown in Figure 4.5. The proposed resonator is a dielectric substrate with etched copper strips on both sides. The effective thickness of the dielectric is a half-wavelength at 11.3 GHz. The strips, arranged to present 3 nH of inductance, contain varactor diodes with a varying capacitance between 0.12 and 0.80 pF. The diodes are assumed to have a series resistance between 0 and 5 Ω for our simulation purposes. These values for the varactor diodes are typical of commercial products. When a beam polarized along the strips is incident on the resonator substrate, total transmission occurs at a single frequency which can be tuned with different capacitances presented by the varactor diodes. The simulation results in Figure 4.6 show a resonance frequency tuning of more than 1.6 GHz between 8.2 and 9.8 GHz. For the cross-polarized fields, the resonator is simply a half-wavelength thick dielectric substrate with a minimal return-loss.

The ideal application for a frequency-selector diode grid in the external feedback oscillator is between the active array and the feedback circuit. In the arrangement shown in Figure 4.7, three different parts are assembled to form a complete oscillator circuit. Each of these three parts performs an independent task. The active array produces an amplified output beam from the input, the feedback circuit converts the output beam back to the input over a wide frequency range without much loss, and the frequency-selector provides the required phase-delay
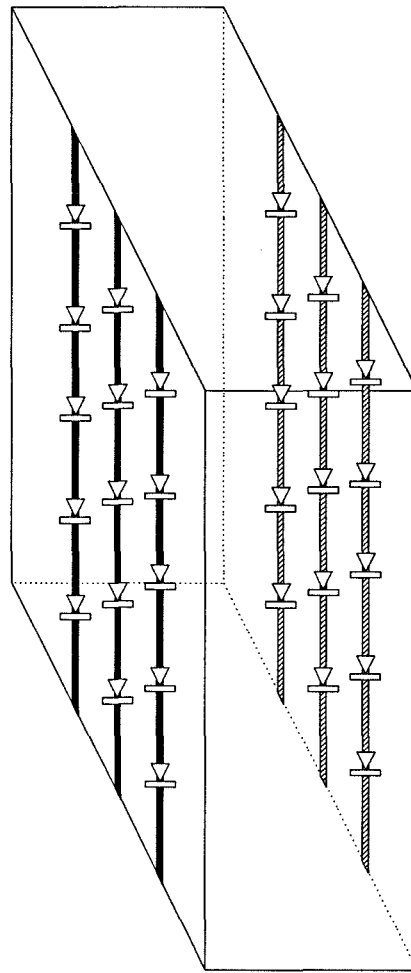
Duroid substrate (9 mm thick, ϵ_r=2.2)

(a)

L=3 nH

$Z_c = 254\,\Omega$

C=0.12~0.80 pF

160° at 10 GHz

R=0~5Ω
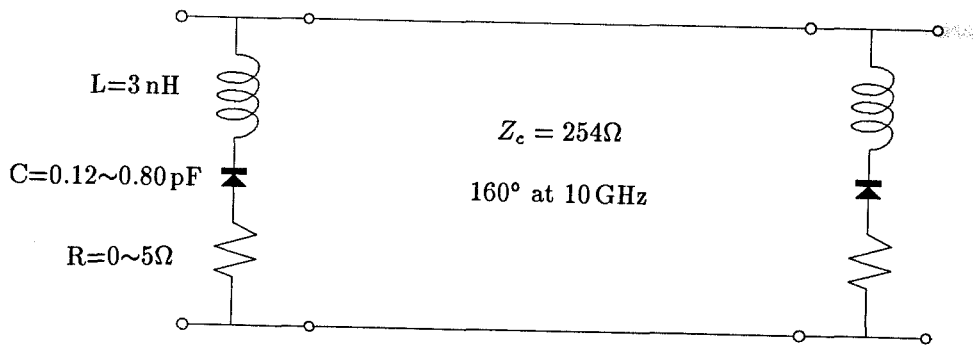
(b)

Figure 4.5 (a) Proposed electronically tunned Fabry-Perot resonator for use as a frequency-selector. (b) Equivalent circuit model for the frequency selector. The width of the strips is chosen to present 3 nH of inductance.
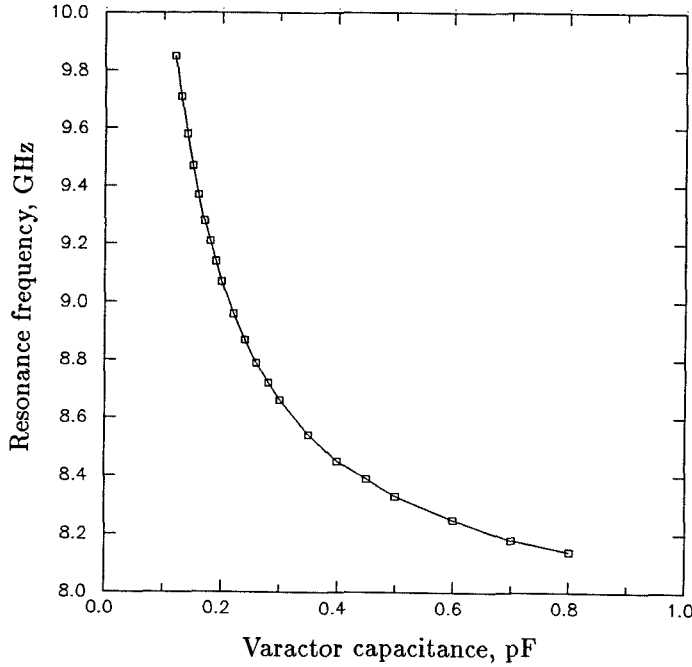
Figure 4.6 Simulated resonance frequency of the selector grid vs. capacitance of the varactor grid, neglecting the series resistance in the diodes

and circuit-matching for the desired frequency. When both of the air-gap spacings between the three parts are fixed at 3.3 mm, the predicted oscillation frequency is tuned from 8.45 to 9.75 GHz by varying the dc-bias to the frequency-selector grid (Figure 4.8a). When a series resistance of 5Ω is added to the varactor diodes, the frequency tuning range shows almost no change. However, the total round-trip loss for the frequency-selector and the feedback circuit increases for larger series resistances (Figure 4.8b). This particular arrangement is not the most efficient way to obtain electronic frequency-tuning. A more sophisticated circuit could be designed for the same purpose.

The quasi-optical feedback circuit was now modified in two different ways to further examine the oscillator. First, the tilted polarizer angle in the half-wave plate feedback circuit was varied from 45° to weaken or strengthen the coupling between the output and input. The results show slight frequency tuning. The
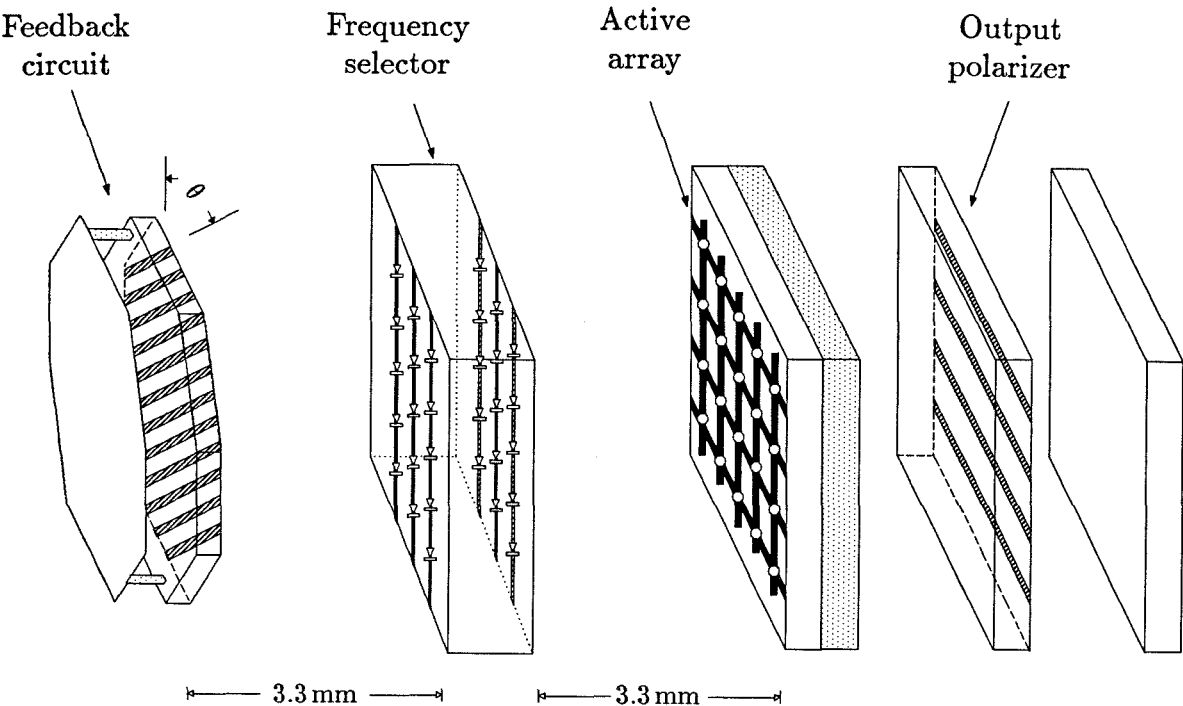
Figure 4.7 An electronically frequency-tuned grid oscillator. The circuit arrangement is identical to that in Figure 4.1 except that the frequency selector is placed between the feedback circuit and the active array.

(a)

(b)
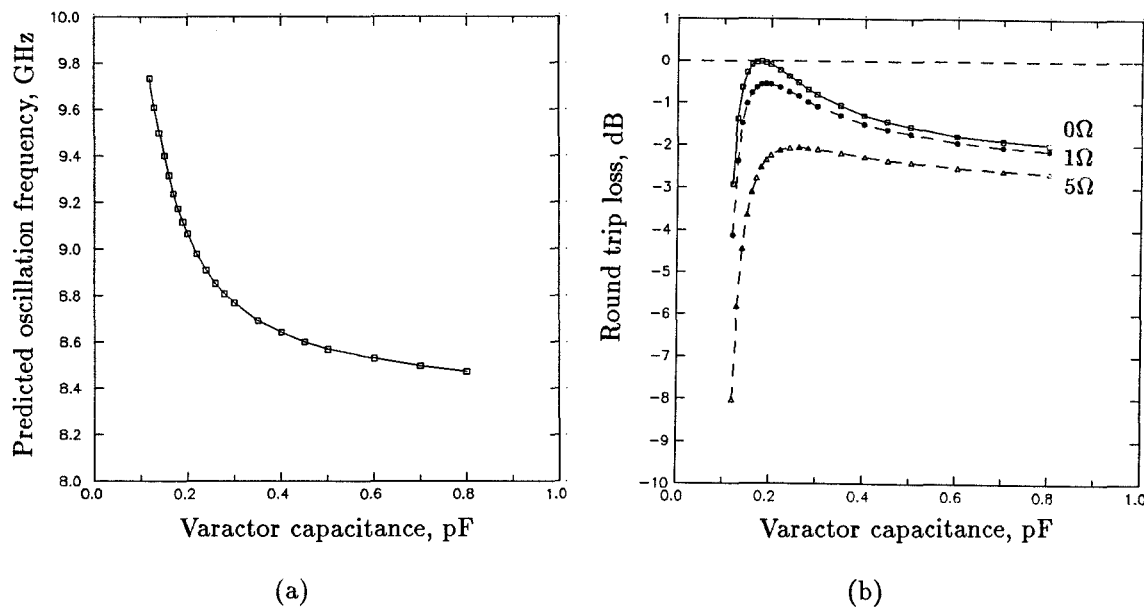
Figure 4.8 (a) Simulated oscillation frequency vs. the capacitance of the varactor diodes embedded in the frequency-selector. (b) The total round trip loss between the feedback circuit and the frequency selector.
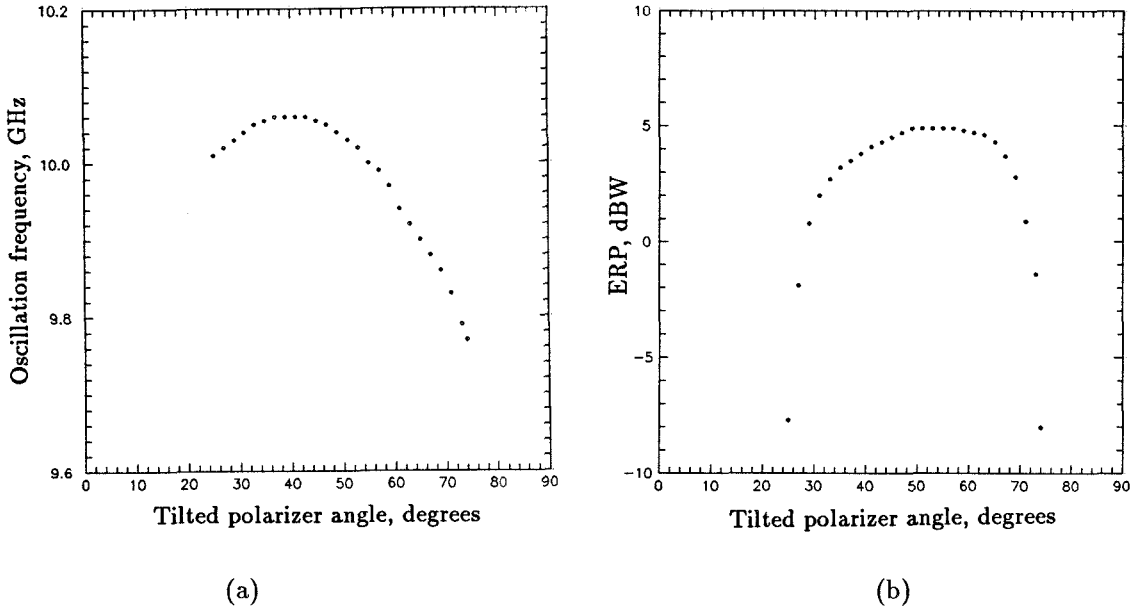
Figure 4.9 (a) Oscillation frequency vs. tilted polarizer rotation angle. (b) ERP vs. rotation angle. The air-gap spacing between the active array and the feedback circuit was fixed at 24 mm.

output power, however, changes drastically with different polarizer angle. When the polarizer was parallel to the horizontal input beam polarization ($\theta = 90°$), or parallel to the vertical output beam polarization ($\theta = 0°$), there was no oscillation. The conversion between the output and the input was sufficient to start an oscillation only when the rotation angle was between 15° and 75°. The optimum output power was achieved when the rotation angle was around 45°. This is illustrated in Figure 4.9.

Another way to modify the feedback circuit is to change the spacing between the tilted polarizer and the back mirror. Different spacings between the tilted polarizer and the mirror change the added phase delay to the beam component polarized normal to the tilted polarizer. For example, a larger spacing shifts the optimum conversion frequency down to the frequency where the spacing distance becomes a quarter-wavelength. A number of different mirror and tilted polarizer spacings were tested. Oscillation frequencies from 6.5 GHz to 11.5 GHz were observed.

4.2 GRID-ARRAY SYSTEM: WAVE-FRONT CONSERVATION EXPERIMENT

A system made of two grid arrays of solid state devices has been demonstrated by Popović *et al.* [9]. A varactor diode grid was placed behind a MESFET oscillator grid to electronically tune the frequency by 10 % at around 3 GHz. A different type of grid array system could be constructed with an amplifier grid and an oscillator grid (Figure 4.10). This type of system is one of the natural applications for a grid amplifier.

A small size grid oscillator with two unit cells along the E-plane and four along the H-plane was built. The unit cell size of this grid was 10 mm. The transistors used in this grid were *Fujitsu* FHX35X HEMT chips. The grid oscillated at 10 GHz with the cross-polarization ratio better than 20 dB at any angle for both the E and H planes. The H-plane pattern of the oscillator grid is shown in Figure 4.11a as a solid line. The oscillator was then moved backward 5 cm away from the original position, where the amplifier grid was placed instead. The distance between active-array surface of the amplifier grid and the oscillator grid was only 1.6λ. The radiation pattern produced by the amplifier is shown as a dashed line in Figure 4.11a. The two patterns were normalized to the peak power of the stand-alone oscillator grid. With the amplifier in front, the peak power density increased by 15 dB even though the pattern was slightly modified. The beam width of the amplifier grid became even narrower as the oscillator grid was moved further away from the amplifier by 34 cm (Figure 4.11b).

The amplifier radiation pattern for a far-field source was presumably determined by the size of the amplifier grid because the beam incident onto the amplifier grid was almost a plane wave. A theoretical power pattern was calculated from an array of 10 dipole elements that are 8 mm apart. These elements have the same phase and amplitude. The theoretical pattern is in very close agreement with the measured pattern of the amplifier grid (Figure 4.12). This indicates that the beam directivity of an amplifier grid can be estimated from its physical size.
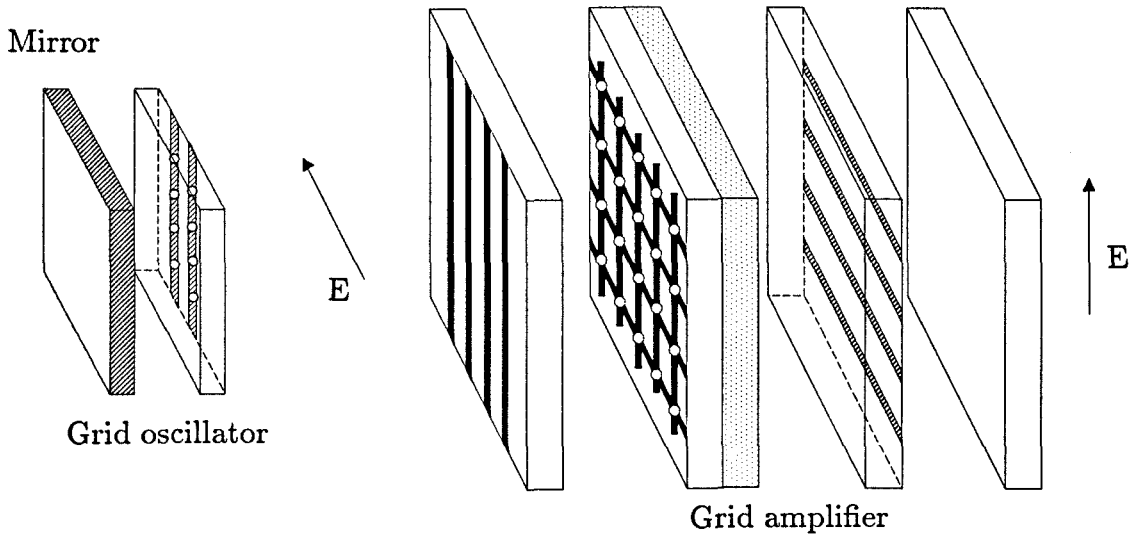
Figure 4.10 A simple grid-array system. The matching circuit for the amplifier grid was adjusted to obtain the most gain at 10 GHz [1]. The oscillator grid was a 2 × 4 HEMT array that produced an oscillation at 10 GHz.

(a)

(b)
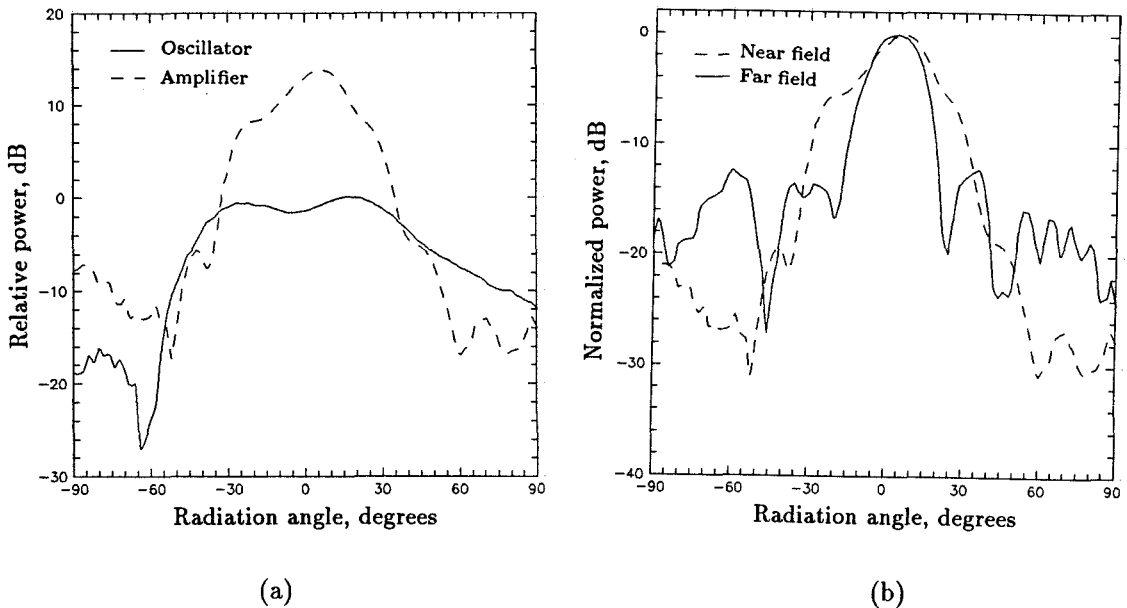
Figure 4.11 (a) H-plane radiation patterns for the stand-alone oscillator grid (solid line), and E-plane pattern for the amplifier grid 1.6λ in front of the oscillator grid (dashed line). The peak power density was improved by 15 dB. (b) The distance between two grids was increased to 11.4λ. This allowed measurement of the radiation pattern when a plane wave was incident on the amplifier grid (solid line). The results are compared with previous near-field source pattern (dashed line).
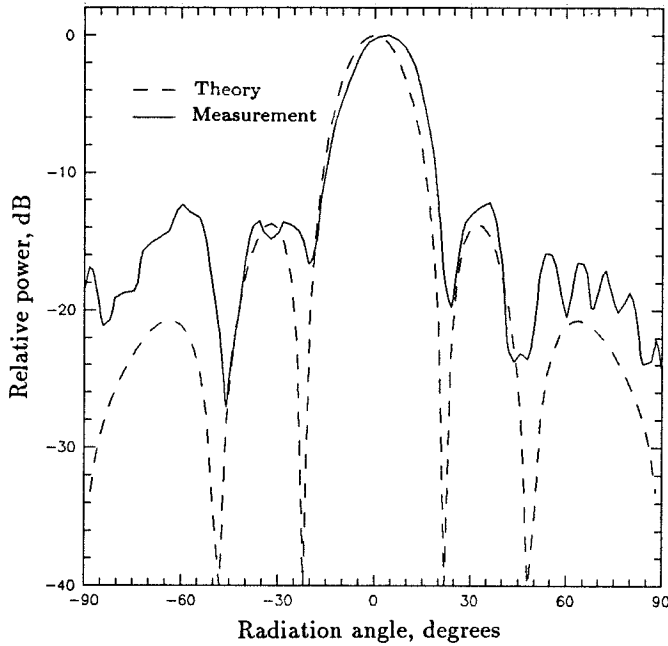
Figure 4.12 Radiation pattern of the amplifier grid when the input beam was a plane wave. Close matches of the theory (dashed line) and experiment (solid line) are shown.

A grid amplifier is a multi-mode linear device that preserves the propagation angles of incident beams. In order to compare the radiation patterns for different incident beam angles, the oscillator grid was first moved to produce an incident beam at 20° angle as in Figure 4.13.a. The peak of the output pattern was then detected at 20° off the normal angle (Figure 4.13 b). All the side lobes were at least 15 dB lower than the main lobe, and the beam width of the main lobe was comparable to the earlier beam width for the normal incidence. Again, the calculated pattern for an uniform source of the amplifier aperture size with a appropriate phase delay closely matched the measured pattern. An input beam was also sent from -20° angle, and similar results were obtained. The peak power changed by less than 1.5 dB for the two different incident angles. The implication of this experiment is that the amplifier can advantageously be placed after a beam-steering array in a transmitter system.

(a)

(b)
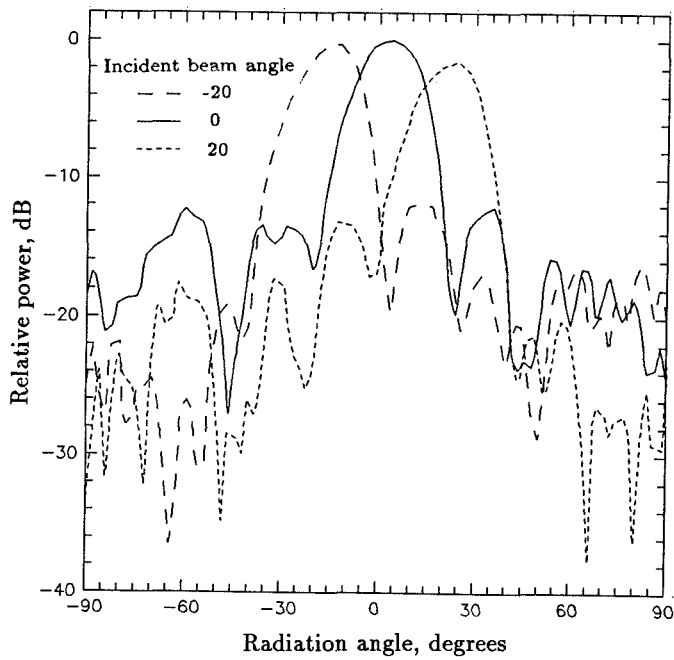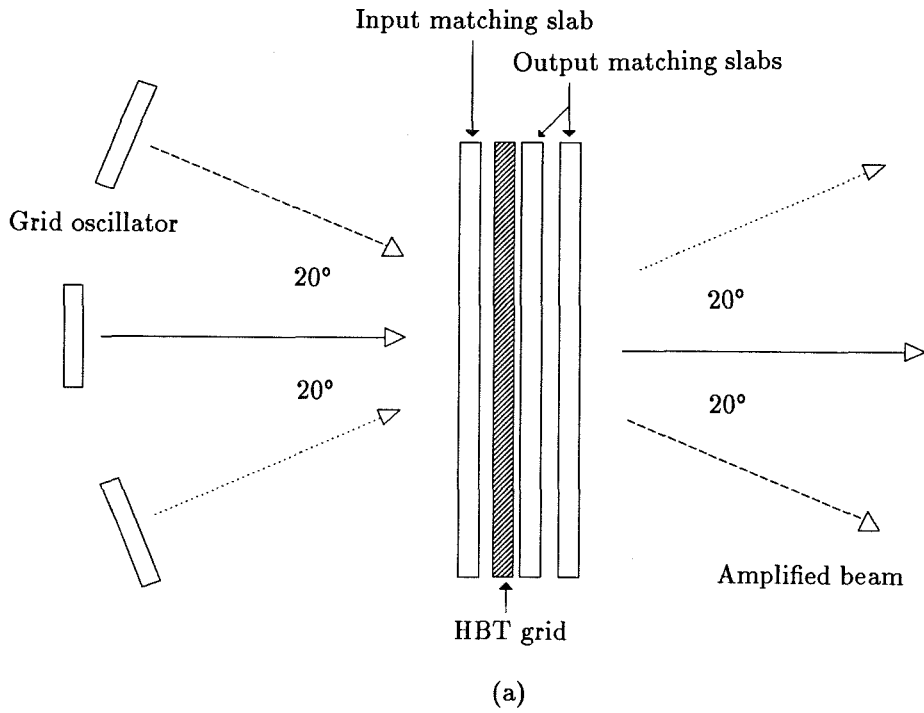
Figure 4.13 (a) Setup to test the change in the propagation angle for a beam passing through the grid amplifier. (b) Radiation patterns for three different incident beam angles.
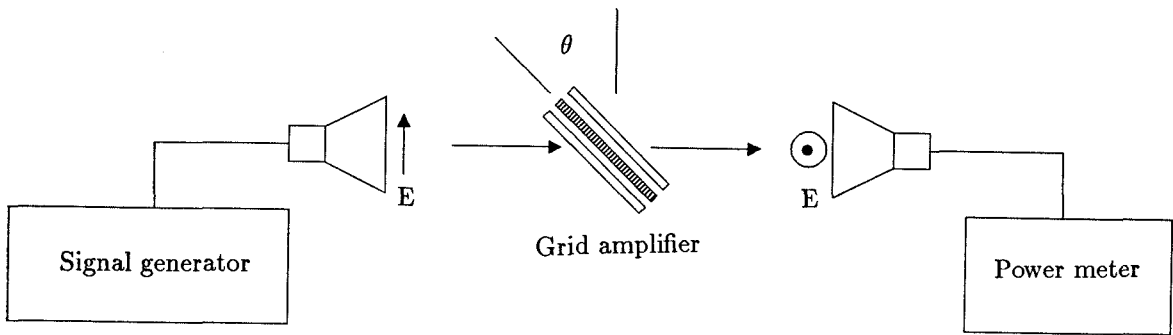
(a)
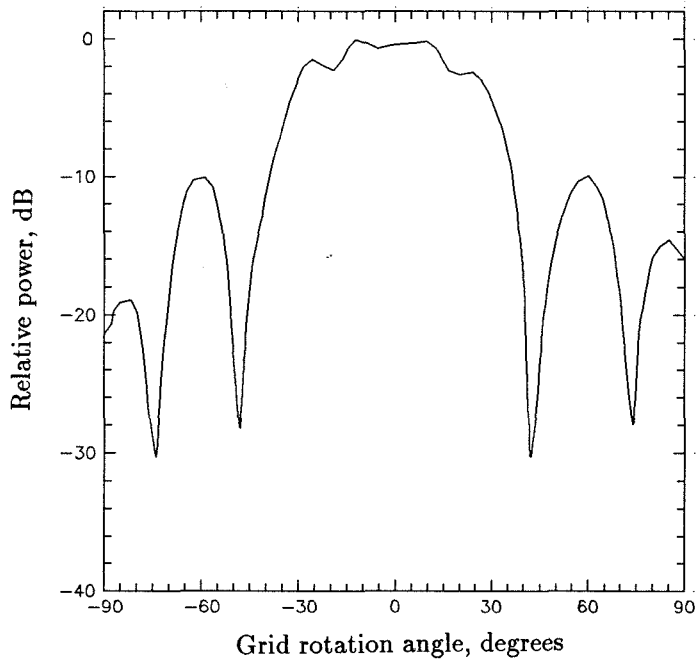
(b)

Figure 4.14 (a) Test setup for larger incident beam angles. The grid amplifier was rotated between two cross-polarized antenna horns. (b) The normalized power received at the same angle as the incident beam.

The tolerance of the amplifier grid to an input beam with larger incidence angles was tested. The amplifier grid was placed in the middle of two cross-polarized antenna horns. When the grid was rotated, the incident beam and the measured output beam had a corresponding angle. Figure 4.14b shows that the received beam power stayed above -3 dB as long as the beam angle was less than 35°. At higher incidence angles, the output power diminished, since the input power collected by the grid amplifier was smaller. The direction of the propagation may also have changed, and the radiation pattern became distorted because of the finite aperture size of the amplifier grid.

4.3 AN AM MODULATOR

One useful aspect of the amplifier grid is that the amplifier gain varies with the dc bias applied to the grid. For vacuum-tube amplifiers, the amplifier gain varies linearly with the applied dc bias voltage even when the amplifier gain is very high [10]. The gain of a solid-state device amplifier on the other hand, reaches a saturation where it does not respond to the changes in dc bias. However, it is still worthwhile to investigate the use of the amplifier grid as an AM modulator for a grid-array system.

For vacuum-tube amplifiers, the gain when the plate bias voltage changes with a modulation frequency of ω_m, may be described as

$$G(t) = G_0(1 + m\cos\omega_m) \tag{4.2}$$

where m is the amplitude modulation index. For the grid amplifier described here, the gain response to applied dc bias was not exactly linear. The response curve of the amplifier grid is shown in Figure 4.16. Below the transistor cutoff bias voltage of 1.3 V, the amplifier gain was not sensitive to changes in dc bias. However, when the DC bias for the grid is modulated around 2 V, the gain response curve could
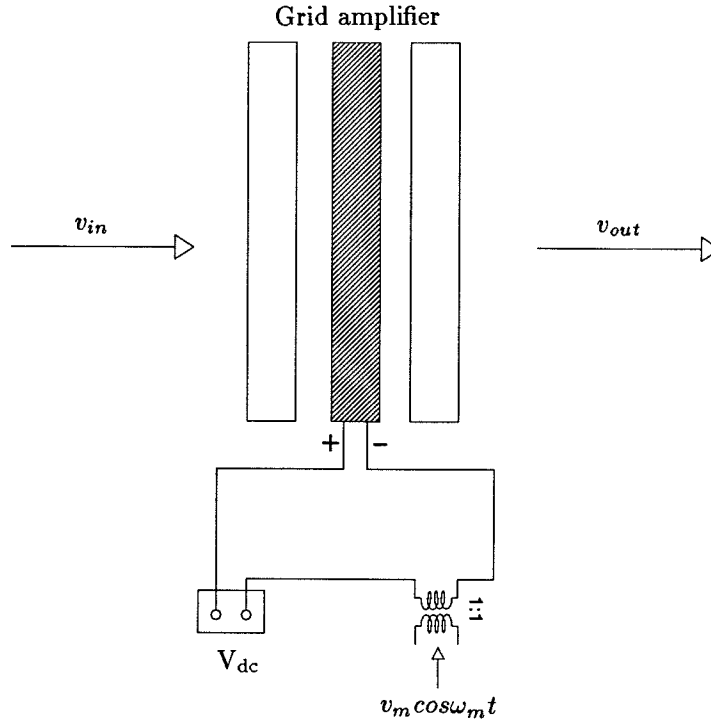
Grid amplifier

Figure 4.15 Grid amplifier as an AM modulator

be roughly approximated with a line, $G = 1.162(1 + 0.823v_m \cos\omega_m t)$, where v_m is the peak amplitude of the modulation voltage. Here, the amplitude modulation index is 0.823 times the peak value of the modulated DC bias signal.

Power measurements on the main carrier and the side band signal were taken at different amplitudes of the modulation signal, v_m. Figure 4.17 shows a frequency spectrum of the modulated signal, with a carrier frequency of 10 GHz and the modulation frequency of 200 KHz. The amplitude of the modulation bias voltage was 0.15 V. From the power difference between two signals, which was 23.7 dB, the modulation index of 0.12 could be calculated. Figure 4.18 shows the measured amplitude modulation index from amplifier grid at various modulation voltages. At low voltages, the measured points closely followed the calculated line from
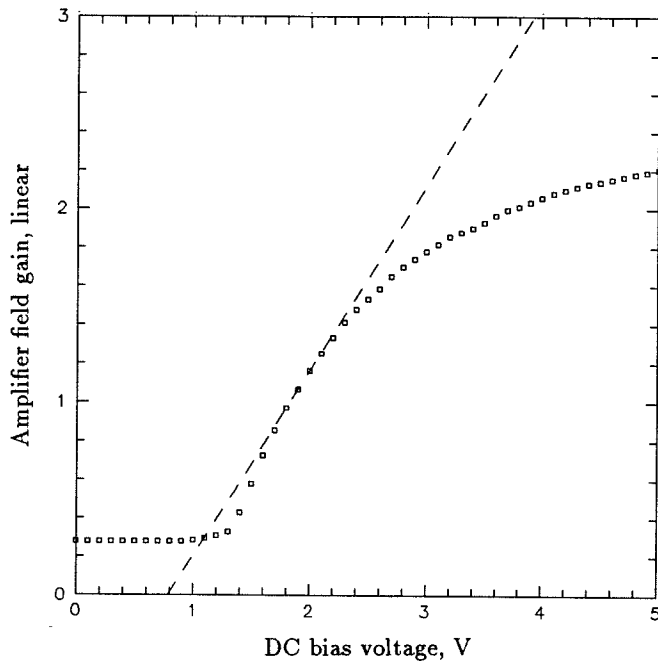
Figure 4.16 The response curve of the grid amplifier. The field gain on a linear scale is shown as a function of the bias voltage. At 2 V of DC bias, the response curve could be approximated with a line $G = 1.162(1 + 0.823v_m cos\omega_m t)$. Therefore, for a small modulation signal around 2 V, the amplitude modulation index was about $0.823v_m$.

Center frequency = 10 GHz, Span = 100 KHz/div
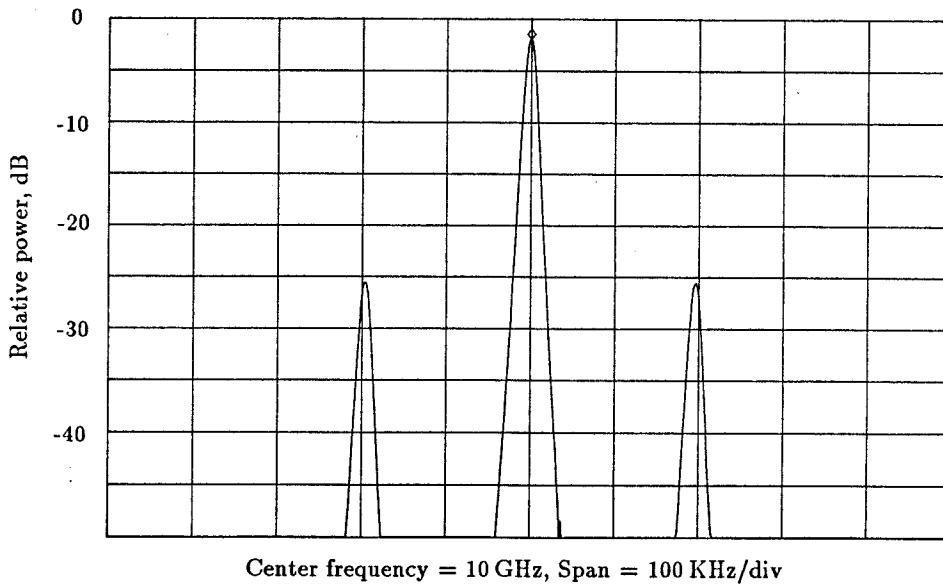
Figure 4.17 A frequency spectrum of the AM modulated signal from the amplifier grid. A modulated signal of 0.15 V at 200 KHz was added on top of the dc bias voltage of 2 V. The calculated modulation index from the gain response line was 0.123. The power difference between the carrier and the side band signal from the screen was -23.7 dB, which matches the calculated modulation index.

the linear gain response approximation. However at larger voltages, the data deviates from the calculated line indicating that the linear approximation is no longer sufficiently accurate.

The response curve might be more appropriately described by a quadratic curve for larger modulation voltages. The gain is then described by $G = G_0(1 + m_1\cos\omega_m t + m_2\cos^2\omega_m t)$. This type of non-linear response curve would give rise to a second side band signal that is $\pm 2\omega_m$ away from the main carrier signal in the frequency spectrum. Figure 4.19 is a plot of the power difference between the main carrier and the first and the second side band signals. The second side band signal was much smaller than the first side band signal indicating that the linear approximation is appropriate. The slope of the second side band signal is $40\,\mathrm{dB/dec}$ whereas the first side band signal has $20\,\mathrm{dB/dec}$ slope.

A Hewlett-Packard HP 8563A Spectrum analyzer was used to demodulate the received rf signal. Figure 4.20 shows a single-tone modulation signal on the dc-bias line of the grid and the demodulated time domain signal produced on the spectrum analyzer screen. When the dc voltage was set to $2\,\mathrm{V}$, the distortion is minimal. As the bias voltage was lowered, the AM modulation increased. When the bias reached $1.1\,\mathrm{V}$ below cutoff for the HBT's, the demodulated signal lost its lower half, as the amplifier gain remains unchanged for the biases under $1.3\,\mathrm{V}$.
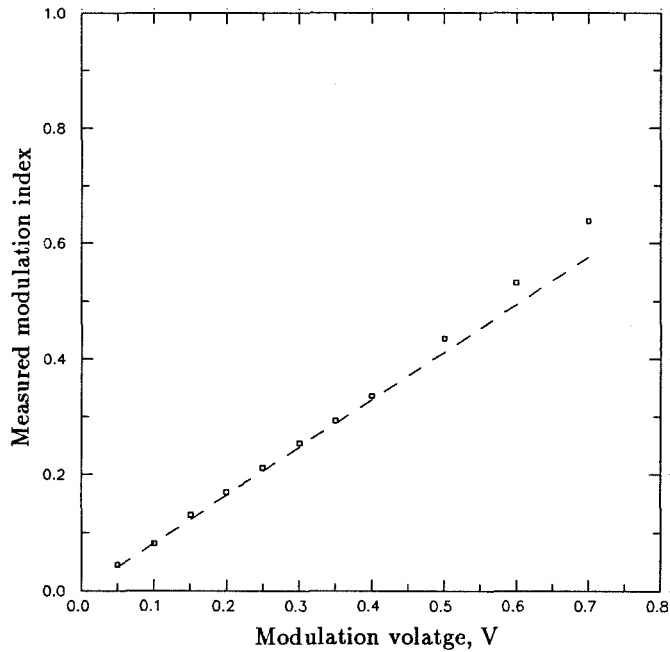
Figure 4.18 Measured amplitude modulation index for the grid amplifier with 2 V of DC bias. The squares show the measured m, and the dashed line is the calculated m from the gain response curve for a small modulation signal. At high modulation voltages, the value of measured m deviates from the calculated line.
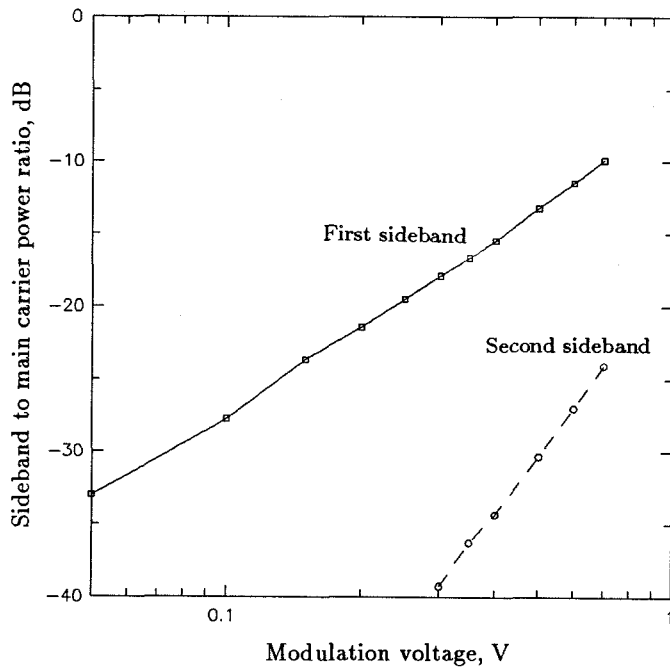
Figure 4.19 Measured power ratio between side band signals and the main carrier. The solid line is for the first harmonic and the second signal is for the second harmonic. Even though the bias reaches a cutoff below 1.3 V, which can happen with 2 V of dc bias and 0.7 V of modulated bias, the two lines can be extrapolated to find an intercept point for the second harmonic, which is 5 dB above the carrier signal.

V_DC = 2.0V   V_DC = 1.7V   V_DC = 1.1V

(a)

$V_{DC} = 2.0V$

$V_{DC} = 1.7V$

$V_{DC} = 1.1V$

(b)
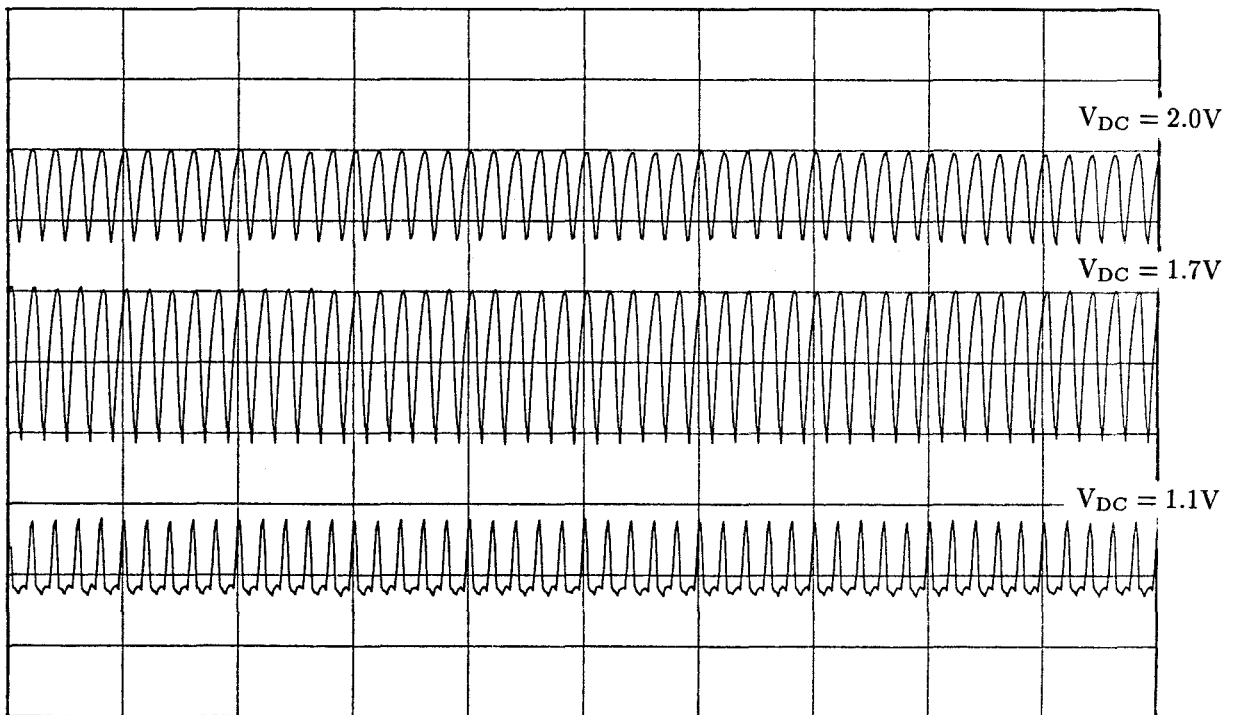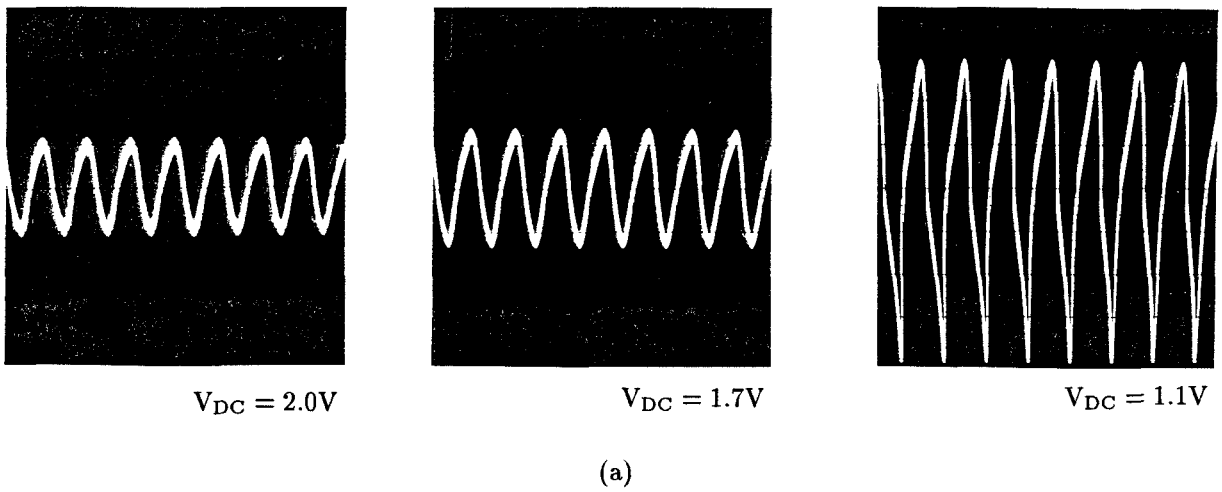
Figure 4.20 (a) Modulation signal on top of a the dc bias line shown on the oscilloscope. (b) Demodulated signal on the spectrum analyzer.

REFERENCES

[1] M. Kim *et al.*, "An X-Band HBT Grid Amplifier," submitted to *IEEE Trans. Microwave Theory Tech.*

[2] M. Kim *et al.*, "A Grid Amplifier," *IEEE Microwave and Guided Wave Letters, MGWL-1*, pp. 322-324, May 1991.

[3] R. M. Weikle *et al.*, "Planar MESFET Grid Oscillators Using Gate Feedback," to be published in *IEEE Trans. Microwave theory Tech.*

[4] Z. B. Popović *et al.*, "A 100-MESFET Planar Grid Oscillator," *IEEE Trans. Microwave Theory Tech., MTT-39*, pp. 193-200, January 1991.

[5] M. Kim, E.A Sovero, R.M. Weikle, J.B. Hacker, M.P. DeLisio, and D.B. Rutledge,"A Ka-Band Monolithic HBT Grid Oscillator ," submitted to *IEEE Trans. Microwave Theory Tech.*

[6] E. Hecht, "Optics," pp. 301-303, Second Edition, Addison-Wesley, 1988.

[7] L. B. Sjogren *et al.*, "Monolithic Millimeter-Wave Diode Array Beam Controllers: Theory and Experiment," *Third International Symposium on Space Terahertz Technology*, pp. 55-67, Ann Arbor, Michigan, March 1992.

[8] W. W. Lam *et al.*, "Millimeter-Wave Diode-Grid Phase Shifters," *IEEE Trans. Microwave Theory Tech., MTT-36*, pp. 902-907, May 1988.

[9] S. Bundy, T.B. Mader, Z.B. Popović, "Quasi-Optical Array VCO's," *IEEE MTT International Symposium*, pp. 1539-1542, Albuquerque, NM, June 1992.

[10] R.G. Buss "Radio Engineer's Handbook," Section 22.5, Second Edition, McGraw-Hill, 1977.

Chapter 5

A 35 GHz HBT Monolithic Grid Oscillator

This chapter presents the first monolithic Ka-Band grid oscillator. The grid consists of 36 heterojunction bipolar transistors (HBT's) at intervals of 1 mm. The grid was built on a 740 μm thick GaAs substrate with gold evaporated on the back side. The oscillation frequency is 34.7 GHz, with an effective radiated power (ERP) of 170 mW at a DC bias power of 370 mW.

5.1 MONOLITHIC GRID FABRICATION

All the grids that contained transistors [1-4] so far have been hybrid circuits where the active devices were mounted on top of an etched circuit board. Therefore, these grids tend to have a relatively large unit cell and consequently a low operation frequency. The smallest unit cell size for grids that used discrete transistors has been 5 mm for a 36-element 17 GHz oscillator grid [1]. Also, as the number of elements on the grid increases, mounting the devices on the substrate becomes a difficult and tedious process. Monolithic fabrication of a grid eliminates these problems and allows operations at higher frequencies. Since the grid oscillators were the first to be explored, and have the most well-established design method among grid components, we have chosen to design, fabricate, and test a monolithic grid oscillator for signal generation in the Ka-Band [5,6].

The fabrication of the monolithic grid was accomplished with the standard HBT process established at Rockwell International. The heterojunction bipolar transistor fabrication utilizes a self-aligned dual lift-off process [7] after an epitaxial growth. The AlGaAs/GaAs HBT has the active emitter area of 40 μm^2 with a
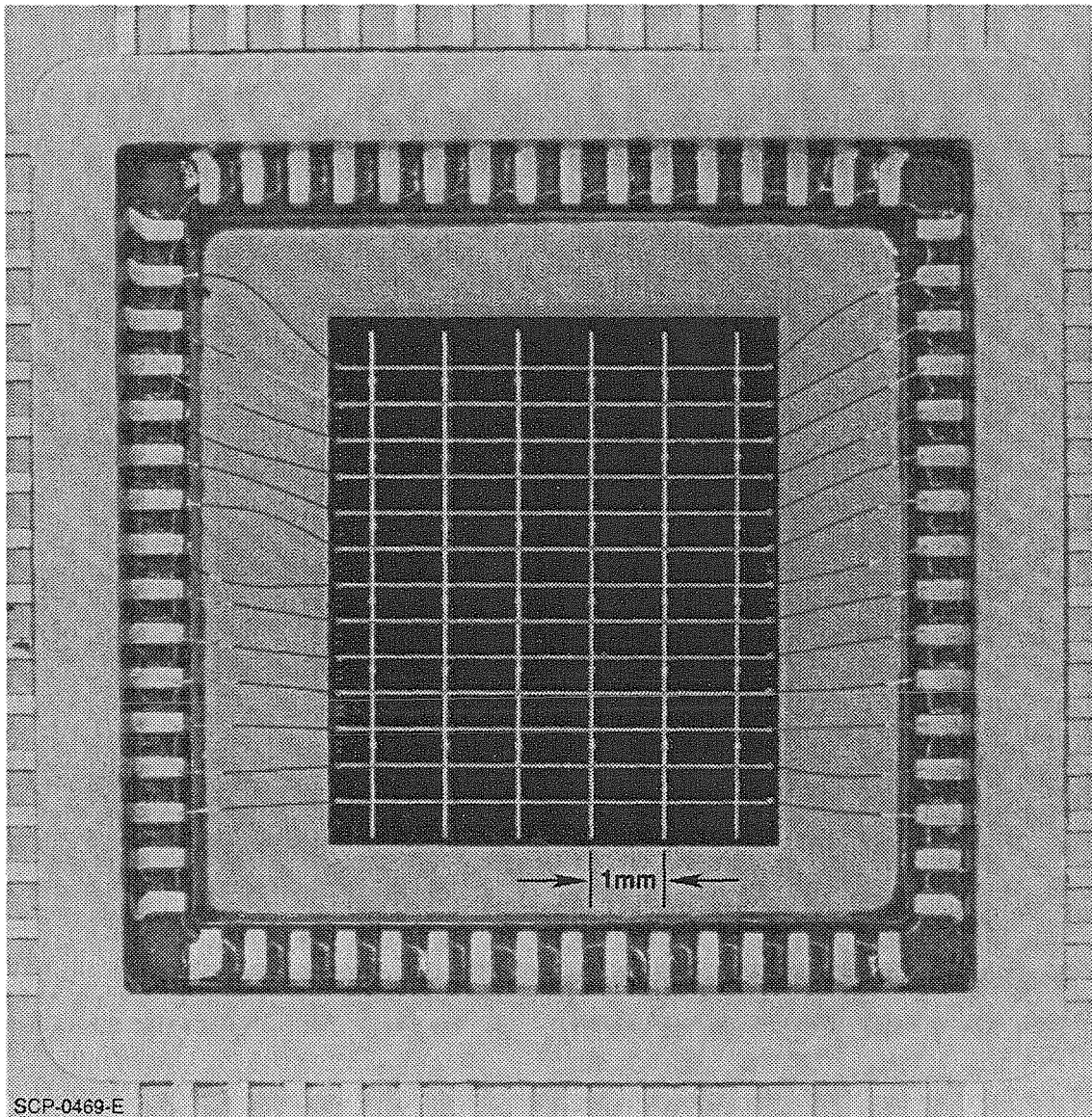
Figure 5.1 Photograph of the Ka-band 36-element HBT monolithic oscillator grid. The unit cell size is 1 mm and all the metal strips including horizontal bias lines are 40 μm wide.
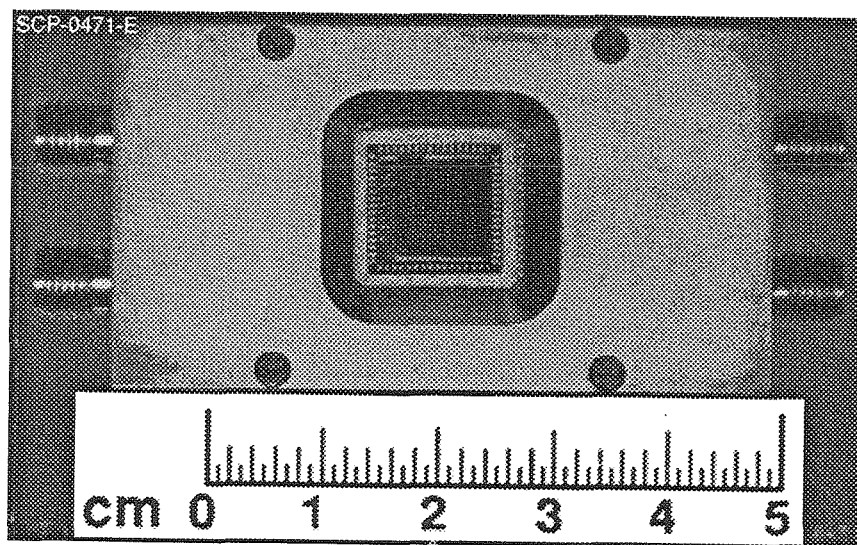
Figure 5.2 Photograph of the grid placed inside a metal case for safety in handling during the measurements.

base layer thickness of 50 to 100 nm. The measured unilateral gain of this HBT is more than 10 dB at the design frequency of 39 GHz. In addition to the HBT fabrication, the grid requires only one extra mask step to lay out the connecting metal strips. The entire grid has a diameter of 6 mm, slightly less than one free-space wavelength. The substrate under the grid is 740 μm thick, and the back surface is covered with gold to act as a back-short. The grid is mounted on a 64-pin IC flat pack carrier with bond-wires connecting the grid and the package (Figure 5.2). For safety in handling, the grid package is then placed inside a metal case with a 4 mm-deep, 20 mm square hole.

5.2 EQUIVALENT CIRCUIT MODEL

The performance of the grid oscillator can be predicted by analyzing a unit cell in the grid. Under the desired rf operation, the output beam is polarized in the vertical direction, and the rf current is distributed in such a way that we can impose boundary conditions on the edge of the unit cell as shown in Figure 5.3a. Previous work on hybrid grid oscillators has developed an equivalent circuit model for the passive grid structure in the shape of a cross [1]. The equivalent circuit

(a)

(b)
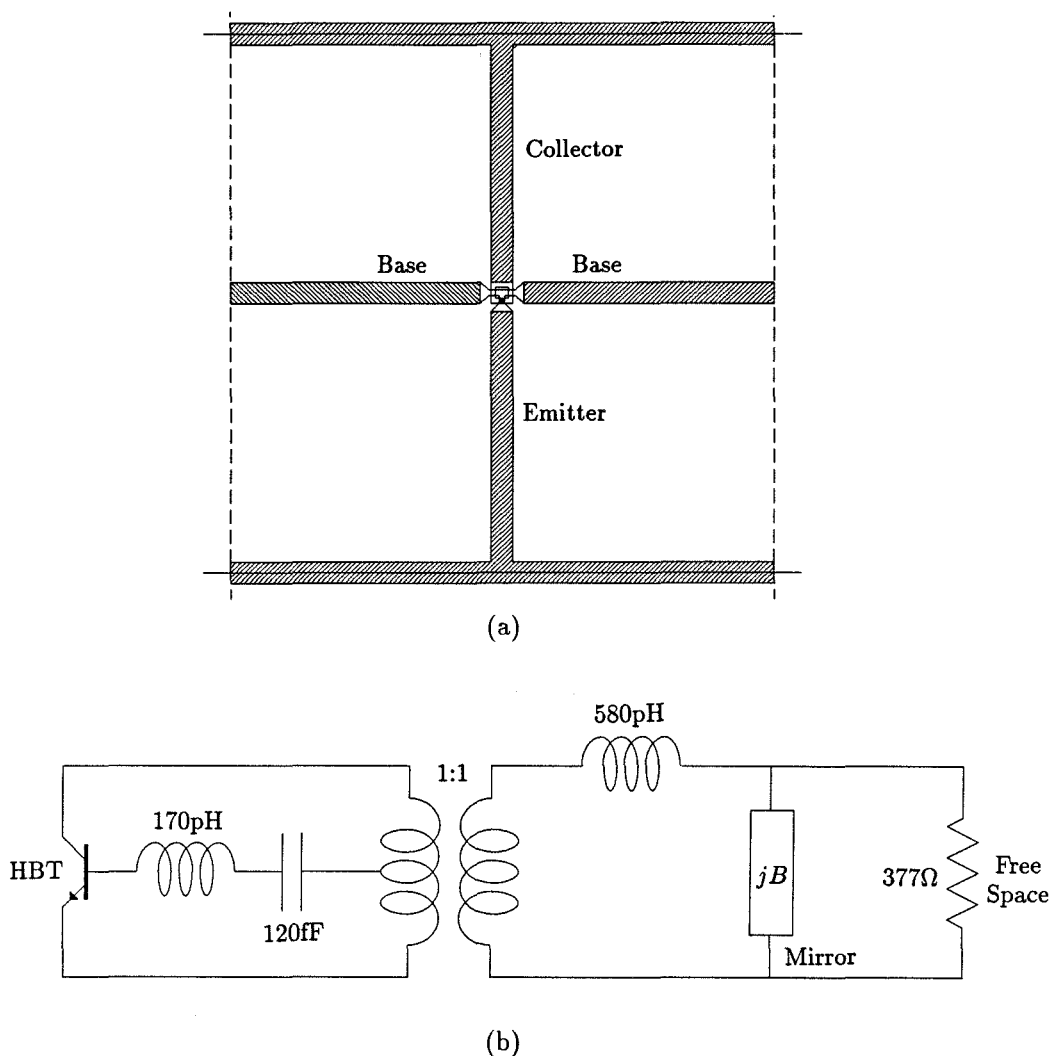
Figure 5.3 (a) The unit cell sketch. The unit cell size is 1 mm and all the metal strips are 40 μm wide. When all the transistor currents have the same magnitude and phase, and edge effects are neglected, an equivalent waveguide circuit can be analyzed with electric walls (solid line) and magetic walls (dashed line) on the boundaries of the unit cell. (b) The equivalent circuit model for the unit cell. The inductances and capacitances shown are appropriate for the entire Ka-band.

for the HBT monolithic grid is shown in Figure 5.3b. The unit cell size of 1 mm is suitable for Ka-Band operation, and the lumped elements are valid throughout the designed frequency range.

Along with the measured S-parameters for a single HBT chip, the equivalent circuit model enables us to predict the oscillation frequency. Weikle [8] describes two different approaches to predict the oscillation frequency: the counter-clockwise loop method, and the gate feedback loop method. For the equivalent circuit

Center frequency = 34. 75 GHz, Frequency span = 100 MHz
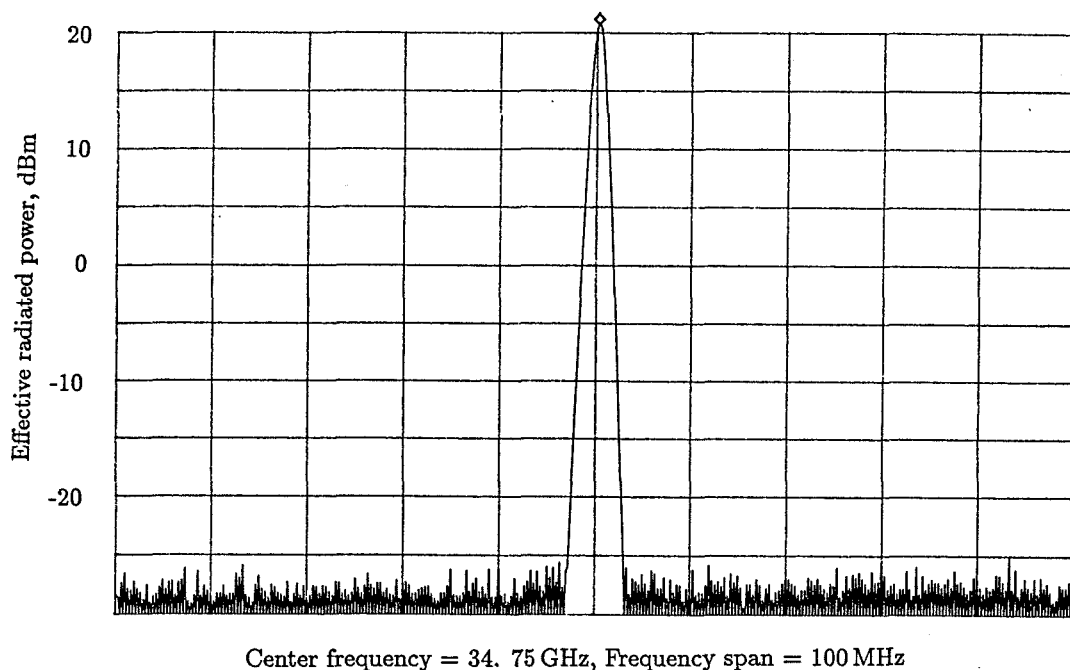
Figure 5.4 Frequency spectrum displaying the oscillation at 34.75 GHz. The peak is 22 dBm. The spectrum analyzer is calibrated to directly show the ERP.

shown in Figure 5.3b, both methods predict an oscillation at 39 GHz.

5.3 RESULTS

One important change for the monolithic grid is the use of a GaAs substrate with a dielectric constant of 12.8 rather than the *Duroid* substrate ($\epsilon_r = 2.2$) previously used in the hybrid grid oscillators. The GaAs substrate may be more susceptible to other oscillation modes because of its high dielectric constant. The grid initially showed oscillations at low frequencies in the range from 2 to 5 GHz. The output was horizontally polarized rather than vertically polarized, indicating that this oscillation was associated with the bias lines. As a measure to attenuate the bias-line rf current, a ferrite slab (Phillips 3E2A) cut to a size of 1 mm × 2 mm × 8 mm was placed on each side of the grid underneath the bond-
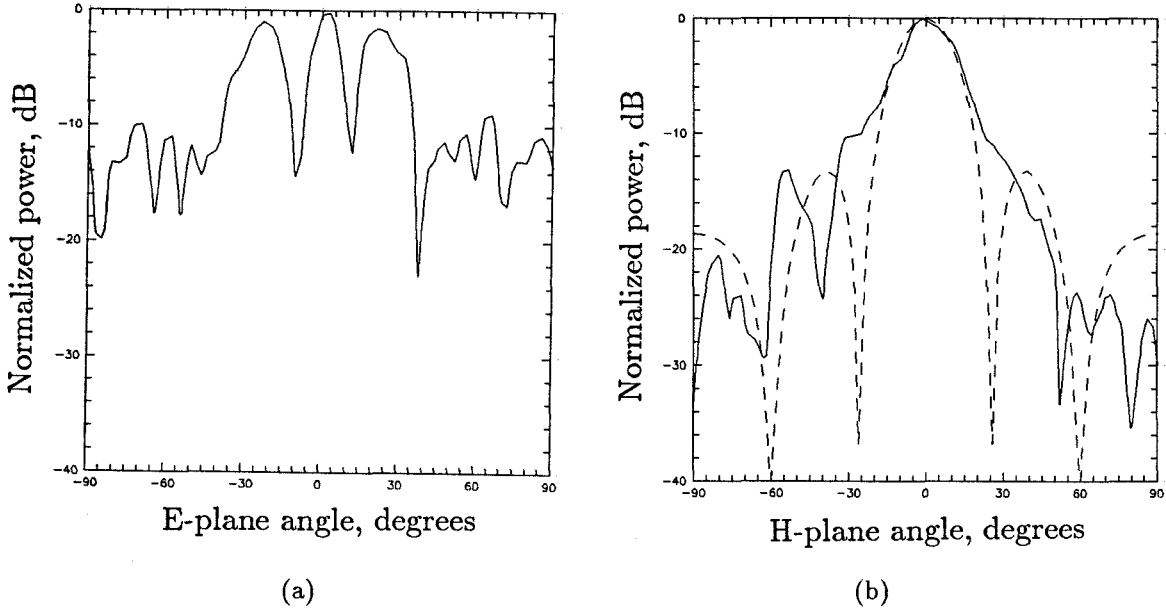
Figure 5.5 (a) H-plane and (b) E-plane patterns for the monolithic grid. In the H-plane plot, the dashed curve is the theoretical pattern for a uniformly illuminated aperture 20 mm wide. This is the width of the hole in the metal case.

wires. In microstrip measurements, we found that the ferrite slab effectively attenuates microwave signals up to 10 GHz.

With the ferrite slabs in place, the grid oscillated at 34.7 GHz. For comparison, the design frequency was 39 GHz. The beam was vertically polarized with a cross-polarization ratio of 20 dB. The maximum ERP was 170 mW. The DC power supplied to the grid was 370 mW. The E and H-plane patterns (Figure 5.5) are measured with a 0.65 mm-thick *Duroid* slab of 10.5 dielectric constant placed 7.6 mm in front of the grid. This slab improves the radiation pattern. The main beam in the H-plane has a 3-dB beamwidth of 22°, and is similar to the theoretical pattern of a uniformly illuminated aperture 20 mm wide. This is the width of the hole in the metal case that holds the grid. The E-plane pattern is poor and shows side-lobes with the peak value only 2 dB less than the main-lobe peak. This split may be associated with the metal case.

This is first report of a successful monolithic grid oscillator. It is significant because it demonstrates that the quasi-optical power-combining approach can be used for millimeter-wave power generation by a monolithic circuit. A variety of improved oscillator grids for high-power, low-noise, and higher-frequencies could be investigated in the future. More importantly, a similar approach can also be applied to build monolithic grid amplifiers, which would enable us to build a millimeter-wave system entirely out of monolithic grid components.

REFERENCES

[1] R.M. Weikle, M. Kim, J.B. Hacker, and D.B. Rutledge, "Planar MESFET Grid Oscillators using Gate Feedback," to be published in *IEEE Trans. Microwave Theory Tech.*

[2] Z.B. Popović, R.M. Weikle, M. Kim, and D.B. Rutledge, "A 100-MESFET Planar Grid Oscillator," *IEEE Trans. Microwave Theory Tech.*, *MTT-39*, pp. 193–200, February 1992.

[3] M. Kim *et al.*, "An X-Band HBT Grid Amplifier," submitted to *IEEE Trans. Microwave Theory Tech.*

[4] M. Kim *et al.*," A Grid Amplifier," *IEEE Microwave Guided Wave Lett.*, *MGWL-1*, pp. 322–324, November 1991.

[5] M. Kim, E.A. Sovero, R.M. Weikle, J.B. Hacker, M.P. De Lisio, S. Li, and D.B. Rutledge, " A 35 GHz HBT Monolithic Grid Oscillator," submitted to *IEEE Trans. Microwave Theory Tech.*

[6] M. Kim *et al.*," A 35 GHz HBT Monolithic Grid Oscillator," *International Conference on Infrared and Millimeter Waves*, Pasadena, CA, December 1992.

[7] F. Chang *et al.*" AlGaAs/GaAs Heterojuction Bipolar Transistors Fabricated Using a Self-Aligned Dual-Lift-Off Process," *IEEE Electron Device Lett. EDL-8*, pp. 303–305, July 1987.

[8] R.M. Weikle, "Quasi-Optical Planar Grids for Microwave and Millimeter-Wave Power Combining," Ph.D. Thesis, California Institute of Technology, Pasadena, CA, 1992.

Chapter 6

A Passive Grid Structure
for 93 GHz Beam-Steering

In this chapter, a passive stucture that produces a fixed beam shift of 30° is presented. The grid was 4×4 wavelengths in size at 93 GHz. The unit cell size is chosen to be $\lambda/5$. In a unit cell, $200\,\mu$m wide gold strips on a silicon substrates provide the inductance. The gap in the middle of the gold strip is varied to produce a changing capacitance. The results show a successful beam shift from 30° to 0° with a peak power density decrease of 2.5 dB.

Reflected beams

Incident beam

Quartz cover

Diode grids

Metal mounting block
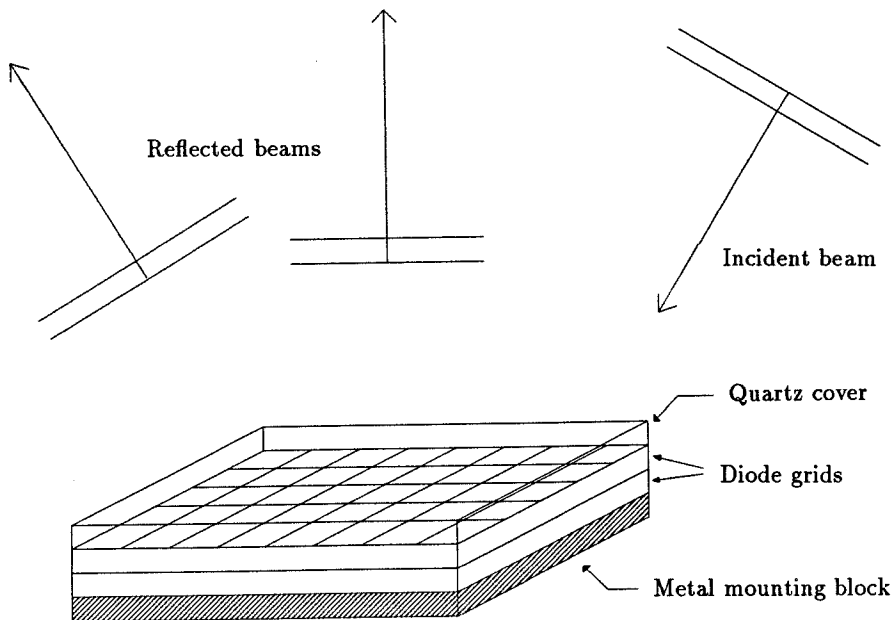
Figure 6.1 Electronically programmable beam-steering array proposed by Lam *et al* [1].

6.1 BACKGROUND

The idea of using diode grids for electronic beam steering was introduced by Lam *et al* [1]. As shown in Figure 6.1, when an incident beam reflects off the diode grid, the direction of the reflected wave can be controlled by progressively varying the reflection phase across the grid. The reflection phase of the diode grid can be controlled by varying the DC bias on the diodes. Later, a monolithic diode grid was fabricated with 1600 varactor diodes, and a relative phase shift of 70° at 93 GHz was measured [2]. This work verified the transmission-line theory used to design the grid, but the phase shift was not sufficient to steer the beam. Recently, Johansson [3] designed and built a passive planar grating-reflector antenna that focused a beam. A rigorous moment-method solution was applied to choose a grating geometry to select the first-order diffracted wave. In the work described here, the goal was to demonstrate that a beam can be steered by building a grid structure without diodes giving a fixed beam shift. In these grids, diodes were replaced by gaps with different sizes to obtain the different capacitances needed to steer the 93 GHz beam.

6.2 THEORY

If the wave has different incident and reflected angles, the characteristic impedance of the incident wave and the reflected wave are different. The formulas for the reflection coefficient are different for the E and the H field,

$$\rho_e = \frac{Y_i - Y}{Y_r + Y} \quad \text{and} \quad \rho_h = \frac{Z_i - Z}{Z_r + Z} \tag{6.1}$$

where Z_i and Z_r are the characteristic impedance of the incident wave and reflected wave, and Z is the impedance of the grid. Y_i, Y_r, and Y are the inverses of Z_i, Z_r, and Z, respectively. When Z is purely imaginary, we can write $Z = jX$, and the phase of the two reflection coefficients differ by a constant, π. In order

to steer the beam, the phase of the reflection coefficient for the grid should vary linearly across the grid as

$$\angle\rho = -k_g x \qquad (6.2)$$
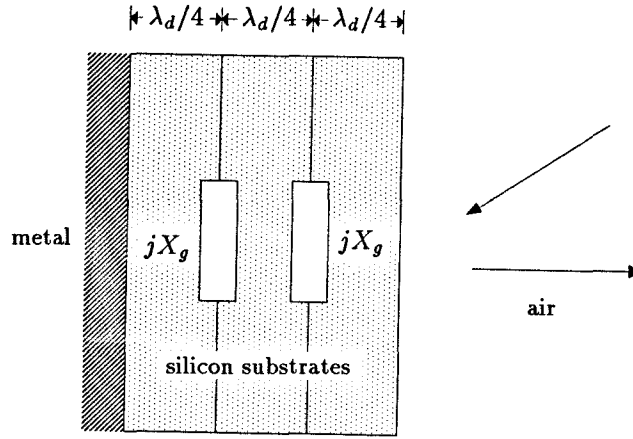
(a)
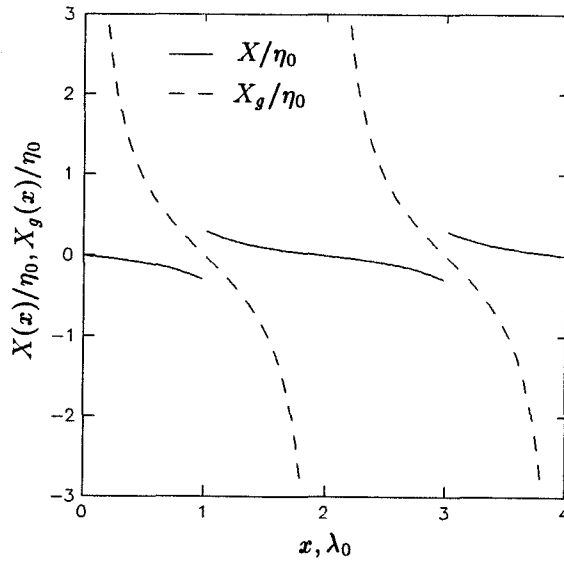
(b)

Figure 6.2 (a) Side view of two-layer stack with variable shunt elements. (b) The total reactance required to shift beam 30° (dashed line) and the required reactance for a single grid in a two-layer stack (solid line).

where x is the coordinate across the grid, and k_g is a constant. The incident beam field will have a variation across the grid of $\exp(-jk_ix)$, where $k_i = k_0\sin\theta_i$. In this formula, k_0 is the free-space propagation constant, and θ_i is the incident angle. The reflected wave will have a corresponding field variation of $\exp(-jk_rx)$ where $k_r = k_0\sin\theta_r$, and θ_r is the reflected angle. We can then write

$$k_g = k_r - k_i \tag{6.3}$$

For given incident and reflected angles, the grid reactance must satisfy

$$k_g x = \tan^{-1}\left(\frac{X(x)}{Z_i}\right) + \tan^{-1}\left(\frac{X(x)}{Z_r}\right) \tag{6.4}$$

The required reactance is plotted in Figure 6.2b as a dashed line for an incidence angle of 30° and a reflected angle of 0° for waves incident with TM polarization. This figure shows that both very large and very small reactances are required to steer the beam. This is difficult to obtain with a single grid. However, we can reduce the required reactance range by stacking two identical grids (Figure 6.2a). If the grids are surrounded by substrates with a high dielectric constant, the wave inside the substrates can be approximated by a TEM wave at normal incidence. The reactance of each grid then can be transformed to the required total surface reactance using the transmission-line model as,

$$X(x) = X_g(x) - \frac{\eta_d^2}{X_g(x)} \tag{6.5}$$

where η_d is the characteristic impedance of the dielectric substrate used. The required range for $X_g(x)$ is then reduced to $0.6\eta_0$, where η_0 is the free-space characteristic impedance (Figure 6.2b).

To determine the shunt reactance produced by a single grid, it is convenient to assume that the grid parameters vary slowly, and to define a unit cell. For a

(a)   (b)
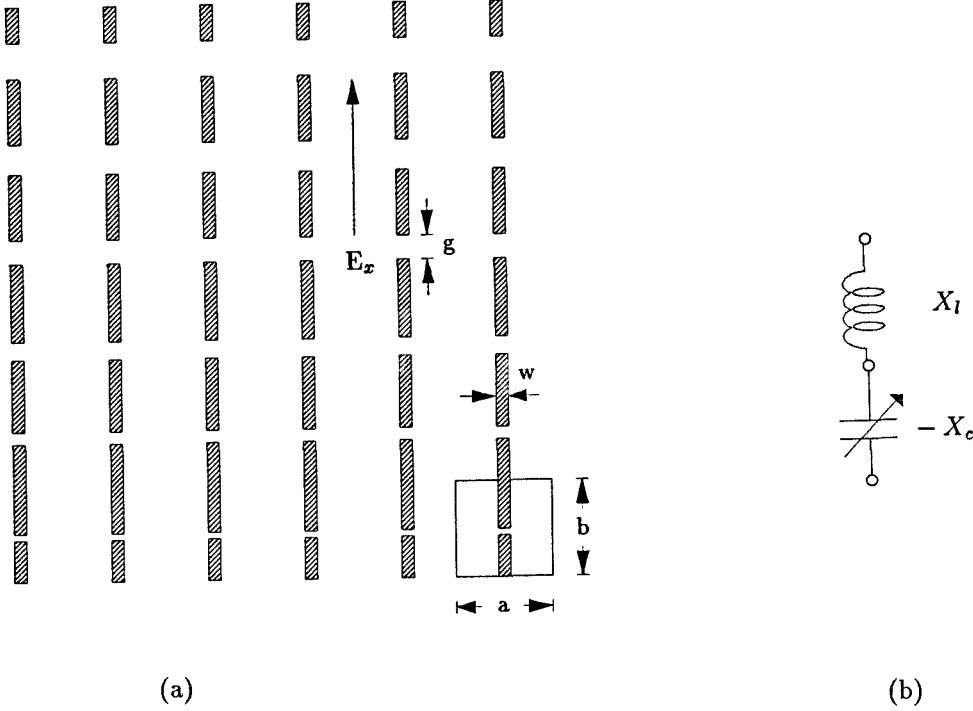
Figure 6.3 (a) A grid with varying gaps. The area enclosed by the rectangle shows a unit cell. (c) The resulting equivalent circuit.

TEM wave, electric walls can be placed anywhere along the direction of the H field and magnetic walls along the E field direction. A unit cell is then defined as the area enclosed by lines that connect the middle points between the gaps (Figure 6.3a). After placing electric walls on the sides and magnetic walls on the top and bottom of the unit cell, the inductive reactance due to the metallic lead can be found using a method developed by Eisenhart and Kahn [4],

$$X_l(\mathrm{w}) = \frac{\mathrm{b}}{\mathrm{a}}\omega\mu \sum_{m=1}^{\infty} \frac{1}{\alpha_z}\mathrm{sinc}^2\left(\frac{m\pi\mathrm{w}}{\mathrm{a}}\right)\left(1 - \frac{\mathrm{w}}{\mathrm{a}}\right) \qquad (6.6)$$

where a and b are the unit cell width and height, w is the width of the metal strip, α_z is the attenuation constant for the given mode, and μ is the permeability of the material that forms a waveguide for the unit cell. Assuming that the inductance can be chosen as the average of the varying capacitive reactance, the

minimum capacitance required should be smaller than $\frac{1}{2\pi f \Delta X_g}$, which is about 7 fF at 93 GHz. This kind of capacitance is smaller than that available from packaged varactor diodes. Unless the grid is made monolithically, the frequency of operation has to be lowered or several diodes must be placed in series.

For the passive grid without diodes, the capacitive reactance produced by the gap can be also obtained using the Eisenhart and Khan method [4],

$$X_c(g) = -\frac{b}{4a}\omega\mu \sum_{m=0}^{\infty} \frac{\epsilon_{0m}\text{sinc}^2(\frac{m\pi w}{a})(1-\frac{w}{a})}{\sum_{n=1}^{\infty}\text{sinc}^2(\frac{n\pi g}{b})\frac{\alpha_z k^2}{k_y^2-k^2}(1-\frac{g}{b})} \qquad (6.7)$$

where g is the size of the gap in the metal strip. ϵ_{0m} is 1 if m is zero, and 2 otherwise. The capacitance given by this formula can easily be small enough to allow the required $0.6\eta_0$ reactance change at 93 GHz.

6.3 EXPERIMENTAL RESULTS

A two-layer grid was built at 93 GHz on 600 Ω-cm silicon substrates. The metal strips were 200 nm thick gold films fabricated by lithographic techniques. The size of the unit cell was chosen to be $\lambda/5$, and the total grid size was 4λ by 4λ. Figure 6.4a shows how the experiment was set up. The reflected power pattern was measured as the incident radiation produced by a 93 GHz klystron was directed onto the grid at a 30° incident angle. Once the data were taken, the grid was replaced by a mirror of the same size for comparison. The beam that was reflected off the grid was found to be shifted by 30° with respect to that reflected off the mirror. The loss was 2.5 dB. At the same time, the unwanted zero-order beam was reduced by 8 dB.

In this work, a passive grid designed using a simple transmission-line model was used to convert the zero-order diffracted wave to the first order. This model is useful because it can easily include semiconductor devices with biasing circuits. Present beam-steering research is directed toward controlling the transmitted
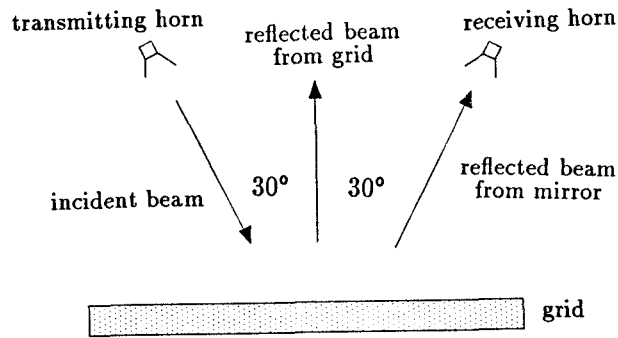
(a)
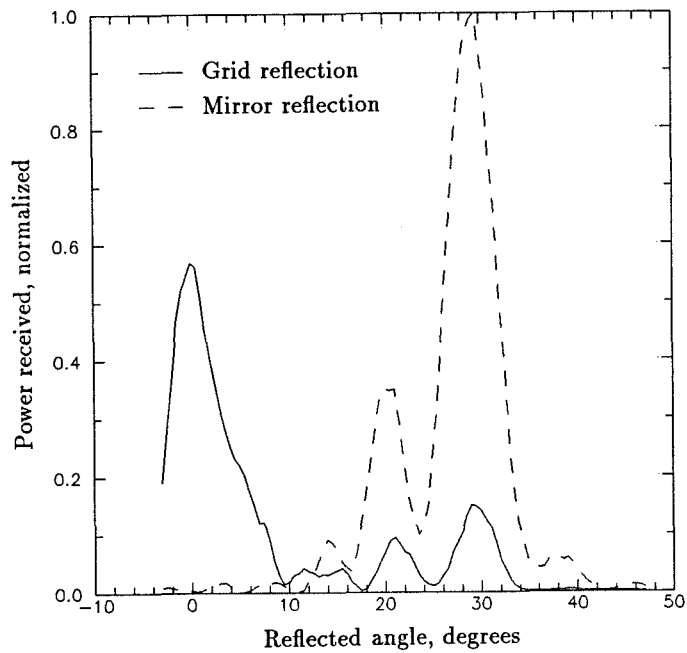
(b)

Figure 6.4 (a) The experimental scheme for passive beam steering grid measurements, and (b) the received power as a function of reflected angle.

beam rather than the reflected beam [5]. Recently, Sjogren *et al.* demonstrated a phase shift of 100° for a transmitted beam from a diode grid at 93 GHz [6]. The loss for the transmitted beam, in this case, was 6 dB. This kind of planar stucture can be integrated together with other active grid structures, such as amplifiers and mixers to form a complete millimeter-wave optical beam system.

REFERENCES

[1] W.Lam, C. F. Jou, N. C. Luhmann, Jr., D. B. Rutledge, "Diode Grids for Electronic Beam Steering and Frequency Multiplication," *International Journal of Infrared and Millimeter Waves, Vol. 7, No. 1,* pp. 27-41, 1986.

[2] W. Lam, C. F. Jou, H.Z. Chen, K.S. Stolt, N. C. Luhmann, Jr., D. B. Rutledge, "Millimeter-Wave Diode-Grid Phase Shifters," *IEEE Trans. on Microwave Theory and Techniques, Vol. 36, No. 5,* pp. 902-907, May 1988.

[3] F. S. Johansson, "A New Planar Grating-Reflector Antenna," *IEEE Trans. on Antennas and Propagation, Vol. 38, No.9,* pp. 1491-1495, September 1990.

[4] R. L. Eisenhart, P.J. Kahn, "Theoretical and Experimental Analysis of a Waveguide Mounting Structure," *IEEE Trans. on Microwave Theory and Techniques, Vol. 19, No. 8,* pp. 706-719, August 1971.

[5] Martin Lee Zimmerman, " An H-Plane Diode Grid Array Phase Shifter Design at 20 GHz," M.S. Thesis, University of Illinois, 1988.

[6] L.B. Sjogren et al., "Monolithic Millimeter-Wave Diode Array Beam Controllers: Theory and Experiment," *Third International Symposium on Space Terahertz Technology,* Ann Arbor, MI, March 1992.

Chapter 7

Suggestions for Future Work

Two important new projects are introduced in this chapter. Hybrid HEMT grid amplifiers are being tested for X-band application in order to obtain better noise performance. A monolithic amplifier array fabrication project has been initiated at Rockwell International. These projects, along with an improved design model, should help us understand grid amplifiers better, and allow us to eventually build monolithic grid array millimeter-waves systems.
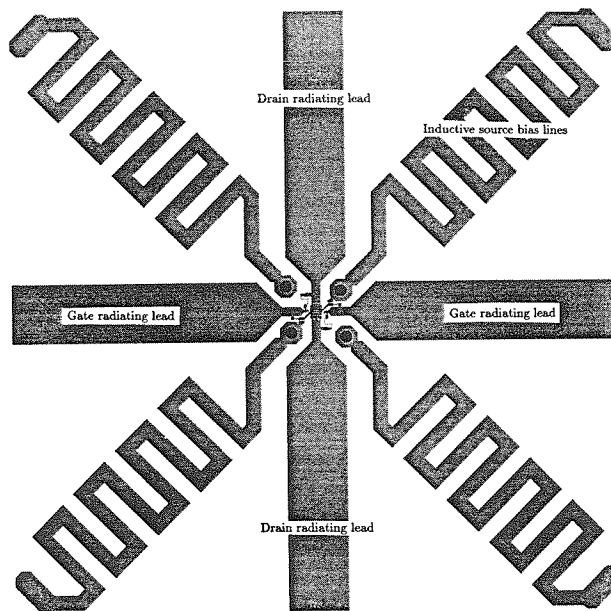
7.1 HYBRID HEMT GRID AMPLIFIERS

Attempts are being made to improve the results of the X-band HBT grid discussed in Chapter 3. One of the shortcomings of the X-band HBT grid was its relatively high noise figure that makes it unsuitable for low-noise amplification. By replacing the HBT chips with High Electron Mobility Transistor chips, the noise performance of the amplifier grid can be improved. HEMT's using pseudo-morphic InGaAs material for the electron channels exhibit even higher electron velocity than is observed in conventional GaAs channel HEMT's, allowing good power performance as well [1]. HEMT's can have maximum frequencies of oscillation (f_{max}) as high as 400 GHz. HEMT-based oscillators can be operated efficiently at frequencies of over 80% of f_{max} [2], and efficient power amplifiers have been made up to 94 GHz [3]. More importantly, HEMT's exhibit the lowest noise of any solid-state amplifying device at room temperature within their currently useful range (5-100 GHz).

Even with the success of the X-Band HBT grid amplifier, more hybrid grid work is needed to develop and fully understand an appropriate passive grid structure
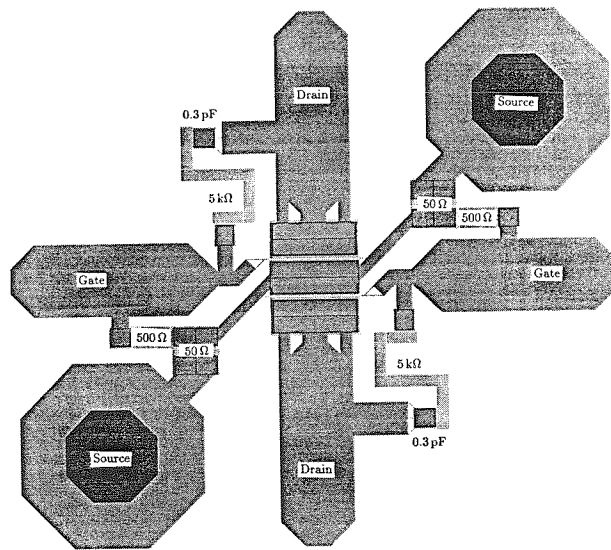
(a)

(b)

Figure 7.1 (a) The layout of the differential-pair chip for a hybrid amplifier grid. The chip consists of two HEMT's and six wire-bonding pads. Resistors are used for stabilization, gate self-bias, and common-mode rejection. (b) Layout for the second generation chip for Ku-Band Hybrid grid proposed by R.P. Smith at JPL. This chip includes parts of the radiative elements. As the size of the unit cell shrinks for higher frequency operation, the chip can be simply tiled onto a substrate to form a unit cell by itself. to control the bias and suppress the spurious oscillations.

for an amplifier. Dr. Peter Smith at Jet Propulsion Laboratory has designed and fabricated differential-pair HEMT chips that are similar to the earlier HBT chips. As shown in the Figure 7.1 (a), there are three types of resistors on the chip: $5\,k\Omega$ feedback resistor between gate and drain to present negative feedback between the input and the output, $500\,\Omega$ to self-bias the gate, and $50\,\Omega$ to increase the common-mode rejection ratio. Again, the integration of the differential-pair on a single chip greatly reduces the parasitic source inductance and the parameter variation that occur when discrete transistors are wired together.

Our experience with the X-band HBT grid indicates that the fabrication of a hybrid grid at frequencies higher than X-band may be difficult. The radiating leads and bias lines have to be placed together in a small unit cell. Dr. Smith again proposed a new chip configuration where the relatively large size chip of $4\,mm$ will include both the radiating leads and the bias lines. A grid can be built by simply tiling these chips over the substrate. This approach seems sound for scaling up in frequency, possibly up to $20\,GHz$.

7.2 MONOLITHIC AMPLIFIER GRID

As was the case for the monolithic oscillator grid [4], the monolithic integration of a grid amplifier will allow fabrication of a smaller unit cell which is necessary for higher frequency operation. Mass production of working amplifier grid arrays will allow many grids to be tiled to obtain even larger grid array.

The high dielectric constant of GaAs substrate underneath the transistors may cause some matching problems. This can be avoided by using a substrate thickness close to $\lambda_e/2$. However, the high dielectric constant material has in many cases produced substrate-modes that were difficult to suppress. In addition, a long design-to-test cycle and the inability to modify monolithic grids present major difficulties.

Design and fabrication processes for monolithic amplifier grids have already been

initiated by Dr. E. Sovero at Rockwell International. The transistors used are identical to those in the X-Band amplifier grid. A similar passive structure to the hybrid HBT grid amplifier was chosen for the monolithic grid except that the overall structure has been shrunk by a factor of four to push up the operation frequency into 44 GHz. A special processing technique is being used to transfer the active layers of the HBT ($\sim$ 4 micron-thick) from the semi-insulating GaAs to a substrate of more desirable dielectric and thermal properties.

7.3 CLOSING REMARKS

In the beginning, we did not think the amplifier grid would work. We were very fortunate to build grids that produced gain and didn't oscillate. The two working amplifier grids presented in this thesis, however, merely implemented the basic concept that was conceived by Professor Jim Rosenberg at Harvey Mudd College. Many things need to be done to improve our knowledge on the amplifier grids. Until now, the theoretical work is so far behind the experimental work, and we still believe that "we don't know anything about the amplifier grid".

Compared to the oscillator grids, the structures of the amplifier grids are much more complicated. However, we hope to soon present a theoretical model which will allow an analytic design of an amplifier grid. Currently, Hewlett-Packard's High Frequency Structure Simulator [5] is being used to help predict the characteristics of the passive structures being used in the grid array. In the near future, improved versions of this software should allow a more rigorous grid design to be accomplished.

REFERENCES

[1] B. Kim, R.S. Matyi, M. Wurtele, K. Bradshaw, M. Ali Khatibzadeh, H. Quen Tserng," Millimeter-Wave Power Operation of an AlGaAs/InGaAs/GaAs Quantum-Well MISFET," *IEEE Electron Device, ED-36,* pp. 2236-2242, October 1989.

[2] D. Pavlidis, URI-ARO Reasearch Program Review, Ann Arbor, Michigan, 1989.

[3] P.M. Smith, L.F. Lester, P.C. Chao, P. Ho, R.P. Smith, J.M. Ballingall, and M.Y. Kao," A $0.25\,\mu$m Gate-Length Psedomorphic HFET with $32\,$mW Output Power at $94\,$GHz," *IEEE Electron Device Letters, EDL-10,* pp. 437–439, October 1989.

[4] M. Kim, E.A. Sovero, R.M. Weikle, J.B. Hacker, M.P. DeLisio, S. Li, D.B. Rutledge, " The $35\,$GHz Monolithic HBT Grid Oscillator," submitted to *IEEE Trans. on Microwave Theory and Tech.*

[5] "HP 85180A High Frequency Structure Simulator," Hewlett-Packard, Networks Measurements Division, 1400 Fountaingrove Parkway, Santa Rosa, CA, 1992.